UNIVERSITY OF CALIFORNIA
RIVERSIDE

Further Applications of Osmotic Transport Device for Penetrating Ballistic Brain Injury and Long-Term Controlled Cortical Impact Spinal Cord Injury

A Dissertation submitted in partial satisfaction
of the requirements for the degree of

Doctor of Philosophy

in

Bioengineering

by

Alan Giglio

September 2025

Dissertation Committee:
Dr. Victor G. J. Rodgers, Chairperson
Dr. William Grover
Dr. Vasileios Christopoulos

The Dissertation of Alan Giglio is approved:

_____

_____

_____

Committee Chairperson

University of California, Riverside

Acknowledgements

First and foremost, I must express my sincere gratitude and thanks to my advisor Dr. Victor G. J. Rodgers. I still remember our conversations in my first graduate course. I had a good job in industry, and I was offered an opportunity to further my education and have it paid for by the company. In my first course with you I was inspired, and I eagerly studied the course material daily and even neglected my work responsibilities. Near the end of the academic year, I was about to graduate with my masters but I wanted to achieve more. It was at that point that I reached out and you encouraged me to apply and pursue a PhD in bioengineering and my life has forever changed. Thank you for all the guidance and mentorship you have provided me over these years, I am forever grateful.

I would like to thank my committee member Dr. William Grover for his time and insight into some of my projects. I was able to gain valuable skills and knowledge by working in your lab and I am grateful for the time you spent with me in supporting my research.

I would be remiss if I did not mention my friends and colleagues within the graduate student community who supported me and made my years at UC Riverside enjoyable and interesting. Your friendship means the world to me.

I would like to thank the entire Biotransport and Bioreactions Kinetics group (B2K) and the undergraduates who worked with me in designing and conducting experiments. I would like to single out and thank Emily Bomortino, Uma Sindha, and Tanzila Akter for their hard work in supporting my research projects.

Finally, I would like to thank my wife Miranda for her unshakeable faith in me during my years. It was your encouragement that gave me the courage to take the leap in the first place and it was your continued support that allowed me to continue my education through these vital years. Our time together has been the happiest time of my life.

ABSTRACT OF THE DISSERTATION

Further Applications of Osmotic Transport Device for Penetrating Ballistic Injury and Long-Term Controlled Cortical Impact Spinal Cord Injury

by

Alan Giglio

Doctor of Philosophy, Graduate Program in Bioengineering
University of California, Riverside, September 2025
Dr. Victor Rodgers, Chairperson

Secondary injury following penetrating traumatic brain injury (pTBI) and spinal cord injury (SCI) is largely driven by edema-induced increases in intracranial (ICP) and intraspinal pressure (ISP). Conventional approaches such as hyperosmolar therapy and decompressive surgery are limited by transient efficacy, systemic side effects, and lack of point-of-injury applicability. To address these limitations, this dissertation advances the osmotic transport device (OTD), a mechanical platform that leverages osmotic pressure gradients across semi-permeable membranes to achieve controlled removal of excess fluid directly from injured tissue.

Theoretical modeling of the OTD was developed from film theory and the Kedem–Katchalsky framework to characterize solvent flux in relation to hydraulic permeability, boundary layer concentration polarization, and osmotic pressure differences. Analytical solutions were derived to establish controllability parameters for

different geometries and flow conditions, guiding membrane selection and device design. These models were further regressed against experimental datasets to validate predicted flux behavior and optimize operating parameters for both spinal and cranial applications.

For SCI applications, a long-term OTD was fabricated using stereolithography (SLA) and biocompatible resin with a flat-sheet membrane sealed by epoxy traps to maintain structural stability during continuous use. Design iterations incorporated custom brackets, rib-anchored base pieces, and hydrogel interfaces to preserve membrane contact under physiological motion. The device demonstrated feasibility of maintaining osmotic flux during a three-day implantation study in a rat model.

For pTBI applications, hollow fiber and flat-sheet OTD configurations were engineered to enhance decompressive craniectomy by introducing sustained osmotic fluid removal. In rodent studies, these designs produced measurable reductions in ICP and favorable histological trends. To enable large-animal testing, the OTD was scaled for porcine ballistic injury models with custom housings, sterilizable flat-sheet membranes, and an integrated circulation system powered by a programmable pump system was embedded into a helmet-vest assembly to simulate fieldable deployment, with preliminary results validating hydraulic permeability and sustained operation over multi-day studies.

This work establishes a rigorous engineering basis for OTD function, demonstrating how principles of osmotically driven transport can be applied across multiple device architectures and scaled for translational models. By integrating mathematical modeling, materials engineering, iterative design, and experimental

validation, the OTD is positioned as a novel platform technology for managing pressure-driven secondary injury in CNS trauma.

Contents

Acknowledgements iv
ABSTRACT OF THE DISSERTATION vi
Contents ix
List Of Figures xii
List of Symbols xvi
Chapter 1. Introduction 1
1.1 Edema in the Central Nervous System 1
1.2 Role of Edema in Secondary Injury 1
1.3 Penetrating Traumatic Brain Secondary Injury 2
1.4 Non-Severed Spinal Cord Secondary Injury 3
1.5 Treatments for pTBI and Non-severed SCI 3
1.6 Osmotic Transport Device 5
1.7 Previous OTD Applications 5
1.8 Scope of this work 7
Chapter 2. Fundamental Mathematical Principles and Model of the Osmotic Transport Device 9
2.0 Scope of Mathematical Principles 9
2.1 Overview of Osmotic Pressure 9
2.2 Thermodynamic Basis of Osmotic Pressure 9
2.3 Previous Development of Forward Osmosis Membrane Processes 13
2.4 Modelling of Flux of the OTD and Understanding Controllability 13
Chapter 3. Application of OTD for Long-Term Spinal Cord Injury 20
3.1 Previous Work 20
3.2 Scope of this work 21
3.3 Modifications for Long Term Studies 21
3.3.1 CAD Design and Iterations 22
3.3.2 Wheelchair and Swivel 27
3.4 Experimental Methodology 30
3.6 Future work 36
Chapter 4. Osmotic Transport Device for Penetrating Traumatic Brain Injury in Rodents 38
4.0 Scope of Work 38

4.1 Penetrating Traumatic Brain Injury 39
4.2 pTBI Rat Model 40
4.3 pTBI-OTD Development 41
4.3.1 Prototype Hollow Fiber Bundle 42
4.3.3 Discussion on Prototype Hollow Fiber Bundle Experiments 48
4.3.4 Hollow Fiber Tube Fitting 49
4.3.5 Flat Sheet Membrane Device for Rodent pTBI-OTD 52
4.3.6 Quantitative and Qualitative Device Evaluation 53
4.4 Rodent pTBI-OTD Long Term Study 57
4.4.1 Rodent pTBI-OTD Methods 57
4.5 Rodent pTBI Results and Discussion 58
Chapter 5. Osmotic Transport Device for Penetrating Traumatic Brain Injury in Porcine 65
5.0 Pig pTBI-OTD Concept and Development 65
5.1 Membrane Housing and Device Development 65
5.1.1 Manufacturing Cost and Production 69
5.2 Quantitative and Qualitative Testing of pTBI-OTD 69
5.3 Swine Helmet and Vest 75
5.3.1 Circulation BoxPump 77
5.4 Device Efficacy and Quantitative Analysis 80
5.5 Conclusion 87
Chapter 6. Conclusions 89
6.1 Findings in This Work 89
6.2 Future Directions 89
Schematics of Flat Sheet Membrane OTD Versions and Full Assemblies 90
A1. Schematic of Base v1.2 90
A2. Schematic of Bracket v1.2 90
A3. Schematic of OTD v1.2 91
A4. Schematic of v1.2 Assembly 91
A5. Schematic of Bracket 1.3 92
A7. Schematic of OTD 1.3 Assembly 93
A8. Schematic Base 1.4 93
A9. Schematic Bracket 1.4 94

A10. Schematic of OTD v1.4 Assembly 94
A11. Schematic of Base 1.6 95
A12. Schematic of Bracket 1.6 95
A13. Schematic of OTD v1.6 Assembly 96
A14. Schematic of OTD v1.8 Base 96
A15. Schematic of OTD v1.8 Bracket 97
A16. Schematic of OTD v1.8 Assembly 97
A17 Schematic of Rat Spinal Cord Harness 98
Appendix b. Hollow Fiber OTD Schematics 98
B1. Schematic of Hollow Fiber Skull Attachment 98
B2. Schematic of Hollow Fiber Housing Bottom 99
B3. Schematic of Hollow Fiber Housing Top 99
B4. Schematic of Hollow Fiber Housing Barbed Tubing Connection 100
B5. Schematic of Barbed Cap 100
B6. Schematic of 180 Degree Barbed Cap 101
B7. Schematic of Hollow Fiber Assembly 101
Appendix c. Rodent Flat Sheet Membrane OTD Schematics 102
C1. Schematic of Flat Sheet Membrane Rodent Model Base 102
C2. Schematic of Flat Sheet Membrane Rodent Model Top 102
C3. Schematic of Flat Sheet Membrane Rodent Model Assembly 103
Appendix d. Porcine Flat Sheet Membrane OTD Schematics 104
D1. Schematic of Impermeable Elastic Membrane for Porcine Model OTD 104
D2. Schematic of Membrane Housing for Porcine Model OTD 104
D3. Schematic of Porcine Model OTD Assembly 105
Appendix e. Matlab Code for the Analysis of Tangential Flux 106
E1. Code for Membrane Series 1 106
E2. Code for Membrane Series 2 Low Speed 108
BoxPump Code and Schematic Design 110
F1. Code for Arduino Boxpump 110
F2. Electric Schematic for the BoxPump Device 113

List Of Figures

Figure 2.1 Osmotic Transport From Tissue 13

Figure 3.1 CAD model of SCI-OTD with tube fittings designed to extend past the skin and outside the animal 22

Figure 3.2 A cross-section view of the original version of the SCI-OTD on the T8 vertebrae of the spinal cord. The device was sealed onto the spinal cord with silicone... 23

Figure 3.3 Original assembly for the first iteration of the SCI-OTD..... 24

Figure 3.4 Bracket for stabilizing the OTD on the spinal cord..... 25

Figure 3.5 Base pieces that were designed to straddle the SCI-OTD from both sides and restrict the lateral movement of the device relative to the spinal cord. 25

Figure 3.6 Epoxy trap for SCI-OTD to eliminate bowing of membrane during study..... 26

Figure 3.7 Final SCI-OTD with housing and bracket in place. 27

Figure 3.8 Schematic representation of the current iteration SCI-OTD in the different phases of placement secured around the spinal cord with screws. 27

Figure 3.9 Wheelchair attachment for rat post-surgery with OTD active. 29

Figure 3.10 Vest with OTD attached 30

Figure 3.11 The experimental setup for the 3-day experiment. The containers on separate top loading balances were used to measure the evaporation in the room with a control container on a separate balance with a small amount of BSA. 32

Figure 3.12 Animal test subject over 3 days of study. 33

Figure 4.1 A. MRI images showing 7-day Edema progression for a pTBI rat model. B. Cerebral Edema volume progression from baseline value over 7 days. Courtesy of Dr. Zach Bailey 41

Figure 4.2 Prototype of the hollow fiber pTBI prototype with the custom attachment for craniotomy fitting..... 43

Figure 4.3 Custom tube fitting for hollow fiber prototype. 44

Figure 4.4 Schematic Representation of Hollow Fiber Prototype Experiment 45

Figure 4.5 Hollow Fiber Prototype test setup with control and sham rat 46

Figure 4.6 ICP chart of preliminary hollow fiber prototype trial 47

Figure 4.7 Short Term Hypertonic OTD Treatment with Hollow Fiber Bundle. 48

Figure 4.8 Prototype Hollow Fiber Tube Fittings..... 50

Figure 4.9 Exploded view of multiple part hollow fiber tube fitting. 51

Figure 4.10 Hollow fiber tube fitting chamber where the main osmotic pressure driving force is generated. 51

Figure 4.11 Rodent pTBI-OTD flat sheet membrane 52
Figure 4.12 Quality testing setup schematic of OTD for rodent pTBI device..... 55
Figure 4.13 OTD hydraulic permeability qualification setup. 56
Figure 4.14 Schematic of rodent pTBI-OTD study 58
Figure 4.15 When examining the raw ICP data, we find that following PBBI, there was not a significant impact of OTD treatment. However, during the 4-hour treatment period a decreasing trend was observed in the hypertonic treated group compared to both isotonic and PBBI only controls. n=9 59
Figure 4.16 ICP increases significantly following injury in all injured groups. The OTD with the hypertonic solution group decreased slightly during treatment, but the differences did not reach statistical significance. n=9 59
Figure 4.17 Isolated OTD conditions in the treatment phase. By the end of the experiment, the difference was approximately 1 mmHg. While not statistically significant, the ICP trends are promising in acute TBI stages. The change in ICP from the first 30 minutes of treatment to the final 30 minutes. n = 9..... 60
Figure 4.18 Brain water content measured using the wet-dry method at 5hrs post injury in the ipsilateral (A) and contralateral (B) hemispheres 60
Figure 4.19 Histological assessment of IBA1 demonstrated a significant reduction of IBA1 levels in the striatum post-injury and OTD treatment with the hypertonic solution compared to isotonic solution ($p<0.05$). A trending reduction was also detected in the thalamus region. 61
Figure 4.20 Histological assessment of silver stain indicated a trending reduction of neuronal damage in the striatum. 62
Figure 4.21 Histological assessment of GFAP showed no changes detected in all the regions examined. 63
Figure 4.22 Rodent MRI Results for Edema and Hemorrhage courtesy of Dr. Joseph Dwyer at WRAIR 64
Figure 5.1 Size and shape differences between human, monkey, swine, and rat brains. [57] 65
Figure 5.2 Swine pTBI-OTD CAD representation 68
Figure 5.3 Hydraulic permeability of the flat sheet membrane. 71
Figure 5.4 Hydraulic permeability of membranes prior to storage. 72
Figure 5.5 Vacuum Sealed pTBI-OTD Ready for Shipment. 72
Figure 5.6 Membrane degradation without vacuum seal to protect membrane..... 74
Figure 5.7 Degradation of Hydraulic Permeability of pTBI-OTD Membrane. 75
Figure 5.8 Helmet prototype design and connection to vest..... 76

Figure 5.9 Vest with OTD BoxPump, Battery pack, and infusion system for the 3-day study courtesy of Dr. Joseph Dwyer 77
Figure 5.10 BoxPump schematic during porcine experimenation 78
Figure 5.11 Box pump activity pie chart per hour. 79
Figure 5.12 Schematic of device efficacy experiment 81
Figure 5.13 Flux comparison of 1% and 2% agarose hydrogel at different tangential flow rates 84
Figure 5.14 Results of shear comparison for the 1% agarose hydrogel study. 85
Figure 5.15 Results of shear comparison for the 2% agarose hydrogel study. 86
Figure 5.16 No tangential flow rate for the 1% agarose hydrogel. 86
Figure 5.17 No tangential flow rate for the 2% agarose hydrogel. 87
Figure a.1 Schematic of Base v1.2 90
Figure a.2 Schematic of Bracket v1.2 90
Figure a.3 Schematic of OTD v1.2 91
Figure a.4 Schematic of v1.2 Assembly 91
Figure a.5 Schematic of Bracket v1.3 92
Figure a.6 Schematic of Base v1.3 92
Figure a.7 Schematic of Assembly v1.3 93
Figure a.8 Schematic of Base v1.4 93
Figure a.9 Schematic of Bracket v1.4 94
Figure a.10 Schematic of Assembly v1.4 94
Figure a.11 Schematic of Base v1.6 95
Figure a.12 Schematic of Bracket v1.6 95
Figure a.13 Schematic of Assembly v1.6 96
Figure a.14 Schematic of Base v1.8 96
Figure a.15 Schematic of Bracket v1.8 97
Figure a.16 Schematic of Assembly v1.8 97
Figure a.17 Schematic of Rat Harness 98
Figure b.1 Schematic of Hollow Fiber Prototype Skull Attachment 98
Figure b.2 Schematic of Hollow fiber housing Bottom v.5 99
Figure b.3 Schematic of Hollow Fiber Housing Top v.5 99

Figure b.4 Schematic of Hollow Fiber Housing Barbed Tubing Connector v.6 100
Figure b.5 Schematic of Hollow Fiber Housing Barbed Cap 100
Figure b.6 Schematic of 180 Degree Barbed Cap..... 101
Figure b.7 Schematic of Hollow Fiber Assembly..... 101
Figure c.1 Schematic of Flat Sheet Membrane Rodent Model Base 102
Figure c.2 Schematic of Flat Sheet Membrane Rodent Model Top 102
Figure c.3 Schematic of Flat Sheet Membrane Rodent Model Assembly..... 103
Figure d.1 Schematic of Impermeable Elastic Membrane for Porcine Model OTD 104
Figure d.2 Schematic of Membrane Housing for Porcine Model OTD..... 104
Figure d.3 Schematic of Porcine Model OTD Assembly 105

List of Symbols

Greek Symbols

β — Geometry-based constant
δ — Boundary layer height
$\Delta\pi$ — Osmotic pressure difference across the membrane as a function of solute concentration
ρ — Density
ΔP — Transmembrane pressure
γ — Cross-flow shear rate
μ_i — Chemical potential of species *i*
π_d — Osmotic pressure contribution due to the Donnan effect
π_p — Osmotic pressure contribution from the permeate
σ — Reflection coefficient
ψ_i — Thermodynamic potential associated with species *i*
∇ — Del (nabla) operator

Latin Symbols

A — Constant
B — e^A
c_i — Concentration of species *i*
D_{ij} — Solute diffusivity tensor component between directions *i* and *j*
E — Constant equal to the concentration of the permeate
G — Gibbs free energy
h — Height of the channel
J_{OTD} — Total flux through the membrane
J_v — Solvent volumetric flowrate per unit membrane area
k^f — Mass transfer coefficient
L — Length of the channel
L_p — Hydraulic permeability of the membrane
ln — Natural logarithm
M_p — Mass of the protein
N — Solute flux, defined as $N = (c_i \mathbf{v}_s - D_{ij} \nabla c_i)$
N_φ — Moles of all other components in the system except species *i*
N_i — Moles of component *i*
R — Ideal gas constant
R_i — Reaction rate of species *i*
S — Entropy
t — Time
T — Temperature
v_γ — Velocity in the *y* direction
V — Volume
$\bar{V}_i$ — Specific volume of species *i*

w_p — Weight of the protein
W — Lambert W function

Subscripts
b — Bulk solution
i — Refers to species i
p — Permeate
w — Membrane wall
$y = 0^-$ — Just before the membrane interface in the y direction
$y = 0^+$ — Just after the membrane interface in the y direction

Chapter 1. Introduction

1.1 Edema in the Central Nervous System

Traumatic injuries to the central nervous system can stem from a multitude of sources with different levels of severity. These injuries are costly and disabling as they disproportionately affect patients under 30 years old. The pathophysiology of any traumatic injury related to the central nervous system (CNS) consists of an initial primary injury that is usually caused by blunt force and is quickly followed by a biological secondary cascade.[1] This secondary cascade is not easily treatable and is commonly referred to as secondary injury and refers to a series of predominantly molecular events and an increasingly restricted set of aberrant biochemical pathways and products which lead to the death of surrounding healthy cells.[2] This facet of injury is characterized by hemorrhage, edema, and ischemia.[3] A cycle of ischemia, edema, elevated pressure, and ischemia then occurs exacerbating the injury for the patient. This cascade of biological processes that occur immediately after the primary injury and continues to exacerbate up to three days post injury.[4]

1.2 Role of Edema in Secondary Injury

Clinical studies have demonstrated that secondary injuries in both the brain and spinal cord result in increased internal pressure which leads to compression against bone and damages vital internal components.[5] This high internal pressure is mainly attributed to the presence of edema.[6]] There are two main causes of edema attributed to neuronal injury: cytotoxic and vasogenic. While both forms of edema are attributed to by the movement of intracellular water to the extracellular space, cytotoxic edema is caused by water movement into the intracellular compartment of neurons while vasogenic edema is

attributed to the direct disruption of the blood brain barrier (BBB) which is responsible for the accumulation of fluid into the extravascular space.[7] This unchecked accumulation into extracellular space increases cellular volume and elevates pressure and triggers a cascade of events with detrimental effects on both the brain and spinal cord. In most cases, the internal pressure created by the buildup of edema is so devastatingly high that fatality is imminent unless drastic measures are taken. While many forms of injury exist, this thesis focuses on penetrating traumatic brain injury and non-severed spinal cord injury.

1.3 Penetrating Traumatic Brain Secondary Injury

Penetrative traumatic brain injury (also known as penetrative ballistic brain injury) is defined as a subset of injuries in which a foreign body pierces the skull and dura, entering the cranial cavity. It represents 0.4 – 1.5% of all TBI cases but is the most lethal form of TBI with a patient mortality rate of 70% to 90%. [8, 9] Firearm-related injuries are the most common cause of pTBI and were responsible for 39,000 deaths in the US in 2017.[10] The projectile crushes soft brain tissue in its path and creates a permanent path of injury. Additional small missile fragments from the bone and metal of the projectile spreading from the site of injury causing further damage.[11] Post injury, ICP increase is assured due to the rigidity of the skull and edema buildup in the brain requiring surgical intervention. This high pressure results in restricted blood flow and local ischemia at the point of injury leading to vascular complications further exacerbating secondary injury.[12]

1.4 Non-Severed Spinal Cord Secondary Injury

The primary injury for SCI is characterized by the disruption of axons of nerves running through the spinal cord leading to an irreversible loss of motor and sensory function to extremities below the level of injury.[13] In the event that the spinal cord is not severed by the primary injury, the direct contusion of the spinal cord initiates an inflammatory response which leads to secondary injury. Global estimates of the annual incidence of non-fatal and non-severed SCI range from 15-40 cases per million and in the United States alone more than 1 million patients currently live with an SCI and over 12,000 new cases every year.[14] Even a less severe non-severed SCI often results in the severe morbidity and permanent disability of its victims leading to a reduced quality of life.[15]

1.5 Treatments for pTBI and Non-severed SCI

It is imperative that ICP be kept in control to improve neurological outcomes after severe injury. Hyperosmolar solutions are a common measure to lower ICP resulting from edema buildup after pTBI by creating an osmotic gradient that draws edema fluid from brain tissue into the circulatory system.[16] Osmotherapy is the medically managed treatment of cerebral edema without raising ICP. It achieves this by circulating hypertonic saline or mannitol solutions to draw fluid from tissue into the circulatory system. While these treatments reduce ICP, they are often ineffective in treating other aspects of severe pTBI and improving neurological outcomes. They also have significant disadvantages including clinical variability, temporary duration of effect, and potential systemic consequences on the cardiovascular and renal physiological systems. [17] Most importantly, these therapies are not specific and therefore ineffective in treating ballistic

wound injuries where fluid buildup is too extreme to be treated vascularly. For instances of pTBI where the injury is not surface level, decompressive craniectomy is usually necessary to alleviate intracranial pressure (ICP) and prevent brain herniation. [18, 19] A craniectomy is the most common surgical treatment for severe cerebral edema following pTBI and removes a part of the skull to allow room for the brain to swell to relieve ICP. Early cranial decompression has been shown to increase survival of pTBI resulting from blast injury in military settings. [20] While more effective than drug alternatives, there are serious risks and limitations to this treatment as it can take several months for the brain to return to a normal size leaving it open to infection by exposure. Furthermore, the brain is still vulnerable during external brain herniation and compression of the cerebral veins can become compressed leading to ischemia around the point of injury. While decompressive craniectomy is a common surgical method for severe pTBI, aimed at relieving ICP, recent findings have shown unfavorable outcomes and limited suitability for point-of-injury care.[21]

To date there are no medical device treatments that improve patient outcomes after non-severed SCI at the point of injury.[22] This injury induces high intraspinal pressure (ISP), significantly contributing to the extent of secondary injury and impeding neurological recovery.[23] For SCI, clinical studies have found that only a slight 15-20 mmHg increase in ISP is required to disrupt autoregulation.[24] This suggests that a relatively small amount of extracellular fluid buildup is necessary to restrict the spinal cord and propagate secondary damage. Even with recent understanding of the pathogenesis of SCI, treatment options remain remarkably slim. Methylprednisolone is a

corticosteroid that has been used as a treatment for SCI secondary injury. This drug is administered intravenously within eight hours of injury but there is little evidence of the drug's efficacy and impact.[25] The general protocol for treating traumatic SCI is to prevent further injury by immobilizing the spinal column which may require surgery that could further magnify secondary injury.[26] There are currently no viable treatment options for reducing edema at the point of injury for SCI. A recent study indicates that high intraspinal pressure is to blame for the lack of neurological recovery and a randomized controlled multicenter trial, DISCUS, is investigating whether bony decompression plus duroplasty improves neurological outcome when compared with just bony decompression.[27]

1.6 Osmotic Transport Device

As previously mentioned, surgical treatment in the event of pTBI is solely to reduce high ICP instead of directly treating cerebral edema. Craniectomy to prevent brain herniation will result in the brain herniating outside of the skull and cause local ischemia which will lead to further secondary injury. Therefore, a new method is required which will treat the high ICP by alleviating the secondary injury buildup. The osmotic transport device (OTD) was developed to draw edematous fluid from swollen tissue without damage to prevent ischemia, oxidative stress, cyst formation and cell death.[28] It removes edematous fluid from brain tissue in a controlled fashion, conformed to the surface of the brain, and did not harm the underlying tissue.

1.7 Previous OTD Applications

Previous research from our lab has shown the effectiveness of the OTD in reducing edema found in both TBI [29] and SCI. [4] The original OTD was developed as a

direct treatment and reversal of brain and spinal cord edema following decompressive surgery. The original work sought to fill the important gap in medical treatment at the point of injury for TBI and SCI by using direct osmotherapy to alleviate edema fluid buildup.

Our laboratory has previously examined the application of the OTD for treating edema following TBI by using a high concentration protein as the lumen solution with semi permeable hollow fibers to facilitate flux from swollen tissue in a TBI mouse model.[28] It consisted of hollow fiber semipermeable membranes embedded in a moldable hydratable material placed directly on the injured tissue. An aqueous solution of highly concentrated bovine serum albumin (BSA) flowed through the lumen of the fibers resulting in an osmotic pressure gradient that gently removed fluid from tissue through the aqueous shell and exited through the fibers. On a controlled cortical impact model with mice, it was found that brain water content was significantly higher for animals treated with an OTD than the control animals. However, studies with TBI mice treated with an OTD the brain water content was not significantly higher than the controls and brain water content of TBI animals was significantly reduced compared to that of untreated animals.[28] The initial study demonstrated a proof of concept for the reduction of cerebral edema using osmotic pressure. A second TBI study with adult mice focused on the functional recovery of neurological systems with an OTD following TBI via neurobehavior testing.[29] The neurological function of mice after TBI with an OTD was examined to determine the neuroprotective properties of the OTD. The OTD improved

functional outcome better than craniectomy alone and advocated for the therapeutic benefits of osmotherapy.[29]

The fundamental principles behind the function of the OTD and its simple mechanical design make it ideal for modification to alleviate edema in SCI. To accommodate the difference in injury, a change in the form factor of the membrane was required to ensure that the osmotic gradient could be created deep within the tissue close to the injury at the spinal column. Instead of hollow fiber membranes through an aqueous shell, a thin, flat sheet, hydrophilic membrane was used to ensure water flux toward the osmotic solution was not hindered with a membrane backing that prevented bowing of the membrane and kept it flat against the solution channel.[4] A non-severed spinal cord contusion was administered at the T8 vertebrae in rats and the SCI-OTD was surgically mounted at the POI. The OTD was applied one hour after the injury followed by three hours of operation. Water content analysis of the spinal cord showed a statistical reduction in water content in tissue following OTD treatment. Even a small reduction in water content in neurological systems can drastically reduce the pressure. Previous work showed that the reduction of edema from 73.3 ± 0.30% to 72.4 ± 0.43% can reduce vascular collapse and open the subarachnoid space.[4] This short-term study, despite only being three hours, formed the basis of this work and a study examining the full fluid buildup time frame over three days was necessary in developing the OTD for spinal cord treatment.

1.8 Scope of this work

Limitations of OTD work previously conducted for SCI was only three hours but also showed that swelling can occur for up to three days. Our goal is to develop a long-

term OTD to mitigate neurological edema following SCI. The devices have the potential to treat spinal cord edema by removing extracellular water through osmotically driven flux without damaging the sensitive tissue of the spinal cord. This treatment will help to prevent secondary damage associated with SCI such as ischemia, oxidative stress, glial scarring, cyst formation, and necrosis.

In addition, the OTD may be advantageous in providing immediate treatment for pTBI. This work describes the modifications made to the OTD and their effectiveness in treating rodent and porcine models in penetrative injuries. The goal of this thesis is to develop new OTD that can improve neurological outcomes for secondary injury relating to non-severed spinal cord injury and penetrative traumatic brain injury.

Chapter 2. Fundamental Mathematical Principles and Model of the Osmotic Transport Device

2.0 Scope of Mathematical Principles

This chapter is divided into two parts: the first focuses on the mathematical principles governing osmotic pressure, and the second explores membrane processes in a forward osmosis system, emphasizing the modeling of the OTD.

2.1 Overview of Osmotic Pressure

Osmotic pressure occurs when a semi-permeable membrane separates a solvent from a concentrated solution containing an impermeable solute. This results in a net flow of the solvent towards the concentrated solution to establish equilibrium by diluting it. In nature, this is an important phenomenon that allows cells to regulate functions such as capillary pressure, water uptake by plants, and cell size. Equilibrium pressure is defined as osmotic pressure and is directly tied to the chemical potential of each species. The OTD functions by utilizing the chemical potential difference across the semipermeable membrane in an aqueous system to generate osmotic pressure and treat excess edema injury in both TBI and SCI.

2.2 Thermodynamic Basis of Osmotic Pressure

Osmosis is defined as the spontaneous net movement of solvent molecules through a selectively permeable membrane from a region of low solute concentration to a region of high solute concentration. The term was coined by Henri Joakim Dutrochet in 1837 who discovered this phenomenon and constructed the first osmometer to prove that osmotic pressure could be generated across a membrane. [30] This process has been utilized for a variety of applications, such as water treatment, food processing, and power generation.

The chemical potential of a species in a system is defined as the change in the free energy with respect to the change in the mole number of that species. Gibbs free energy is the standard for measuring the thermodynamic potential of a system in constant temperature and pressure. The chemical potential of species i, μ_i, defined as the change in Gibbs free energy, G, for a change in the moles of component i changes, N_i, at fixed temperature, T, pressure, P, and moles of all other components, N_q, is described as

$$\mu_i = \left(\frac{\partial G}{\partial N_i}\right)_{T,P,N_q} \tag{2.1}$$

Therefore, we can describe the change in Gibbs free energy as

$$dG = -SdT + VdP + \sum_i \mu_i dN_i, \tag{2.2}$$

however, because we are assuming that the process is at constant temperature and pressure, Eqn 2.2 reduces to

$$dG = \sum_i \mu_i dN_i. \tag{2.3}$$

Now for a system with several phases, ψ_i, and at equilibrium where the change in Gibbs free energy is zero,

$$dG = dG^{\psi_1} + dG^{\psi_2} + \cdots = 0\ . \tag{2.4}$$

For a two-phase system, Eqn 2.3 and 2.4 can be combined for each phase,

$$dG = \sum_i \mu_i^{\psi_1} dN_i^{\psi_1} + \sum_i \mu_i^{\psi_2} dN_i^{\psi_2} = 0\ , \tag{2.5}$$

and, for each component, it follows that

$$\mu_i^1 dN_i^1 + \mu_i^2 dN_i^2 = 0. \tag{2.6}$$

The conservation of mass law requires that, for each component which transports from one phase to the other,

$$N_i^1 = -N_i^2, \tag{2.7}$$

at equilibrium, the chemical potential of each component must be equal in the two phases,

$$\mu_i^1 = \mu_i^2. \tag{2.8}$$

For a system consisting of two solutions separated by a semi-permeable membrane, and one solution contains a solute impermeable to the membrane, at equilibrium, the chemical potential of the diffusible species, i, must be equal. Let the chemical potential of species i in chamber 2, at pressure P, be $(\mu_i^2)_P$ and the chemical potential of species i in the solute free chamber 1, at pressure P, be $(\mu_i^1)_P$, such that

$$\left(\mu_i^2\right)_P < \left(\mu_i^1\right)_P. \tag{2.9}$$

At equilibrium with temperature and pressure constant and with the number of all diffusible species moving across the membrane then,

$$\left(\mu_i^2\right)_{P+\pi} = \left(\mu_i^1\right)_P, \tag{2.10}$$

where π is the increase in the pressure required to satisfy chemical potential equivalence of species i in the two chambers as seen in Eqn 2.10.

The chemical potential of species i at equilibrium is given as

$$\left(\mu_i^2\right)_{P+\pi} = \left(\mu_i^2\right)_P + \int_P^{P+\pi} \left(\frac{\partial \mu_i}{\partial P}\right)_T dP \tag{2.11}$$

where the chemical potential of species of species i at the initial pressure P is $(\mu_i^2)_P$. The specific volume can then be defined as

$$\overline{V_i} = \left(\frac{\partial \mu_i}{\partial P}\right)_{T,n_k}, \tag{2.12}$$

with Eqn 2.11 becoming

$$\left(\mu_i^2\right)_{P+\pi} = \left(\mu_i^2\right)_P + \int_P^{P+\pi} \overline{V_i} dP \tag{2.13}$$

and upon integration and simplification yields

$$\left(\mu_i^2\right)_{P+\pi} = \left(\mu_i^2\right)_P + \overline{V_i}\pi. \tag{2.14}$$

Now we can combine Eqns 2.10 with 2.14 to yield

$$\left(\mu_i^2\right)_P + \overline{V_i}\pi = \left(\mu_i^1\right)_P \quad , \tag{2.15}$$

which can then be rearranged to represent the osmotic pressure as the difference in chemical potential of species i in the two chambers, or

$$\pi = \frac{\left(\mu_i^1\right)_P - \left(\mu_i^2\right)_P}{\overline{V_i}}. \tag{2.16}$$

Several models have been devised to correlate the osmotic pressure of a solution at specific concentration with physical parameters. For dilute solutions, the van't Hoff equation is used to determine the molecular weight of the solute. [31] Relying on the ideal gas constant and chemical equilibrium, the van't Hoff equation is an excellent approximation of osmotic pressure at dilute concentrations. Yet, highly concentrated solutions depart from ideality and require consideration of phenomena leading to non-idealities in osmotic pressure. Numerous models in the literature have been devised to address these observations, primarily rooted in the McMillan-Mayer theory which requires fitted parameters. One such model that does not require fitted parameters is the free-solvent based model which accounts for the hydration and ion binding of the solute.[32] This model has been previously utilized for concentrated single protein solutions and binary protein solutions.

2.3 Previous Development of Forward Osmosis Membrane Processes

Previous models considered concentration polarization on both sides of the membrane for industrial applications. Because our focus is only on the medical device application and relatively short-term function, only boundary layer effects on the solute side of the membrane is examined. The most important parameters for controlling the flux of the device are hydraulic permeability, osmotic pressure gradient, and transmembrane pressure.

2.4 Modelling of Flux of the OTD and Understanding Controllability

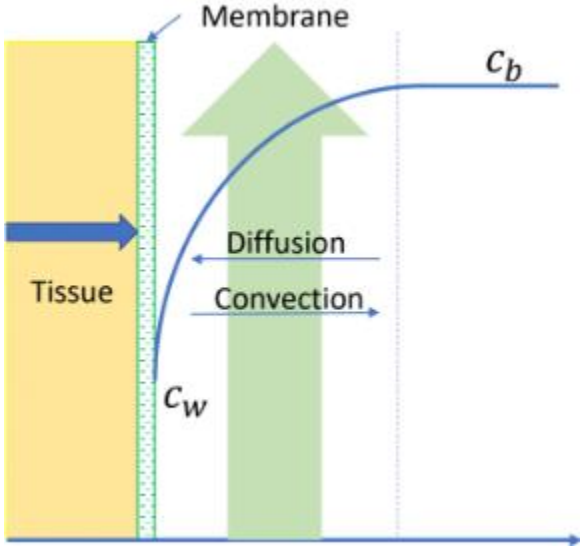

Figure 2.1 Osmotic Transport From Tissue

The flux of the OTD can be represented by Figure 2.1, which shows a one-dimensional model for the fluid being pulled through the tissue. assumes that the flux is only in the y direction thus making it one dimensional.

The differential equation that models the film theory for the OTD, using the rectangular cartesian coordinate system (RCCS), is

$$\frac{\partial c_i}{\partial t} = \nabla \cdot D_{ij} \nabla c_i + R_i. \tag{2.17}$$

Assuming steady-state and no chemical reactions with either the membrane or the draw solution we can simplify to

$$v_y \frac{dc_i}{dy} = D_{ij} \frac{d^2 c_i}{dy^2} \tag{2.18}$$

For a non-linear differential equation, we assume that the flux from the tissue is constant, and we can set our boundary condition as follows for the boundary layer.

$$y = \delta, c = c_b \tag{2.19}$$

The second boundary condition denotes the flux balance equation which is $N_{y=0^-} = N_{y=0^+}$ and assuming a dilute solution, where N = $\left(c_i \vec{v}_s - D_{ij} \nabla c_i\right)$ we can modify this for one dimensional transport

$$y = 0, \left(c_p v_y\right)_{y=0^-} = \left(c_w v_y - D_{ij} \frac{d}{dy} c_w\right)_{y=0^+} \tag{2.20}$$

Returning to Equation 2.18 governing the one-dimensional diffusion across the membrane where the dependent variable is not in the equation. P-substitution can then be used for the partial differential equation, P = $\frac{dc_i}{dy}$, and solving the differential equations yields

$$v_y P = D_{ij} \frac{dP}{dy} \tag{2.21}$$

$$\int \frac{1}{P} dP = \int \frac{v_y}{D_{ij}} dy \tag{2.22}$$

$$lnP = \frac{v_y}{D_{ij}} y + A \tag{2.23}$$

$$P = e^{\frac{v_y}{D_{ij}} y + A} = e^{\frac{v_y}{D_{ij}} y} e^A = B e^{\frac{v_y}{D_{ij}} y} \tag{2.24}$$

The constant e^A is simplified to the constant B. With the differential equation simplified, $\frac{dc_i}{dy}$ can be resubstituted

$$\frac{dc_i}{dy} = Be^{\frac{v_y}{D_{ij}}y} \tag{2.25}$$

$$c_i = B\frac{D_{ij}}{v_y}e^{\frac{v_y}{D_{ij}}y} + E \tag{2.26}$$

$$\frac{d}{dy}c_i = Be^{\frac{v_y}{D_{ij}}y} \tag{2.27}$$

The concentration gradient can now be substituted into the flux balance boundary condition at y = 0

$$c_p v_y = (B\frac{D_{ij}}{v_y}e^{\frac{v_y}{D_{ij}}y} + E)v_y - D_{ij}(Be^{\frac{v_y}{D_{ij}}y}) \tag{2.28}$$

and simplified into

$$c_p v_y = \left(B\frac{D_{ij}}{v_y} + E\right)v_y - D_{ij}(B) \rightarrow E = c_p. \tag{2.29}$$

Therefore, we can conclude that at the initial boundary condition at the membrane y=0, $E = c_p$.

For the second boundary condition at $y = \delta$ where the film boundary ends and the concentration of the draw solution represents the bulk, $c = c_b$. Substituting this boundary condition and using the solution derived that $c_p = E$ we derive the bulk concentration as

$$c_b = B\frac{D_{ij}}{v_y}e^{\frac{v_y}{D_{ij}}\delta} + c_w. \tag{2.30}$$

With this equation we can then solve for constant B

$$B = (c_b - c_p)\frac{v_y}{D_{ij}}e^{-\frac{v_y}{D_{ij}}\delta}. \tag{2.31}$$

Both constants are solved and can be resubstituted into Eqn 2.25 which yields

$$c_i = (c_b - c_p)e^{-\frac{v_y}{D_{ij}}(\delta - y)} + c_p \tag{2.32}$$

Now it is important to find out how the solvent flux relates to the concentration at the wall, c_w. We can accomplish this by referring to the concentration of the draw solution at the boundary, y = 0, and solving the concentration at the wall, c_w, by defining

$$k_f \equiv \frac{D_{ij}}{\delta}, \tag{2.33}$$

with this constant we can solve equation 2.30 for c_w,

$$\frac{c_w - c_p}{c_b - c_p} = e^{-\frac{v_y}{k_f}} \tag{2.34}$$

$$-v_y = k_f ln\left(\frac{c_w - c_p}{c_b - c_p}\right) \tag{2.35}$$

$$v_y = k_f ln\left(\frac{c_b - c_p}{c_w - c_p}\right) \tag{2.36}$$

Now that the relationship for one dimensional flux through a membrane has been determined it must now be related back to the one-dimensional model OTD shown in figure 2.1 where $v_y = J_{OTD}$ representing the total flux through the membrane. Assuming that $c_p = 0$,

$$J_{\mathrm{OTD}} = k_f ln\left(\frac{c_b}{c_w}\right) \tag{2.36}$$

describing the inverse relationship between the concentration at the wall, c_w, and the flux from tissue, J_{OTD}.

Now we can pair our model for flux from tissue with the OTD with the Kedem-Katchalsky equation for permeate flux,

$$J_v = L_p(\Delta P - \sigma\Delta\pi), \tag{2.37}$$

where ΔP is the transmembrane pressure, J_v is solvent volumetric flowrate per membrane area, L_p is the hydraulic permeability of the membrane, σ is the reflection coefficient, and $\Delta\pi$ is the osmotic pressure difference across the membrane as a function of concentration across the membrane.[33] For the OTD model this equation can be approximated to

$$J_{OTD} = L_p \sigma \pi(c_w) \tag{2.38}$$

assuming that the membrane is completely reflective then σ = 1 and $c_p = 0$. Vilker *et al* summarizes the osmotic pressure contribution from the permeate and the Donnan effect,

$$\pi = \pi_p + \pi_d, \tag{2.39}$$

which can be ignored as the Donnan effect is negligible for ion balanced solutions.[34] Their work summarizes the osmotic pressure contribution of the permeate solution as

$$\pi_p = \frac{RT}{M_p}\left(w_p + A_1 w_p^2 + A_2 w_p^3\right) \tag{2.40}$$

With R being the ideal gas constant, M_p is the mass of the protein and w_p being the weight of the protein. The model for the OTD can then be expressed as

$$J_{OTD} = L_p(\pi_p) = L_p(B_1 c_w + B_2 {c_w}^2 + B_3 {c_w}^3) \tag{2.41}$$

because of the concentration at the wall boundary condition, π_p, and modelling for the osmotic pressure with with the $\frac{RT}{M}$ terms being absorbed into the A constants to form constant B. This equation can be regressed with

$$J_{OTD} = k_f \ln\left(\frac{c_b}{c_w}\right). \tag{2.42}$$

The mass transfer coefficient k_f can then be evaluated using the Graetz-Lévêque equation,

$$k_f = \beta \left(\gamma \frac{D_{ij}^2}{L_c} \right)^{1/3}, \tag{2.43}$$

which defines the mass transfer coefficient in terms of channel length and shear rate for flow through a channel where β is a geometry-based constant, γ represents the crossflow shear rate, L_c is the length of the channel, and D_{ij} is the solute diffusivity. For our OTD application we can approximate the length of the channel as less than $0.1\gamma h^3/D_{ij}$.

Now if we assume that the concentration at the wall is substantially reduced so that it can be modelled as an ideal solution where we can now solve for c_w,

$$J_{OTD} = L_p(B_1 c_w) \rightarrow c_w = \frac{J_{OTD}}{L_p B_1}. \tag{2.44}$$

With c_w put in terms of flux, we solve for the flux of the OTD with W is the Lambert W function.

$$J_{\mathrm{OTD}} = k_f ln \left(\frac{L_p B_1 c_b}{J_{OTD}} \right) \rightarrow J_{OTD} = k_f W\left(L_p B_1 c_b \right) \tag{2.45}$$

Our lab has used these osmotic principles to design different variations of the osmotic transport device, and each variant contains these principles inherent to its design. A highly concentrated protein solute creates osmotic pressure while an aqueous gel with similar chemical properties as the neurological system is in contact with the physiological system. They are separated by a semi-permeable membrane that completely rejects the solute while allowing water to pass through unimpeded. The aqueous gel solution eliminates the possibility of a liquid-air interface which would impede flux while keeping the membrane wetted. The shell of the OTD consists of an inlet and outlet which flushes the solute solution allowing for a new osmotic solution to flush the chamber and maintain osmotic pressure. All OTD variations contain these fundamental principles pairing the

Kedem-Katchalsky model for permeate flux with physiological principles to gently remove water from swollen tissue. My work on advancing this body of knowledge will be examined in upcoming chapters.

Chapter 3. Application of OTD for Long-Term Spinal Cord Injury

3.1 Previous Work

Previous studies showed potential for the development of the first OTD indicated the potential for the device to treat other types of neurological edema swelling such as spinal cord swelling. Several modifications were made to the OTD to address design limitations relative to the treatment of the spinal cord injury. These modifications to the OTD for use in treating spinal cord injury (SCI-OTD) included a change in form factor to the membrane. The original OTD utilized hollow fibers with high surface area which were implanted in a moldable hydratable shell which conformed to the shape of the injury. The change in the form of injury from an external to an internal injury meant that the moldable hydratable surface could not be implanted on the surface of the spinal cord injury. Previous iterations of the OTD were fabricated using direct metal laser sintering of titanium alloy (Ti-6Al-4V) which is widely used as hard tissue replacements in artificial bones, joints, and dental implants due to its nonreactive nature. The original design was intended for anesthetized animals and did not account for the mobility of animals for long term osmotherapy. OTD efficacy is dependent on the osmotic gradient created via the semi permeable membrane. The change in injury meant that the hollow fiber membranes could not be used in the same manner for SCI. Therefore, a flat sheet membrane with a molecular weight cutoff and non-reactive chemical composition was deemed suitable.[4]

The reality of an implantable device requires that the membrane conforms to the injured area to maximize flux by ensuring contact between the injured site and the membrane as well as keeping the membrane hydrated. An agar-based hydrogel was

placed in contact with the membrane and the tissue allowing for water to travel from the tissue to the SCI-OTD which accounted for variability in animal and injury size. *In-vivo* testing of the SCI-OTD for 3 hours determined the effect on the water content of an injured spinal cord showed a greater than 1% reduction in water content in the tissue, which was determined to be effective in improving vasculature, but further testing was needed over longer periods of time to determine the viability of this treatment option for SCI.[4]

3.2 Scope of this work

The 3-hour treatment with the previous iteration of the SCI-OTD was found to have significantly reduced spinal cord edema compared to the injured controls.[4] To show device efficacy, it must maintain contact over an extended period of 3 days while implanted within the animal.

3.3 Modifications for Long Term Studies

The chamber design is designed in a CAD program (Dassault Systemes, Veliz-Villacoublay, France) and then manufactured with a Form 3B printer (Formlabs inc, Somerville, MA) using SLA 3D printing technology. The current iteration is fabricated with Biomed Clear Resin: a medical-grade material designed for rigid, non-brittle, biocompatible parts that require long-term skin and mucosal membrane contact. It is certified as USP Class VI which is suitable for applications that require wear resistance and low water absorption over time.[31] This material is also advantageous as it is permeable to MRI imaging. The SCI-OTD maintains an osmotic gradient with a flat semi-permeable membrane (10 kDa NADIR® PM UP010) allowing the osmotic gradient to draw fluid from the POI. Epoxy (Masterbond EP42HT-2 ND-2Med Black) is used

around the edges of the membrane to seal the membrane to the device. The finished device is left to cure for 3 days in a press to ensure glue contact and drying. The updated device maintained the same form factor but slightly modified the overall size and footprint of the device for implantation.

3.3.1 CAD Design and Iterations

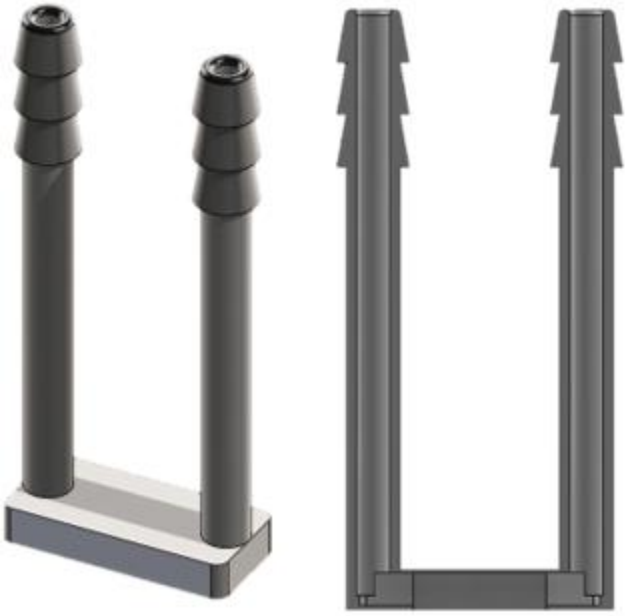

Figure 3.1 CAD model of SCI-OTD with tube fittings designed to extend past the skin and outside the animal

It was determined early on that the previous design of the SCI-OTD had a large footprint and would not be suitable for long-term study. Therefore, a new design was required to reduce torsional strain and keep the device in contact with the spinal cord over the length of the study. Several fitting surgeries were conducted where prototypes were tested for fit and footprint over the spinal cord injury site. These iterations facilitate surgical concerns while improving device function. The membrane was attached to an inflow-outflow resin compartment which would facilitate the tangential flow of the lumen solution at the membrane. The solution would then flow out via the outflow tube

to the waste container. The advantages of the device are its simplicity in function, rapid fabrication, and durability.

Previously, the SCI-OTD was placed over the injury site post laminectomy with a bracket to ensure that it would maintain contact. This bracket was then secured with screws at the anterior and posterior thoracic vertebrae to the injury. After successful implantation of the device, this system was then sutured and monitored over a 3-hour study. While simple and efficient in application, this system was unable to provide lateral stability to the animal post-surgery and was unable to maintain contact in long term studies. In order to provide long term therapy to the spinal cord at the point of injury, the system was modified to ensure that the SCI-OTD maintained contact with the point of injury on the spinal cord as shown in figure 3.2. The SCI-OTD was updated to have a smaller membrane footprint to reduce the amount of surgery required to affix the device. The inflow and outflow barbed connectors were lengthened to allow easy access to the tubing carrying the lumen solution post-surgery.

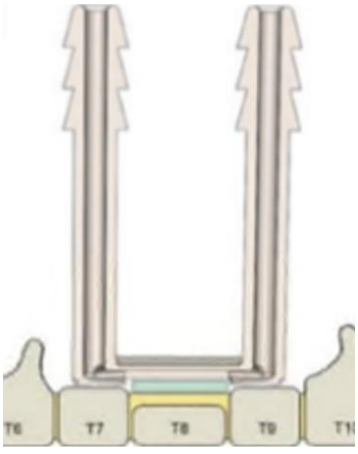

Figure 3.2 A cross-section view of the original version of the SCI-OTD on the T8 vertebrae of the spinal cord. The device was sealed onto the spinal cord with silicone.

The bracket secured the SCI-OTD along the length of the spine but did not secure the device against the lateral twisting and turning of the animal. This torsional strain was expected to increase as the animal recovers from the injury so a bracket was designed which would fit over the membrane chamber and into the base pieces, as shown in figure 3.3. This restricted lateral device strain by adding base pieces that would keep the device in place during treatment. Inspiration was taken from a mouse model that utilized spinal cord clamps to affix an optical window to the spinal cord for several days.[35] However, test surgeries revealed that the bracket in this original design was too large and fit tests of the rodent subject were unsuccessful due to the lack of space around the spinal cord to affix the base pieces.

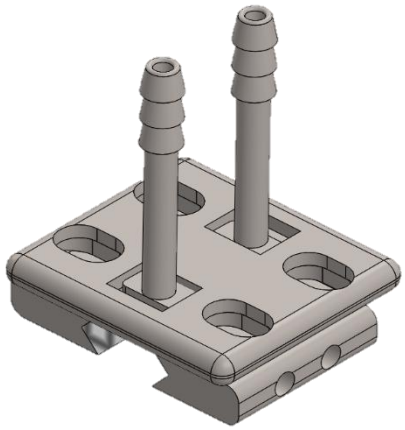

Figure 3.3 Original assembly for the first iteration of the SCI-OTD.

Surgical testing revealed that there was no longer any need for a second bracket and that the system could rely on a single bracket to maintain contact with the dura. This updated bracket piece, as shown in figure 3.4, was secured along the dura and sealed the membrane from any proximal or distal interference.

Figure 3.4 Bracket for stabilizing the OTD on the spinal cord

Surgical testing showed that the base pieces required a stabilization anchor which would ensure that the bracket would secure to the spinal cord. The base pieces had their depth adjusted and angle around the ribcage fine-tuned for the diameter of a rat spinal cord as shown in figure 3.5. Further iterations of the device implemented hooks that penetrated around the spinal cord and rested on the ribcage. These hooks were designed to fit between the ribcage and act as an anchor for the device after placement.

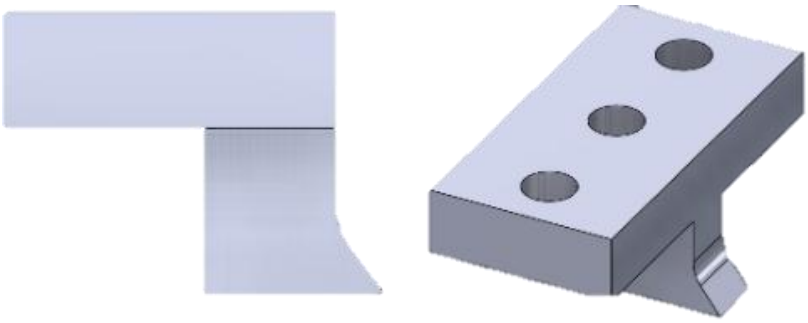

Figure 3.5 Base pieces that were designed to straddle the SCI-OTD from both sides and restrict the lateral movement of the device relative to the spinal cord.

An epoxy trap was designed in order to better grip on to the membrane. It was finely tuned to fit around the chamber to hold the membrane tightly and reduce any bowing of the membrane due to the velocity of the lumen solution as shown in figure 3.6.

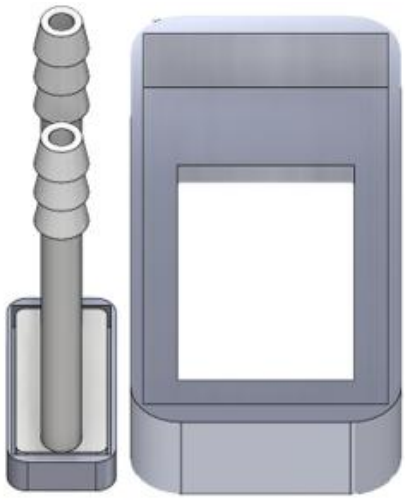

Figure 3.6 Epoxy trap for SCI-OTD to eliminate bowing of membrane during study

The final version of the SCI-OTD housing secured the membrane against the spinal cord while restricting all lateral and proximal motion. The membrane was secured via an epoxy trap that sealed the membrane against the OTD housing while a bracket provided stability onto the spinal cord itself. The membrane housing tube fittings were long enough to penetrate through the skin and connect to the overall system. This bracket was secured via metric M1.2 screws onto base pieces which penetrated in between the ribs and secured the OTD laterally. The full build of the device fits securely between the T7 and T9 vertebrae with the SCI-OTD membrane centered on the T8 vertebrae as shown in figures 3.7 and 3.8.

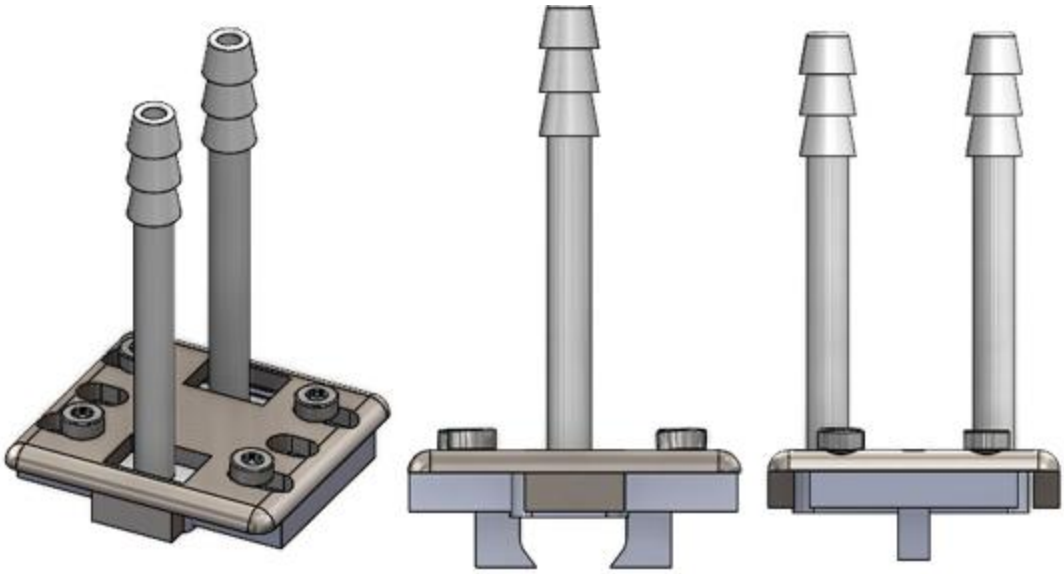

Figure 3.7 Final SCI-OTD with housing and bracket in place.

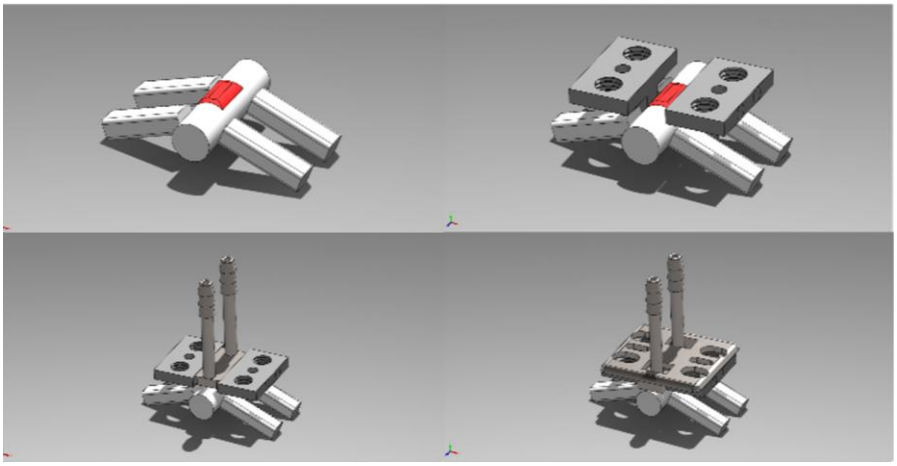

Figure 3.8 Schematic representation of the current iteration SCI-OTD in the different phases of placement secured around the spinal cord with screws.

3.3.2 Wheelchair and Swivel

Initial understanding of animal movement post injury indicated high torsional strain on the device and required a restraint that would keep the animal comfortable while restricting it to a 2D plane of motion. A wheelchair was designed and fabricated that would allow the animal to comfortably move to and from food and water sources while

keeping the OTD in place for the length of the study. This wheelchair consisted of a flat plate for the injured portion with two wheels with an independent axis. Due to the injury immobilizing hind limb movement, this allows the animal freedom of movement via front limbs while recovering from the injury and restricting the torsional movement which would keep the SCI-OTD in place. This attachment was not utilized because appropriate approval was not secured prior to the SCI-OTD study.

The previous study included an hour post injury time before the start of the OTD which made the total time length 4 hours with the animal under anesthesia for the majority of the study. A longer 3-day study introduces new factors to consider in terms of maintaining contact with the injured area. Over the span of the long-term study, the animal will be lucid and perform necessary daily functions in order to survive such as eating and drinking along with other movements such as twisting and turning. In order to achieve this, modifications were made to the SCI-OTD which include a vertebral mount situated around the SCI with a bracket to ensure constant contact.

Figure 3.9 Wheelchair attachment for rat post-surgery with OTD active.

Bases affixed along the axis of the spinal cord with hooks wrapping around the spinal cord create a stable frame around the injury site. The SCI-OTD is then placed over the injury site and bracketed in place with screws onto the base pieces. Furthermore, to prevent twisting of the tubing, a 'vest' support, which allows the tubing to be kept tangle free above the rat, was affixed to a swivel above the cage via a spring. The spring was a P95 spring from Instech labs (Instech Laboratories Inc, Plymouth, PA) and allowed the free motion of the rat without the inlet and outlet tubing from tangling together. This vest was fabricated with elastic resin which was created by the same SLA manufacturing process as the rest of the devices. This design benefits from a bracket which affixes the SCI-OTD laterally. It is expected that future translation of this device to human trials would not require invasive restraints of the OTD onto the subject.

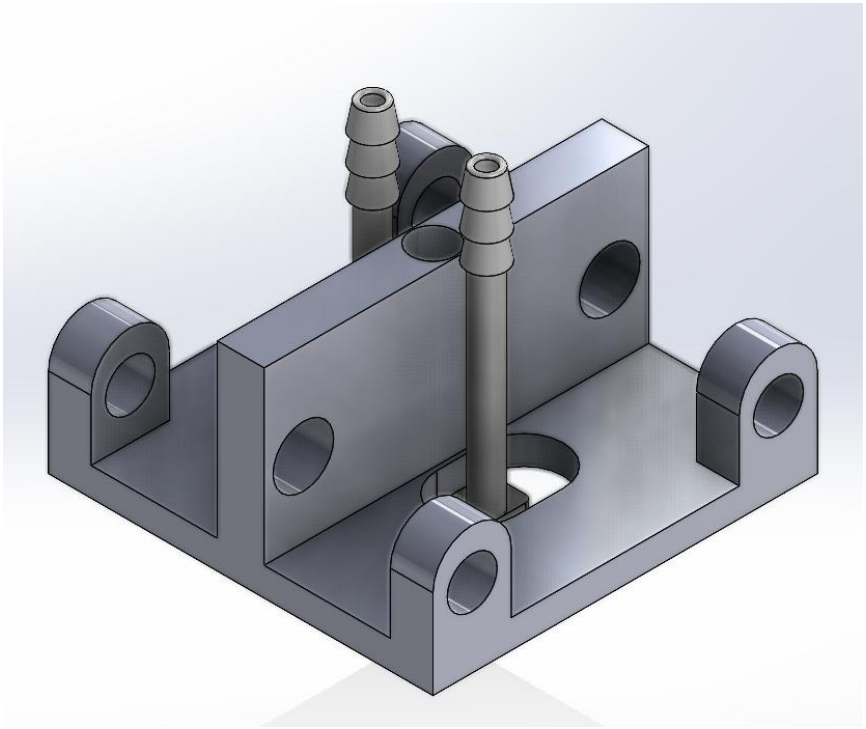

Figure 3.10 Vest with OTD attached

3.4 Experimental Methodology

The duration of the edema progression following severe SCI lasts for days. Therefore, the device must continuously ameliorate edema at the POI the entire time to prevent edema progression. Post-surgery, animals will move and shift in position and cause the SCI-OTD to potentially shift and lose contact with the POI. To prevent this, the device is designed to fit under the animal's tissue and seals the device in location to the surrounding issue and prevents the surgical site from exposure to the environment. The SCI-OTD mounting design addresses potential shifts in SCI-OTD and ensures that it remains firmly in place. The device contact at the POI is also addressed by 0.3% agar hydrogel solution which conforms to the uneven tissue surface and allows fluid flux from the edema into the SCI-OTD. The hydrogel was placed over the injury site to ensure

contact between the OTD and the POI. This concentration was chosen due to the water content level not being high enough to worsen the edema in the spinal cord but was still hydrated enough to facilitate osmotherapy.

The osmotic gradient that governed the osmotherapy was established by artificial cerebrospinal fluid (aCSF) containing 350 g/L BSA circulating through the device beginning 1 hour post injury. An IV bag suspended 11 inches over the animal determined the head pressure. The device was active for 3 days at a constant flow rate (1 drop per 10 seconds) with the IV bag being monitored and refilled at intervals to maintain head pressure. A custom vest will restrain the rat and prevent the SCI-OTD tubing from entanglement via a specialized swivel mount (Single-Axis Counter-Balance Swivel Mounts, CM375BS, Instech Laboratories Inc, Plymouth, PA). The animal was monitored every 4 hours with the flow rate adjustment. The setup for this experiment is shown below.

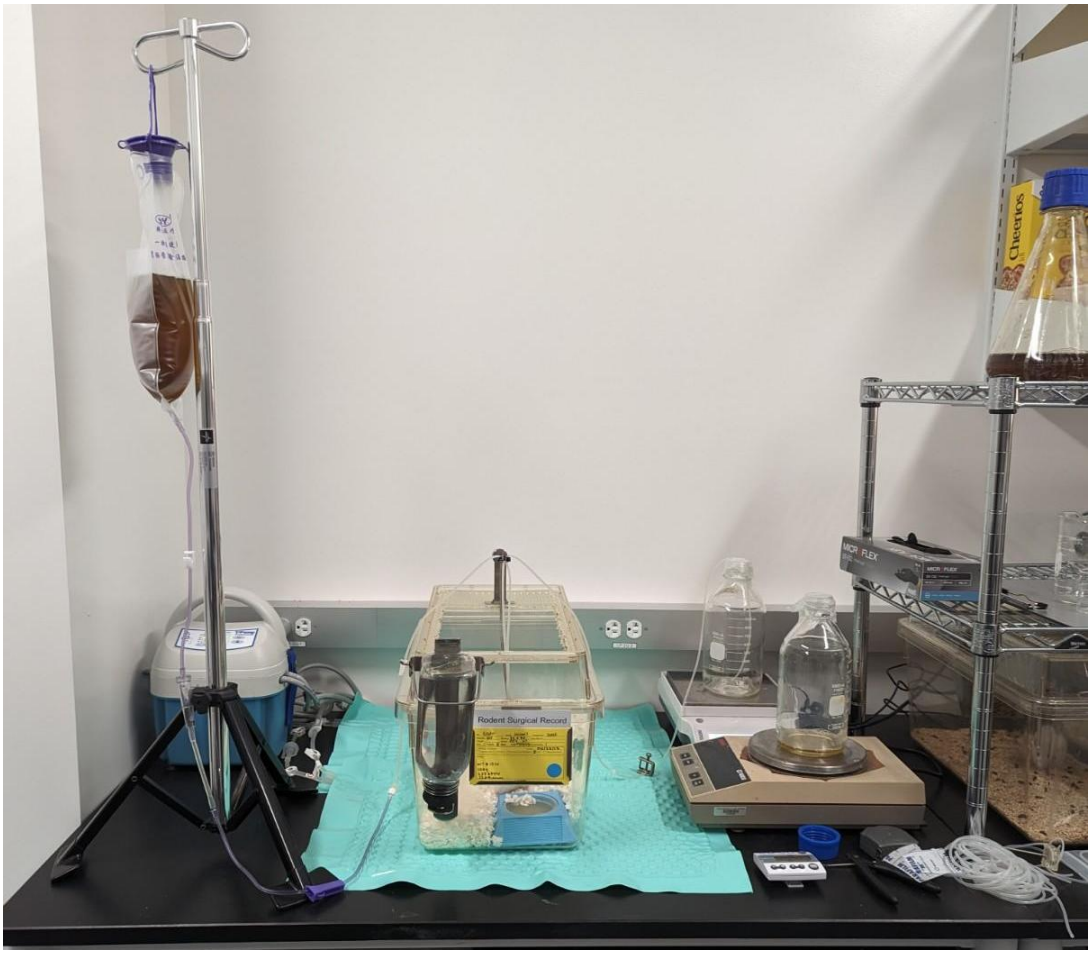

Figure 3.11 The experimental setup for the 3-day experiment. The containers on separate top loading balances were used to measure the evaporation in the room with a control container on a separate balance with a small amount of BSA.

SCI experiments began with a Sprague Dawley female rat, between 8-10 weeks old and 300 to 350 grams, being anesthetized (ketamine/xylazine mixture (80mg/kg)) before a midline incision is made along the spine. The muscles are then separated to expose the bone before a T8 laminectomy is performed. After the spinal cord has been exposed, a 250 kilodyne contusion is performed (Infinite Horizons Impactor, Precision Systems and Instrumentation, LLC, Fairfax Station, VA) and the T7 and T9 dorsal processes are removed and flattened. The tissue between the ribs at this point are then removed and the base pieces are inserted between the bone. The OTD is then placed on

top of the injury site affixed to the base with screws and the muscles are sutured together before the skin is stapled and sutured around the device. Following site closure and 1-hour post injury, the device is connected to 350 g L BSA solution in aCSF at pH 7.4 and an 11-inch head height flow rate. Over the course of the experiment the height of the bag was monitored and refilled if necessary to maintain head pressure. The drip rate was controlled via screw clamps at the end point. At the conclusion of treatment, the protein solution is removed from the device, if applicable, and the animal is euthanized by Fatal Plus™ and cardiac puncture. After expiration, a 5 mm segment of the spinal cord tissue is removed at the epicenter of the contusion site. The tissue is weighed before and after processed (at 85°C for 48 h) to determine tissue water content.

Figure 3.12 Animal test subject over 3 days of study.

The results of the study are summarized in Table 3.1. Three sets of rat cohorts of varying size were conducted: laminectomy only, SCI, and SCI+OTD. Due to difficulties in creating the injury and administering the treatment only two animals out of the proposed 5 were treated in the key SCI+OTD group. No histology, neurological, or

qualitative data was collected to assess the condition of rat post-treatment. However, the following observations were made on each day at promptly 8 am each morning. Immediately after surgery the hind limbs and tail were paralyzed and the rat was able to crawl around on its front limbs to access food and water. On the second day, the harness remained attached and intact with the swivel accommodating animal movement and needs hind limb and tail twitching was observed. On the final day, rat movement and stretching is observed but the device remains sealed due to the harness with minor hind limb motor control being observed.

Laminectomy 3 days post injury						
Animal #	1	2	3	4	5	
Epicenter	71.89	67.41	70.12	67.71	69.93	
Spinal Cord Injury 3 days post injury						
Animal #	6	7	8	9	10	11
Epicenter	77.06	77.46	77.25	76.98	75.30	78.41
Spinal Cord Injury with OTD 3 days post injury with treatment						
Animal #	12	13				
Epicenter	75.72	79.23				

Table 3.1 Raw Data of the percent water content of the spinal cord for all 3 rat cohorts encompassing the 3-day study.

The percent water content of the spinal cord as shown in Table 3.2 was statistically analyzed and compared to the previous work conducted by our lab as shown in Table 3.3. The percent water content of the spinal cord was compared to the water content of the laminectomy and showed that the SCI without OTD treatment had lower error when compared to the control and the treatment group. The dataset of the treatment group encompassed the injury only dataset at both extremes leading to the observed high standard deviation. Despite the small dataset, the mean water content is much higher when compared to the previous study conducted by Hale *et al*. [4]

Treatment Group	Sample Size	Mean (%)	Standard Error
Laminectomy 3 days post injury	5	69.41 ± 1.86	0.83
SCI 3 days post injury	6	77.08 ± 1.01	0.41
SCI + OTD 3 days post injury with treatment	2	77.48 ± 2.48	1.76

Table 3.2 Effects of the OTD treatment compared to Laminectomy and SCI data. Percent (%) water content calculated Laminectomy only, SCI, and SCI + OTD rats following 3 days post injury.

Treatment Group	Sample Size	Mean (%)	Standard Error
SCI + Hydrogel	5	73.26 ± 0.19	0.09
SCI + OTD	5	72.42 ± 0.43	0.19
SCI	5	73.34 ± 0.30	0.13

Table 3.3 Previous dataset from Hale et al [4] showcasing the effects of OTD treatment percent (%) water content after severe SCI at T8. Percent (%) water content calculated SCI only, SCI + hydrogel, and SCI + OTD rats following 3 hours of treatment.

It is worth discussing that the mean water content for the treatment group with a laminectomy 3 days post injury shows a mean average percent water content that can be

considered baseline for the mean water content of an uninjured spinal cord 3 days post-surgery. Therefore, it can be considered the normal water content of a rat spinal cord prior to any injury assuming that the extravasation of bone does not injure the nervous tissue or cause inflammation within the spinal cord 3 days post-surgery. This baseline can then be compared to the previous SCI 3 hours post injury and SCI 3 days post injury. The mean water content for the group 3 hours post injury in table 3 is significantly lower than the group 3 days post injury in table 2. This supports the conclusions asserted by Hale *et al* that the injury progressed post injury and peaked at 28 days post injury without treatment. [4] The high variability of both the standard deviation and standard error in Table 2 suggests that a factor change from the previous study 3-hour study to the 3-day study was the cause of such high deviation. With the limited dataset it could not be determined what the cause of this variability was.

3.6 Future work

This work shows that an implantation of a device that directly interacts with the spinal cord post impact does not injure the animal further than the SCI. This is significant as it is the first implantation of SLA manufactured biocompatible material in an animal model. Future work would refine the study to reduce error and include alternative imaging methods such as focused ultrasound (fUS) to observe the change in vasculature within the spinal cord. The hydrogel can also be improved upon by adding neuroprotective drugs which can reduce inflammation within the system while the SCI-OTD is implanted. Histological and neurological analysis may also illuminate the efficacy. Although the evaluation of spinal percent water content is important when

examining the effectiveness of the SCI-OTD, it is necessary to pair histological data with neurological analysis that shows improvement over the sham animals.

Chapter 4. Osmotic Transport Device for Penetrating Traumatic Brain Injury in Rodents

4.0 Scope of Work

Traumatic Brain Injury (TBI) is the leading cause of morbidity and mortality in individuals under 45 worldwide, claiming over 50,000 lives annually in the United States. According to the CDC, TBI accounts for more casualties in the Iraq and Afghanistan conflicts than any other recent U.S. wars.[36, 37] One of the critical complications following TBI is a delayed increase in intracranial pressure (ICP), driven by cerebral edema—an accumulation of excess brain water content that results in increased brain volume. Approximately 10% of TBI patients develop rapid tissue swelling, qualifying them for decompressive craniectomy (DC), which involves removing a section of the skull to alleviate pressure, prevent brain herniation, and create space for the swollen brain tissue to expand. It is considered a last-resort surgical intervention. Despite advances in surgical interventions like DC, there are no current therapies that directly target the biochemical mechanisms driving cerebral edema. Cerebral edema in severe pTBI is multifaceted making it difficult to treat effectively. Currently, therapeutic options for managing ICP caused by cerebral edema remain limited. To address this gap, a novel application of the osmotic transport device (OTD) was developed. This innovative technology utilizes osmotic principles to enhance fluid transport in cerebral tissue, effectively reducing swelling and mitigating the risk of secondary injury. It is the only POI device for treating cerebral edema.

Osmolar therapy, using intravenous mannitol or hypertonic saline, is the primary treatment for cerebral edema, leveraging osmotic gradients to draw excess water from

swollen brain tissue into the bloodstream. These therapies are aimed at osmotically removing water from edematous brain tissue via the bloodstream. While effective at acutely reducing intracranial pressure (ICP), these therapies are limited by their transient effects and systemic side effects, particularly on cardiovascular and renal functions.[38, 39] At maximum doses, these therapies can fail to treat cerebral edema and may, in some cases, exacerbate it.[40-43] Decompressive craniectomy, often used for severe edema, primarily reduces ICP and prevents transtentorial herniation, rather than directly treating cerebral edema. Following craniectomy, external brain herniation can lead to venous compression, ischemia, and further secondary damage. Recent findings from the DECRA trial indicate no significant improvement in outcomes following decompressive craniectomy for diffuse TBI.[44] This suggests that a more direct POI intervention is necessary to effectively reduce and combat cerebral edema following severe TBI.

The goal of this work was to develop a device that could enhance the decompressive craniectomy procedure currently widely used for penetrating injury and evaluate the device over a 3-day study for both a rat and pig model.

4.1 Penetrating Traumatic Brain Injury

A retrospective study of 1,255 moderate-severe TBI patients within the Joint Theater Trauma Registry, revealed that 774 injuries were penetrating by nature with the majority (94.3%) occurring in battle settings.[45] Notably, 96.8% of all pTBI injuries were classified as survivable. pTBI are associated with the worst outcomes and highest death rates of any form of TBI and predominantly affect younger adults with no therapies outside of surgery available.[46] The acute onset and progression of cerebral edema following injury makes the time course for cerebral damage imminent without

intervention. Consequently, managing cerebral edema and intracranial pressure (ICP) is a critical priority in combat casualty care, given their strong correlation with morbidity and mortality.[47]This gap in treatment ultimately led to the refined application that the original OTD was intended to treat.

Despite the importance of early intervention, point-of-injury (POI) therapeutic strategies for these patients remain severely limited. This treatment gap directly informed the refined application of the original osmotic transport device (OTD), which was developed for pTBI patients undergoing decompressive craniectomy (DC). This updated device was classified as the pTBI-OTD and was designed to: 1) control cerebral edema and 2) stimulate effective convective flux across tissue at risk of imminent damage.

4.2 pTBI Rat Model

Previous studies at the Walter Reed Army Institute of Research (WRAIR) developed and extensively characterized a rat model of pTBI designed to replicate the injury sequelae of ballistic impact. A 5mm craniotomy was performed on the rodent subject and a specialized probe was inserted 10mm into the rodent brain at which point a water pressure pulse rapidly expanded an elastic balloon at the tip of the probe thereby producing a temporary cavity. The balloon would inflate and deflate in less than 40 milliseconds, leaving a significant brain injury within the cranium. This model depicted the neuropathologic consequences of a survivable pTBI injury in humans with a high degree of accuracy.[48] Furthermore, the time course of the edema was verified via MRI as shown in Figure 4.1.

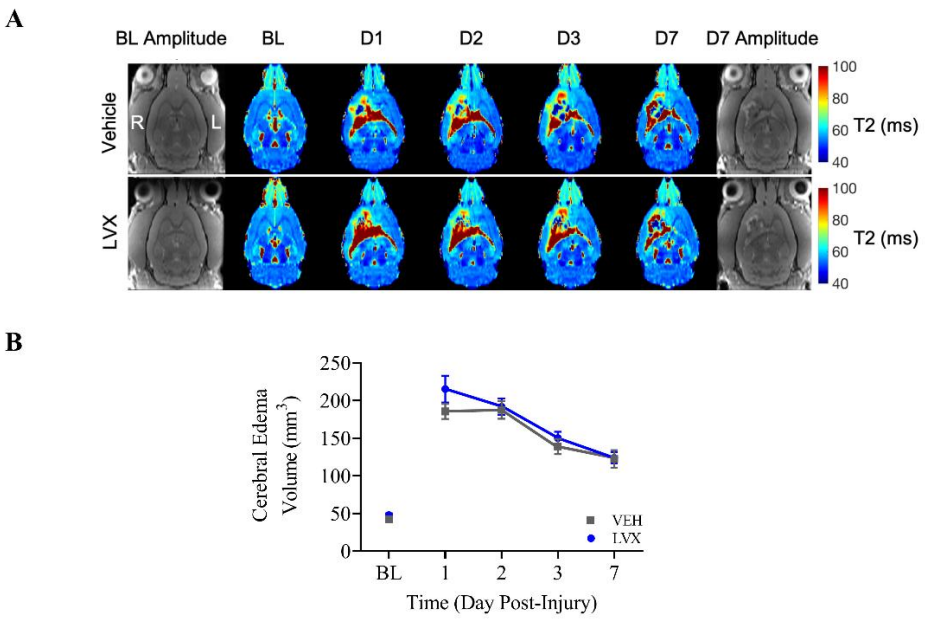

Figure 4.1 A. MRI images showing 7-day Edema progression for a pTBI rat model. B. Cerebral Edema volume progression from baseline value over 7 days. Courtesy of Dr. Zach Bailey

Other studies evaluated the injury severity was like humans in terms of BBB permeability, brain edema progression, and neuro functional impairment that was clinically relevant for studying potentially therapeutic devices.[49-52] This model proved to be an excellent platform for the testing and development of the penetrating traumatic injury osmotic transport device (pTBI-OTD) which would seek to draw edematous fluid from the cranium using osmotic pressure. Craniotomy surgery alone is usually sufficient to reduce ICP to manageable levels. The pTBI-OTD was designed to address the high concentration of edematous fluid within cells thereby reducing the cascade of secondary injury and improving long term neurological outcomes.

4.3 pTBI-OTD Development

The original OTD consisted of a hollow fiber semi-permeable membrane system embedded in a moldable, soft hydrogel which was placed directly over the injured tissue.

The hydratable material conformed to the injury site to ensure contact between the hollow fibers and tissue was maintained. Due to the nature of injury pertaining to the brain and the irregularity of the surface, hollow fibers were again examined for their viability in a penetrating injury. These design choices were limited by the mouse model used to test the device. For larger animal models, such as rats and pigs, more fluid removal would be required because of the larger brain surface area.

4.3.1 Prototype Hollow Fiber Bundle

Hollow fibers are semi-permeable membrane typically used for a wide range of applications such as industrial separations, water filtrations, and dialysis. Due to their flexibility, lightweight, and ability to be packed into large bundles they were selected for the initial pTBI-OTD development. The original version of the OTD had these hollow fibers extracted from the modules and packed into small tube fittings which would then have the protein solution run through the hollow fibers. These hollow fibers increase the surface area of the device with a controlled flowrate. The restriction of surface area on the rat cranium required a new device which would draw a higher amount of fluid from the skull, reduce ICP, and show reduced extracellular fluid via MRI.

A proof-of-concept prototype system was devised using a dialysis hollow fiber bundle Revaclear 300 (Baxter International, Deerfield, IL). The Revaclear 300 shown in Figure 4.2 was developed as a part of a series of dialyzers designed to provide high flux with their proprietary hollow fiber membrane that increased permeability while resisting diffusion. These modules are typically used for dialysis and renal care for those suffering from acute kidney injury to filter the blood of the patient. The membrane pore size (minimum weight cut off) was 15kDa and designed to reject albumin and allowed the

system to build an osmotic pressure gradient throughout the hollow fiber bundle with a hydraulic permeability of 7.14 x 10^{-11} $\frac{m}{Pa*s}$. [53] These hollow fibers were contained in a plastic module with several thousand hollow fibers for a combined surface area of 1.4m^2.

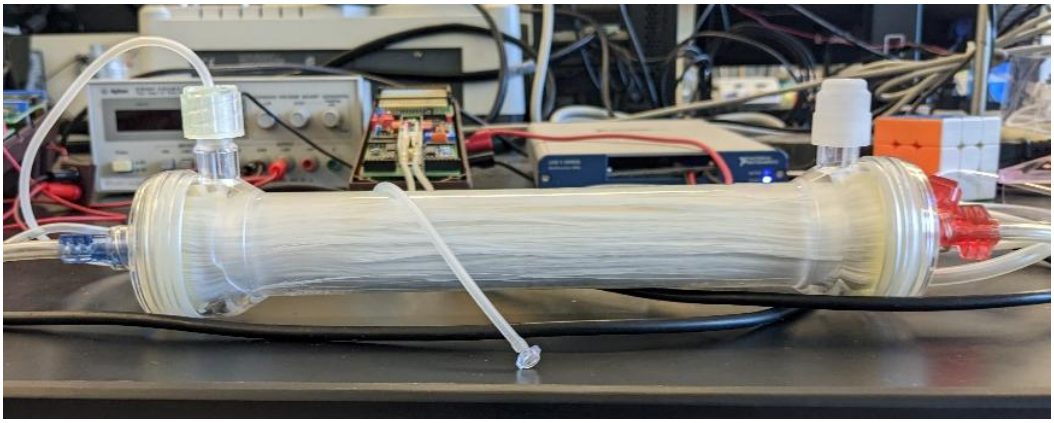

Figure 4.2 Prototype of the hollow fiber pTBI prototype with the custom attachment for craniotomy fitting

The Revaclear 300 hollow fiber bundle proved to be an excellent testing platform for creating a prototype with all tools necessary to create and configure an osmotic pressure gradient. With the MWCO of the hollow fibers fully rejecting bovine serum albumin with a weight of 66 kDa. Due to the high surface area of the Revaclear 300 hollow fiber bundle the bundle can be placed off the cranium with only a simple connection on the craniotomy. In the future, this device could be further developed to enhance Burr hole decompression.

The sealed module and dialysis airtight design also allowed the device to be sterilized until used and the high osmotic pressure prevented the permeation of the lumen solution towards the subject. This permeation is usually considered irrelevant in the face of drawing pressure from the point of injury, but it is important when considering the selection and practical application of a lumen solution.

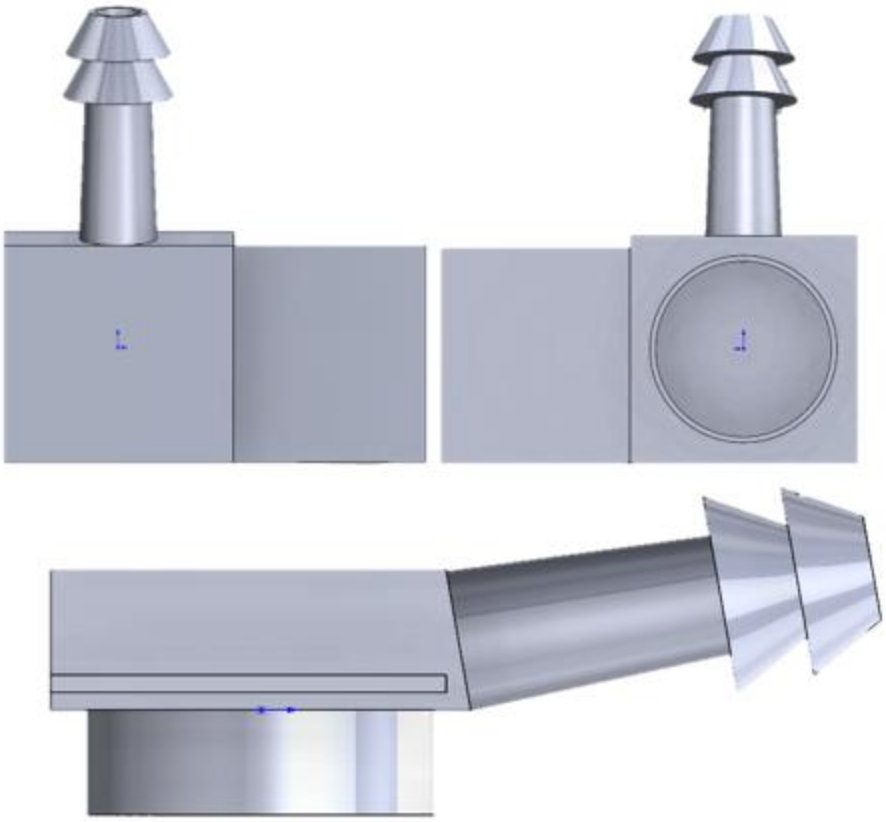

Figure 4.3 Custom tube fitting for hollow fiber prototype.

The biological laws that allow the creation of high osmotic pressure also restrict the lumen solution that can be used. Highly concentrated protein solutions are used to create high osmotic pressure, but these protein solutions are difficult to sterilize and therefore must be made and used immediately. Practically, this makes the long-term storage and use of a device that treats pTBI in the field nearly impossible as the anti-bacterial chemicals, such as sodium azide, required to sterilize the solution would have a slight possibility of seeping through the membrane and causing immense damage to the subject.

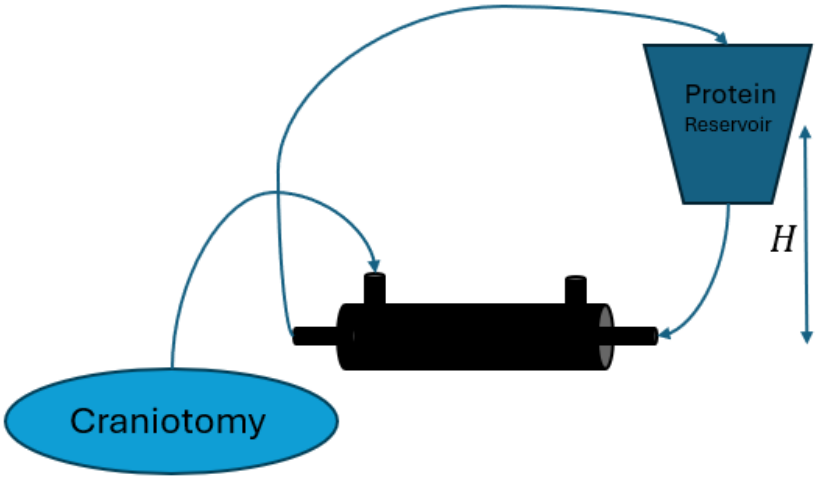

Figure 4.4 Schematic Representation of Hollow Fiber Prototype Experiment

Its high surface area, selective hollow fiber membranes, and relatively compact point of injury application was more than adequate for creating a working prototype for treating penetrating injury. A simple tube fitting was designed and 3D printed to fit the 5 mm craniotomy and made airtight against the subject skull with the use of silicone. Two rat test subjects (sham and control) were subjected to a ballistic injury and had their ICP and mean arterial pressure (MAP) monitored as shown in Figure 4.4. One hour after the rats were subjected to the injury, the hollow fiber modules were activated. The control rat was affixed with the modified hollow fiber device with a 350 g/L solution of bovine serum albumin (BSA) used as the lumen solution.

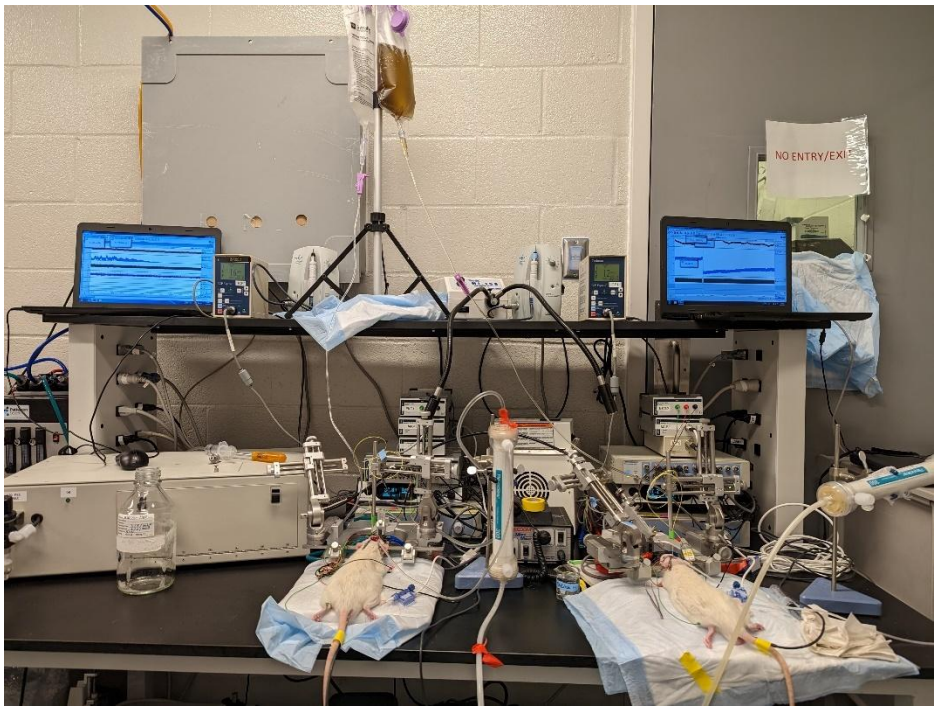

Figure 4.5 Hollow Fiber Prototype test setup with control and sham rat

The hollow fiber prototype seal was difficult to control due to the shape of the rat skull and the area below the fitting. The initial result of the ICP for the control are shown in Figure 4.5 where an immediate and prolonged drop in ICP can be observed for a period of half an hour after the seal was maintained. The results were promising and achieved the desired outcome. With a single module, the ICP was lowered to nominal levels and the decompressive craniectomy was successfully enhanced for penetrating traumatic injury. However, the other factors, most importantly the sustained control in ICP reduction over 3 days, had to be considered before committing to the device for the long-term study.

A second study was conducted with the hollow fiber prototype to determine if the pressure drop would be expressed over a longer timeframe. The study was then conducted with identical parameters but over a longer timeframe. The ICP was monitored

and is shown in Figure 4.6. The custom tube fitting faced the same sealing problems as the initial study, and it took approximately 1 hour for the hypertonic solution to affect the ICP of the subject. Once the seal is verified and the ICP drops to nominal levels again but steadily rises until blood and air bubbles appear in the feed line despite the tube fitting being completely sealed.

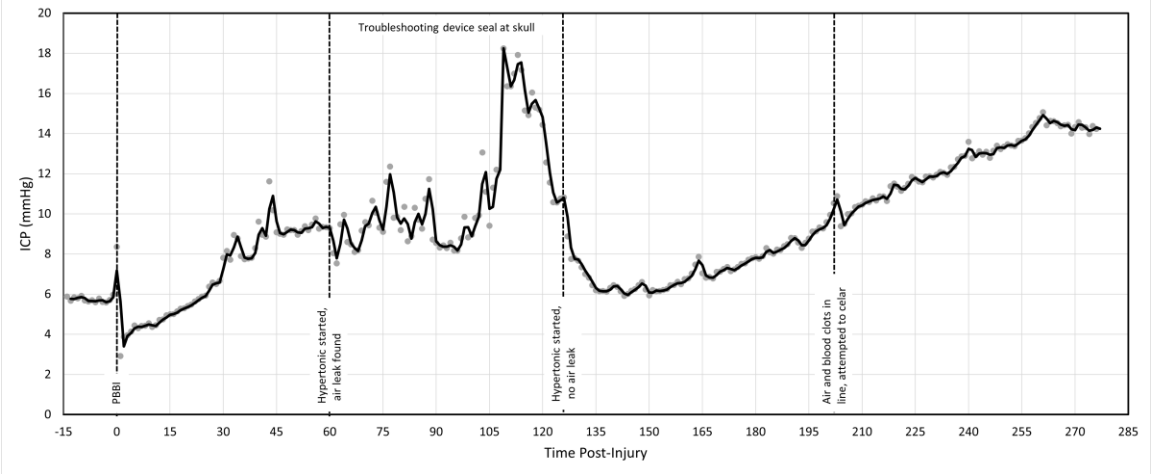

Figure 4.6 ICP chart of preliminary hollow fiber prototype trial

To verify the efficacy of the study on ICP, three more studies were conducted on rats which showed an immediate and sustained drop in pressure over a short time frame as shown in Figure 4.7. These results showed promise for short term treatment as an emergency fieldable care option. However, the lack of sustained treatment as shown in Figure 4.6 indicates that this option would not be a viable long term solution.

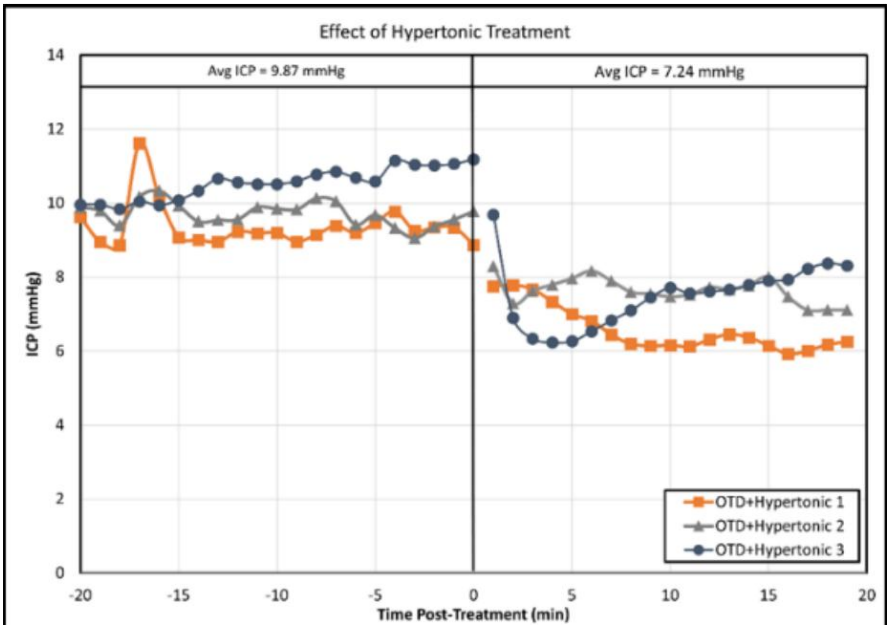

Figure 4.7 Short Term Hypertonic OTD Treatment with Hollow Fiber Bundle.

4.3.3 Discussion on Prototype Hollow Fiber Bundle Experiments

The tube fittings were difficult to seal, and this troubleshooting was the biggest problem in both experiments. What should have been a simple seal was instead difficult to create due to the irregularity in the subject skull and small working area which made it difficult to identify and seal air leaks. However, this could be rectified with an iterative process that would better conform to the subject skull and allow an easier sealing process. The initial sharp drop in ICP shows that the seal is successful, and the osmotic driving force is enough to draw fluid from the cranium. However, the drop in pressure is not maintained for the longer period. A relatively large amount of fluid was observed to be taken into the line from the test subject. As seen in figure 4.1, the test subject should have about 200 mm^3 (~ 0.2mL) of extracellular fluid 24-hour post-injury. The sharp drop in ICP most likely shows the rapid removal of this fluid. The buildup of ICP could then be attributed to the strong driving force drawing fluid from other parts of the test subject and

increasing cranial pressure. Furthermore, the hollow fiber bundle high surface area which was initially thought to be beneficial by providing a high osmotic pressure driving force was thought to be too powerful and therefore uncontrollable. A similar effect could be achieved by reducing the membrane surface area. A similar effect could be achieved while controlling the ICP reduction over a longer period of time. There were several avenues to pursue with hollow fibers but the most conventional path to pursue would be to create a tube fitting embedded with hollow fibers.

4.3.4 Hollow Fiber Tube Fitting

The inability to control the driving force of the osmotic pressure module necessitated a reduction in the membrane surface area and a better sealing method against the skull to enhance the driving force. The concept had hollow fibers run through the tube fitting and connect to specialized connectors similar to the original OTD but our device required a hard shell that would protect the membrane over the longer time frame. These membrane shells would have to be durable to endure a 3-day study and house the hollow fiber membranes. The original OTD used a hydratable hydrogel as the casing for the hollow fibers and as a connection between the soft tissue and the osmotic driving force. The hollow fiber tube fittings were designed in a CAD program (Dassault Systemes, Veliz-Villacoublay, France) and then manufactured with a Form 3B printer (Formlabs inc, Somerville, MA) using SLA 3D printing technology. The same biocompatible resin as the SCI-OTD was used to rapid prototype these tube fittings. This device would miniaturize the hollow fiber module system to fit on a rat skull for the length of the study. Initial prototypes would try to conform the device design to the rat skull.

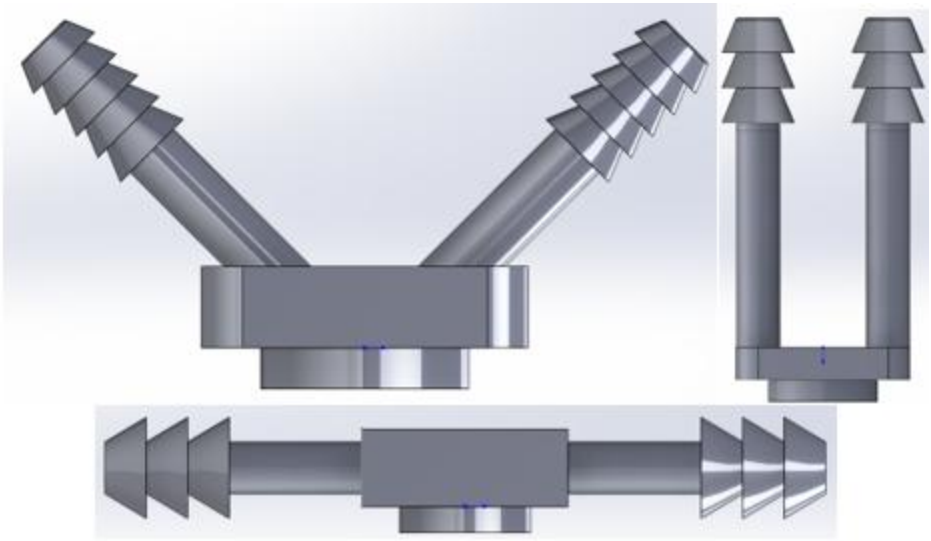

Figure 4.8 Prototype Hollow Fiber Tube Fittings

For a semi-permeable membrane with smaller surface area, tangential fluid flow would be used to enhance the osmotic pressure driving force in the hollow fiber membranes. The hollow fiber module had thousands of membranes with a combined surface area of 1.4 m^2 whereas these smaller hollow fibers embedded in the fitting would have a smaller surface area of around 50 mm^2. These hollow fibers were extracted from the module, wrapped sequentially in Teflon tape and then packed with cotton into the inlets and outlets of the tube fittings to ensure that they were watertight. A low viscosity two-part resin would then be soaked into the cotton which would harden and ensure a watertight seal at the end of the tube fitting.

The prototype hollow fiber tube fitting concepts in Figure 4.8 had too large of a footprint to fit on the skull of a rodent subject and had difficulties packing the hollow fibers into the inlets and outlets to create a seal. A multi-part housing was developed to allow the hollow fibers to be potted and sealed at the inlets and outlets of the device as

shown in Figure 4.9 with the inlet/outlet barbs, seal fitting, and open chamber for the hollow fibers to generate osmotic pressure.

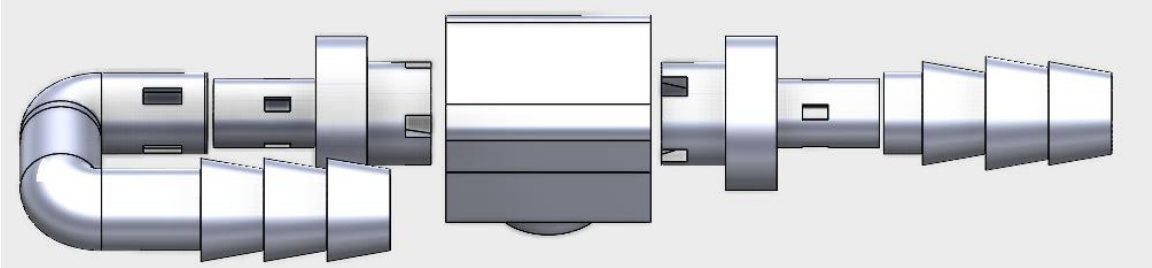

Figure 4.9 Exploded view of multiple part hollow fiber tube fitting.

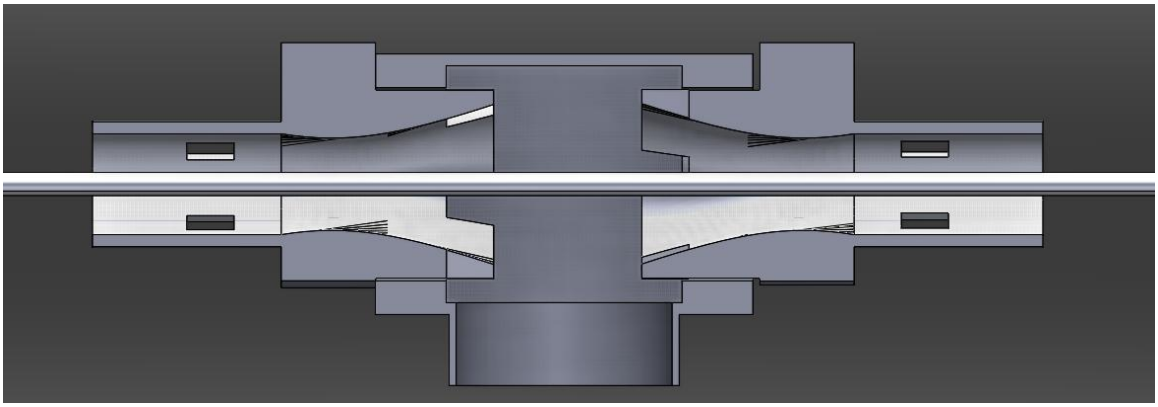

Figure 4.10 Hollow fiber tube fitting chamber where the main osmotic pressure driving force is generated.

This multi part fitting allowed the hollow fibers to be packed easily before the tube fitting barbed. To circumvent sealing issues that the previous iteration faced, these devices were manufactured in phases. By building the device in phases, the hollow fibers could be packed and sealed safely without compromising their integrity. The compact design allowed the device showed in Figures 4.9 and 4.10 could only hold about 30 hollow fibers in the tube fittings. Furthermore, the average rodent test subject had a skull length of 35mm. With a craniotomy diameter of 5 mm, the device had to fit on the test subject skull for a period of 3 days. Therefore, the device had to not only seal but maintain the integrity of the seal on the skull for the duration of the experiment. It was

inefficient to miniaturize the hollow fiber device further without a change in form factor to incorporate the same flat sheet semi permeable membranes discussed in the previous spinal cord injury study in chapter 2 that would be successfully used for the 3-day rodent study.

4.3.5 Flat Sheet Membrane Device for Rodent pTBI-OTD

With my previous experience in manufacturing flat sheet membrane devices for the SCI-OTD, the design would need to incorporate three main design features; a membrane bracket to secure the membrane, a two-chamber housing design to separate the lumen solution from the permeate, and a way to facilitate tangential flow. This device would also need to be small enough to fit on the length of the rodent skull and maintain a seal with the craniotomy without compromising membrane surface area. Hydrogel was used to facilitate the connection between the brain surface and the flat sheet membrane. A simple single inlet/outlet chamber that would contain the inlet and outlet barb attachments could be 3D printed in one piece with advancements in SLA printing technology as depicted as the feed solution housing in Figure 4.11. The barb attachment points are greatly reduced in order to save space and securely stay on the subject skull. These barbs are also angled 15 degrees from the baseline skull to accommodate 1mm inner diameter tubing.

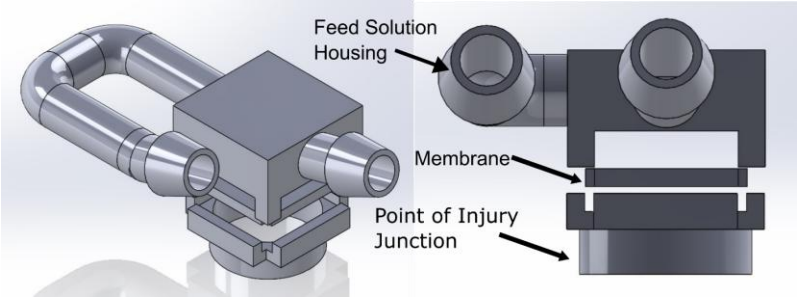

Figure 4.11 Rodent pTBI-OTD flat sheet membrane

In order to address the issue of sealing the device at the point of injury, a thin extrusion was designed to provide a junction through the skull of the subject and directly interface with the point of injury. In between these two pieces a flat sheet membrane was packed and sealed with a two-part epoxy (Masterbond EP42HT-2 ND-2Med Black, Hackensack, NJ). The semi permeable membrane selected for this study, 10 kDa NADIR® PM UP010, was the same as the spinal cord injury study (Sterlitech, Auburn, WA) which is ideal for facilitating the osmotic driving force. The radius of the point of the injury junction was 2.25mm which was the effective surface area that the membrane could interact with the brain. The membranes were cut out of their sheets with a Silhouette Cameo 3 (Silhouette inc, Lindon, UT) and had an effective surface area of 15.9 mm^2. These membranes were then shock-tested to show that they could withstand pressure without leaking and then stored in a 5% formaldehyde solution for storage until the animal studies.

4.3.6 Quantitative and Qualitative Device Evaluation

The minimum qualification standard that the devices underwent post manufacturing was the shock test. This was a test where the device membrane was placed under relatively high pressure compared to the study for a short period of time. The purpose of the shock test was qualitative and quantitative and ensured that the membrane and other components were sealed and secured with epoxy. The shock testing for each version of the OTD but for the rodent pTBI-OTD it consisted of an IV bag filled with water on a stand a height above the device inlet. The device would then be wetted and the outlet would be closed. The device would pass the shock test if the epoxy seal was

maintained and the membrane did not leak at a pressure twice that of the head pressure utilized for the study which was 24 inches of water. Water beading on the membrane surface would be observed ensuring that the membrane was not blocked by epoxy and the device would pass the shock test. If no beading was observed or if the device leaked an amount of water higher than the theoretical value, it would be discarded.

Once the qualitative requirement that the device membrane functioned had been satisfied, quantitative testing was conducted before shipment to the animal study collaborators at Walter Reed Army Institute of Research. This test was similar to the shock test and resembled a batch system. Fouling membranes is dangerous for quality tested membranes as it can foster bacteria within the membrane scaffold as well as reduction of the membrane effective area. Therefore, to prevent damage to the membrane, quality testing could not be conducted with the draw solution at all, and hydraulic permeability was used. The flux calculated from the membrane using a method known as differential densimetry. In collaboration with Dr. William Grover, the method involves using commercial density meters (DMA 35, Anton-Paar, Austria) in series as shown in figure 4.12. First the system was calibrated using sodium chloride salt solutions are varying densities within a range that would encompass the range of the draw solution. The device was then saturated for 24 hours with 350 g/L BSA and then submerged in a solution reservoir of aCSF. These devices were then left in the reservoir solution for 24 hours. The upstream density meter measured the draw solution density before the membrane and the downstream density measures the density after uptake from the membrane as shown in Figure 4.12. The difference in density would then be used to

accurately calculate the precise amount of flux that occurred in the device over the period of time. While this method works in theory, the volume uptake was too small and the densimetry devices were too inaccurate. Both density devices were able to be calibrated over a small range but could not consistently qualify the membranes, so a new method was developed.

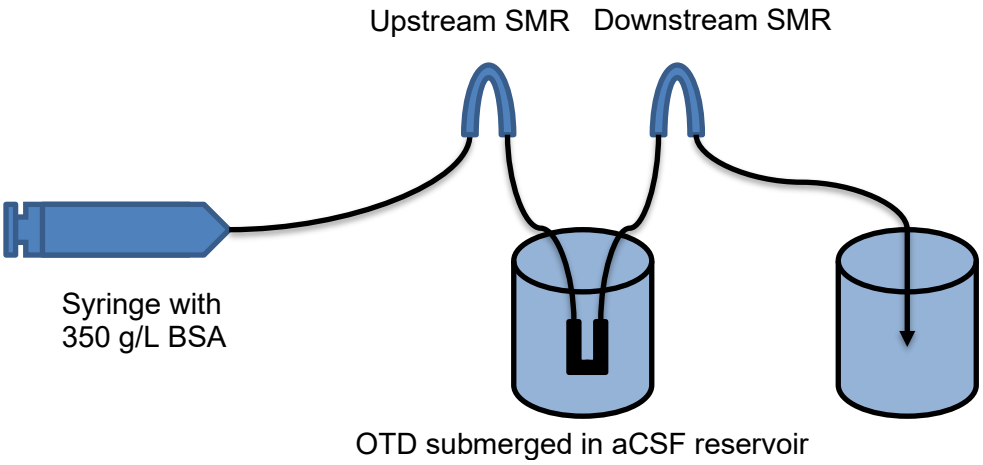

Figure 4.12 Quality testing setup schematic of OTD for rodent pTBI device

The shock testing that was used qualitatively was expanded with a pressure monitor gauge to encompass quantitative testing. The amount of solvent that would be taken up by a flat sheet membrane at a certain pressure over a period of time is dictated by the Kedem-Katchalsky equation 2.37, $J_v = L_p(\Delta P - \sigma\Delta\pi)$. The process of qualifying the membranes was similar to the qualitative testing with a clamp at the end of the tubing and a pressure sensor. The syringe would depress until the internal pressure monitored reached 5 psi and then the clamp would be tightened to completely close the tubing. Pressure would be maintained via the syringe plunger and the reverse flux of the aCSF through the membrane into the reservoir would be measured via the balance. The aCSF

reservoir would have aCSF in it already and the weight would be tared to show the change in weight over the period of time. This value multiplied by the density would show the flux in the system. This weight would then allow us to calculate the hydraulic permeability as shown in Eqn. 2.41, $J_{OTD} = L_p(\pi_p)$. The manufacturer hydraulic permeability, $\frac{J_v}{P}$, was 116/58 Gallons per feet per day per psi which, when converted using dimensional analysis, equals to 0.00095 $\frac{mm^3}{(mm^2 \cdot s)psi}$. For the rodent OTD, over a 5-minute time period at 5 psi transmembrane pressure, the theoretical hydraulic permeability for a 15.9mm^2 membrane is 0.91 mL.

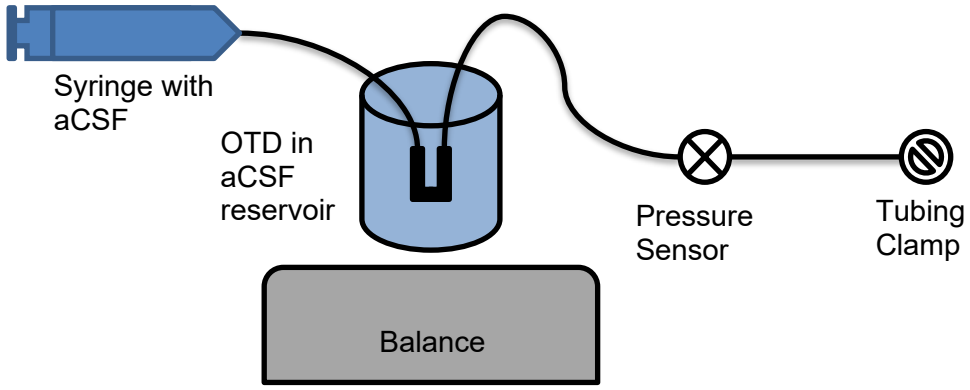

Figure 4.13 OTD hydraulic permeability qualification setup.

The OTD for the rodent study was qualified in groups with each group containing 20 devices. Extra devices were created and qualified to replace any failures in either the membrane or resin during transit. The hydraulic permeability for each group is shown in Table 4.1 with the average percent of the theoretical value. Later studies for the porcine OTD determine that the membranes are able to attain about 70% of manufacturer flux specification.

Group #	Mean Hydraulic Permeability (mL)	Standard Deviation	Average Percent of Theoretical
1	0.589	± 0.034	64.9%
2	0.612	± 0.056	67.5%
3	0.583	± 0.042	64.3%

Table 4.1 Qualitative analysis of rodent OTD hydraulic permeability

4.4 Rodent pTBI-OTD Long Term Study

Therapeutics for traumatic brain injury (TBI)-induced cerebral edema represent a critical gap for battlefield point-of-injury care. Animal studies show that an osmotic transport device (OTD) can reduce acute edema development through surface treatment of edematous tissue that removes water via osmosis. However, the safety and efficacy of OTDs need to be further tested. The objective of this study was to examine the acute effect of OTD treatment on cerebral edema, intracranial pressure (ICP) and neuropathology in a rat model of penetrating TBI.

4.4.1 Rodent pTBI-OTD Methods

The objective of the study was to examine the safety and efficacy of the OTD on cerebral edema, ICP, and neuropathology in a rat pTBI model. ICP and mean arterial pressure (MAP) were measured in adult male Sprague-Dawley rats between 8-10 weeks old and within a 250 to 300 g range, prior to and following right unilateral pTBI. Four groups of animals were studied with 9 animals per group: sham (no injury), Injury only (no device), OTD with isotonic fluid (OTDiso), and OTD with the hypertonic 350 g/L BSA solution (OTDhyp) and treated from 1 to 5 hours post-injury. The feed solution was suspended in an IV bag and a stand a certain height from the subject and a pump was used to circulate the fluid back into the IV bag as shown in figure 4.11. Cerebral edema

progression was characterized via MRI during and following a 72-hour treatment with isotonic and hypertonic fluid. Lesion volume, neuroinflammation, and neuronal damage were assessed.

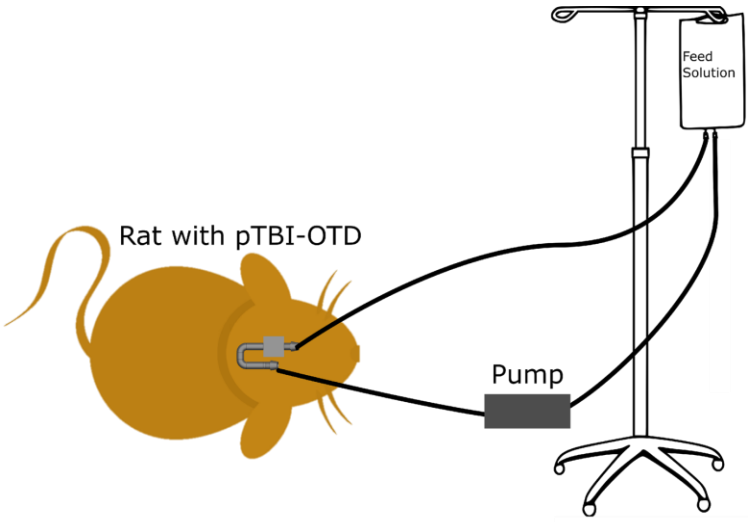

Figure 4.14 Schematic of rodent pTBI-OTD study

4.5 Rodent pTBI Results and Discussion

ICP was decreased in the hypertonic treated group compared to both isotonic and pTBI-only controls approximately 1 mmHg, however, this change was not significant as shown in the figures below. While not statistically significant, the ICP trends are promising in acute TBI stages. A gradual decrease in pressure may be more feasible as opposed to our initial experiments which resulted in rapid reduction and damage to the underlying tissue. As expected, all treatment groups remained above sham values as shown in Figure 4.13. OTD treatment, with isotonic or hypertonic treatment, elicited a reduction in brain water content in the ipsilateral hemisphere.

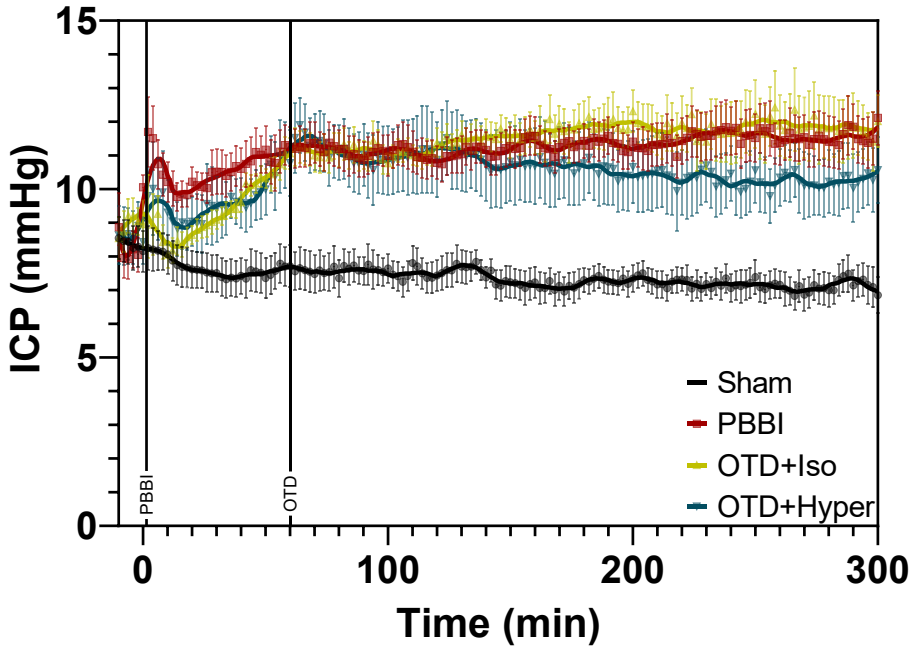

Figure 4.15 When examining the raw ICP data, we find that following PBBI, there was not a significant impact of OTD treatment. However, during the 4-hour treatment period a decreasing trend was observed in the hypertonic treated group compared to both isotonic and PBBI only controls. n=9

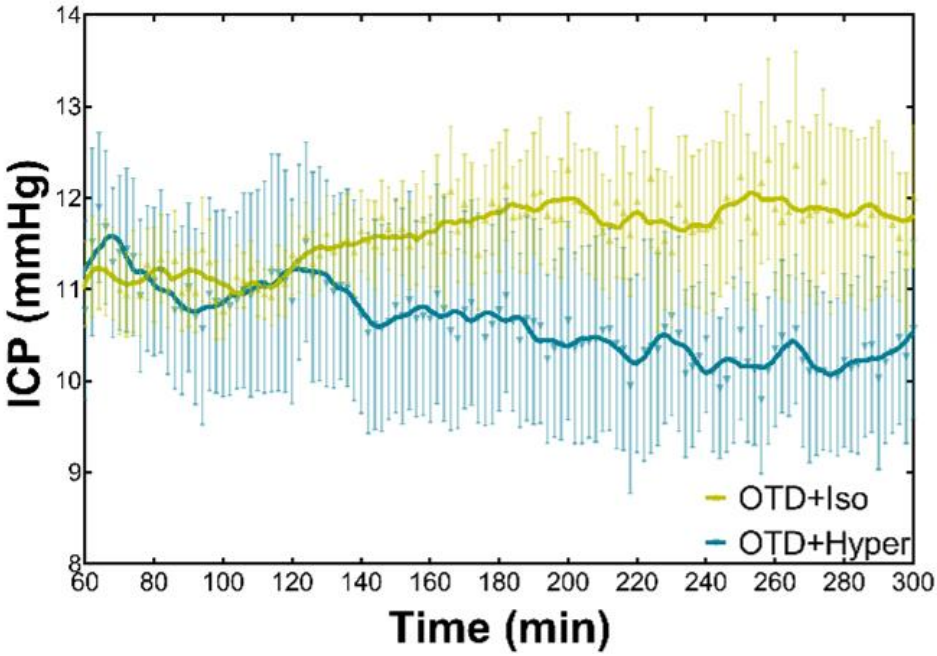

Figure 4.16 ICP increases significantly following injury in all injured groups. The OTD with the hypertonic solution group decreased slightly during treatment, but the differences did not reach statistical significance. n=9

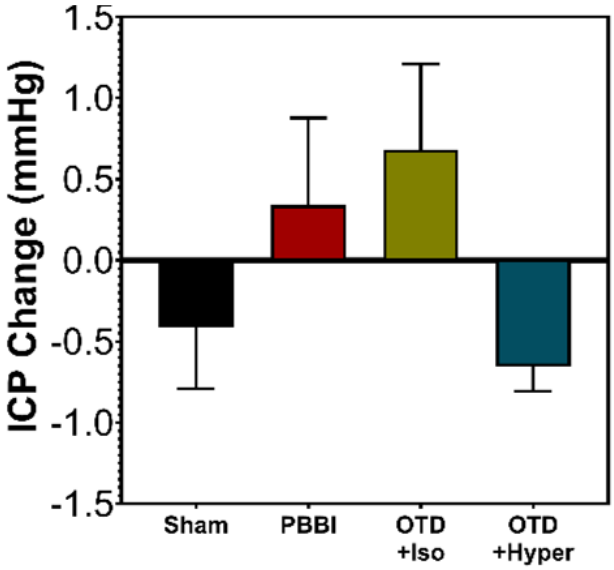

Figure 4.17 Isolated OTD conditions in the treatment phase. By the end of the experiment, the difference was approximately 1 mmHg. While not statistically significant, the ICP trends are promising in acute TBI stages. The change in ICP from the first 30 minutes of treatment to the final 30 minutes. n = 9

Brain water content significantly increased in the injured rats. There was a significant reduction in the brain water content for both the isotonic and hypertonic solution indicating that the OTD had a similar with both solutions effect on brain water content.

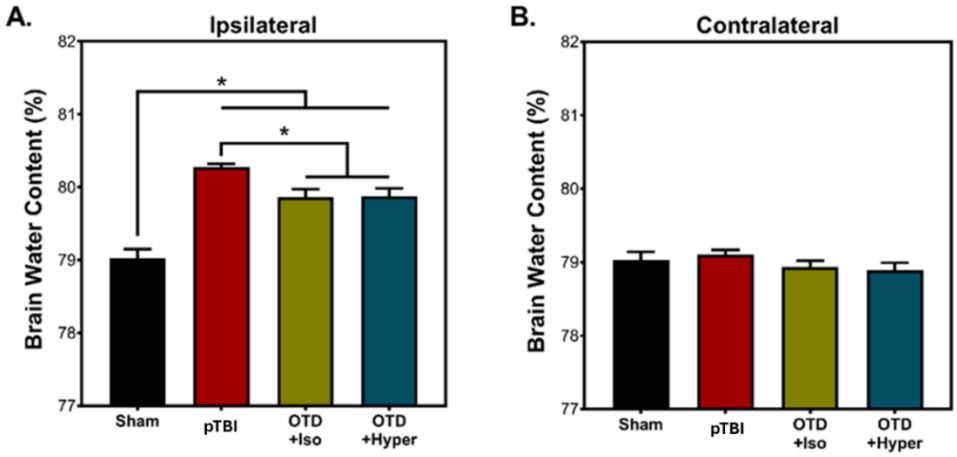

Figure 4.18 Brain water content measured using the wet-dry method at 5hrs post injury in the ipsilateral (A) and contralateral (B) hemispheres

Histological analysis was conducted for the striatum, cortex, hippocampus, and thalamus were conducted for IBA1, silver stain, and GFAP.

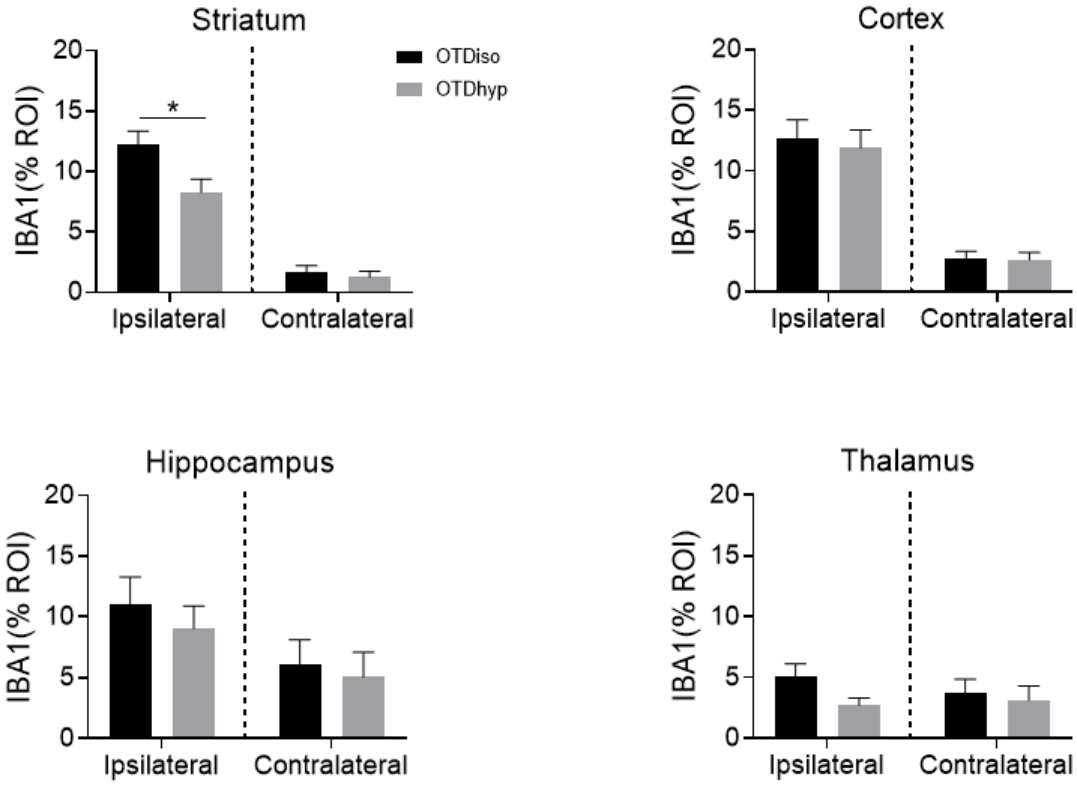

Figure 4.19 Histological assessment of IBA1 demonstrated a significant reduction of IBA1 levels in the striatum post-injury and OTD treatment with the hypertonic solution compared to isotonic solution ($p<0.05$). A trending reduction was also detected in the thalamus region.

IBA1 (Ionized Calcium Binding Adapter Molecule 1) is a highly sensitive calcium binding protein biomarker that indicates microglial and macrophage specific activity. Expression of IBA1 in the striatum and a trending reduction in neural damage via silver stain analysis in Figure 4.20 indicates the OTD reduces neuronal damage. [54] A significant activation in this protein would indicate the neuroregenerative effects on the brain. Silver staining is a sensitive method for detecting small amounts of proteins and low-molecular-weight nucleic acids in polyacrylamide gels. [55] Finally, GFAP (Glial fibrillary acidic protein) immunoreactivity is viewed as an index of gliosis or a relatively

slow-developing correlation of neural damage. [56] Histological data suggests reduced neuronal damage with the hypertonic solution group and supports the previous data.

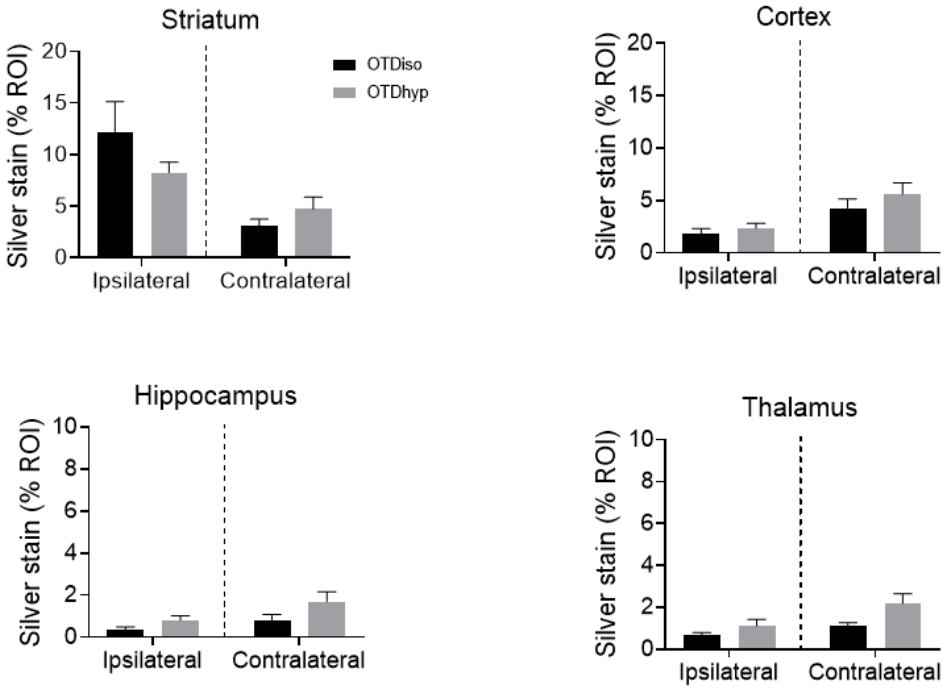

Figure 4.20 Histological assessment of silver stain indicated a trending reduction of neuronal damage in the striatum.

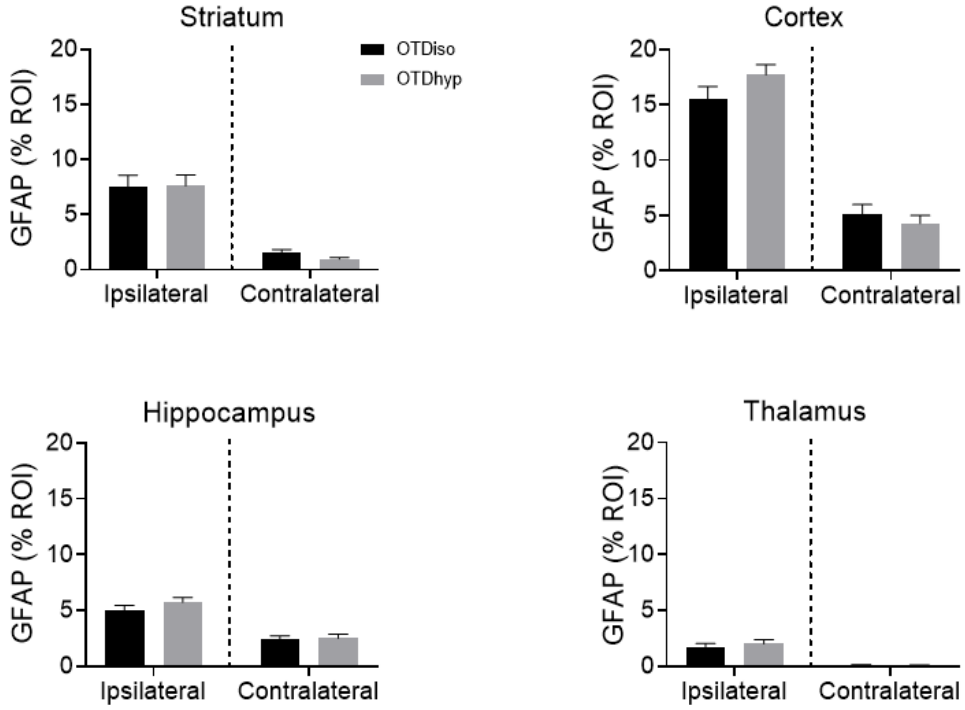

Figure 4.21 Histological assessment of GFAP showed no changes detected in all the regions examined.

Histological assessment demonstrated a significant reduction of IBA1 levels in the striatum, and silver stain analysis also indicated a trending reduction of neuronal damage while GFAP showed no changes detected in all the regions examined. MRI data for the 3-day animal trial indicates that there is no significant difference in cerebral edema progression over the study. Brain water content comparing the ipsilateral and contralateral hemispheres show the effect of the penetrating injury on different hemispheres.

The MRI scans show that there is no significant difference between the hypertonic, isotonic, or injury compared to the control over the time course, however, it does appear that the application of the OTD increased edema volume throughout the study. Additionally, MRI scans for the hypertonic OTD group seemed to have higher

water content in the brain compared to the other groups. While this data suggests that the OTD is detrimental, other data shows that the OTD improved neuropathology and decreased hemorrhage volume over a 7-day timeframe.

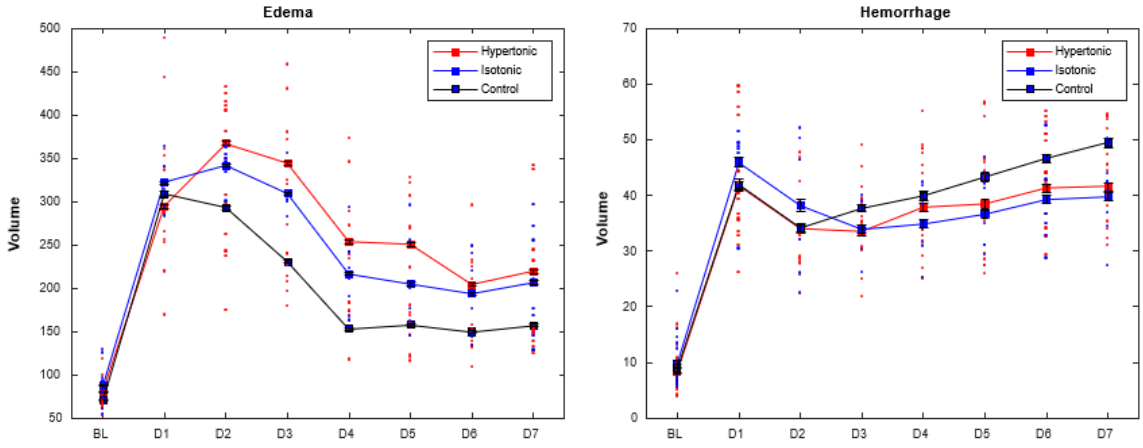

Figure 4.22 Rodent MRI Results for Edema and Hemorrhage courtesy of Dr. Joseph Dwyer at WRAIR

A likely explanation regarding the increase in brain water content relates to the first study with the OTD conducted by Dr. McBride. In this study the animals treated with the OTD had the highest brain water content after death which mirrors the results above.[28] While the brain water content of the OTD treated mice in the original study was higher, the mortality was significantly lower and indicates that the OTD may increase the tolerance for cerebral edema after injury.

Chapter 5. Osmotic Transport Device for Penetrating Traumatic Brain Injury in Porcine

5.0 Pig pTBI-OTD Concept and Development

The size difference and lissenphalic nature of rodent test subjects prevented the study from completely replicating the effect of the enhancing decompressive craniectomy on human test subjects. The need for further animal studies to verify results required subjects with brains and neuropathy like humans. Pigs are natural analogs to humans with similar gyrencephalic structure, and anatomy. To modify the OTD for a porcine pTBI model, the membrane surface area must be increased to increase the flowrate for a larger brain surface area and mass. Figure 5.1 illustrates the difference in size and volume between a rat brain and a pig brain as well as the similarity in contours between a human and a pig brain.

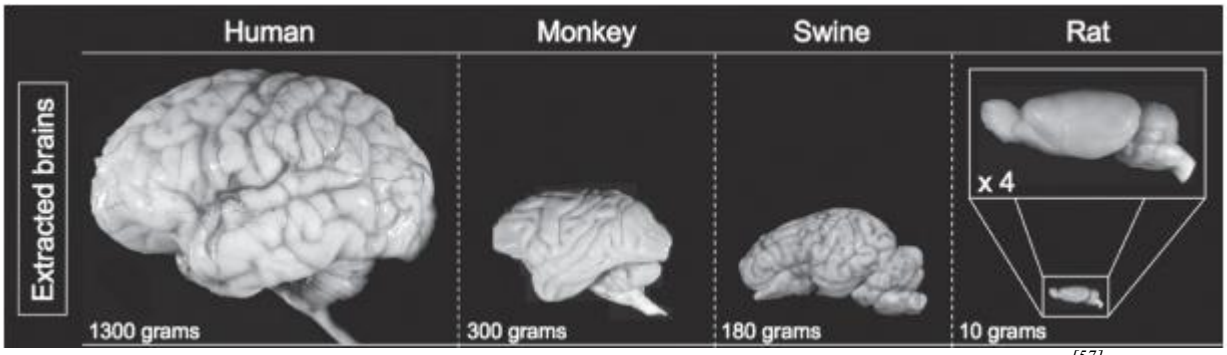

Figure 5.1 Size and shape differences between human, monkey, swine, and rat brains. [57]

5.1 Membrane Housing and Device Development

The membrane housing was designed via CAD (Dassault Systemes, Veliz-Villacoublay, France) and utilized the same biomed clear resin which was biomedically compatible and allowed for long term mucosal membrane contact which would eliminate the chance of resin toxicity and cellular damage. The design of the membrane housing was a similar two chamber design to the rodent version, but a thin elastic membrane was

attached to the lumen solution chamber which allowed the system to expand when fluid was removed. Several elastic materials were tested for their expansion capabilities, durability, and ability to return to original shape after stretching. The material chosen was Elastic 50A Resin V2 (Formlabs inc, Somerville, MA) which was compatible with the current Form 3B printers in our lab and was able to be manufactured via SLA printing which allowed custom designs and variable thickness of the elastic membrane. This resin is a soft, translucent elastomer with a 50A Shore durometer that is ideal for prototyping parts that will bend, stretch, compress, and hold up to repeated cycles without tearing. The manufacturer data sheet gives it a 3.4 MPa tensile strength with a 160% elongation before breaking. All these factors make it an ideal elastic for testing a larger pTBI-OTD for a larger animal.

The elastic membrane was fitted to the shell of the device and sealed as shown in Figure 5.2. Early prototypes of the devices showed that the breaking point was always the seal around the elastic and not the elastic itself therefore placing great importance on the sealing of the elastic membrane to the shell. Several different sealants were tested and quantified where the pressure of the device was measured until a leak emerged. From the epoxy sealants testing UV resin was the strongest.

Prototype Test	JB Weld Epoxy Two-part Clear Weld	JB Weld Epoxy Two-part Cold Weld	Vida Rosa UV Resin Hard Clear
1	8.84 Psi	9.16 Psi	19.38 Psi
2	14.36 Psi	9.36 Psi	22.13 Psi

Table 5.1 The breaking point of the different sealants of the Elastic Membrane.

The rodent pTBI-OTD utilized an effective membrane surface area of 15.2 mm^2. With an 18-time increase in mass and a significant increase in surface area from rodent to pig, 36 times increase in membrane surface area was necessary to produce the higher driving force necessary to draw edematous fluid from the brain with the updated pTBI-OTD had an effective membrane surface area of 569 mm^2. The membrane was sealed to the device using UV resin which had a viscosity that allowed it to soak into the membrane on the edges and create a unified binding between the membrane and the shell with a UV light source. The resin was added to the edges of the membrane and allowed to soak slightly and then quickly set with a UV flashlight before being placed into a UV cure station that would rotate the device while blasting it with UV light from 360 degrees. This made a strong bond that would seal the membrane against the shell permanently. All tests to determine the breaking point of the membrane were inconclusive as other parts of the device failed before the membrane.

An elliptical housing was designed to fit this larger membrane with tube fittings for inlet and outlet flow. The outlet tube fitting was inspired by the rodent device and incorporated a 90-degree elbow that allowed the tubing to be wrapped around to conserve space. Swine skull thickness and skin ranged from 5-10mm deep. The large variation of this thickness required different lengths for the point of injury junction that would sit within the craniotomy gap. To avoid creating a range of devices with different junction lengths, the devices were manufactured at the longest possible length of the craniotomy and then cut down as necessary with a Dremel with a rotary saw attachment.

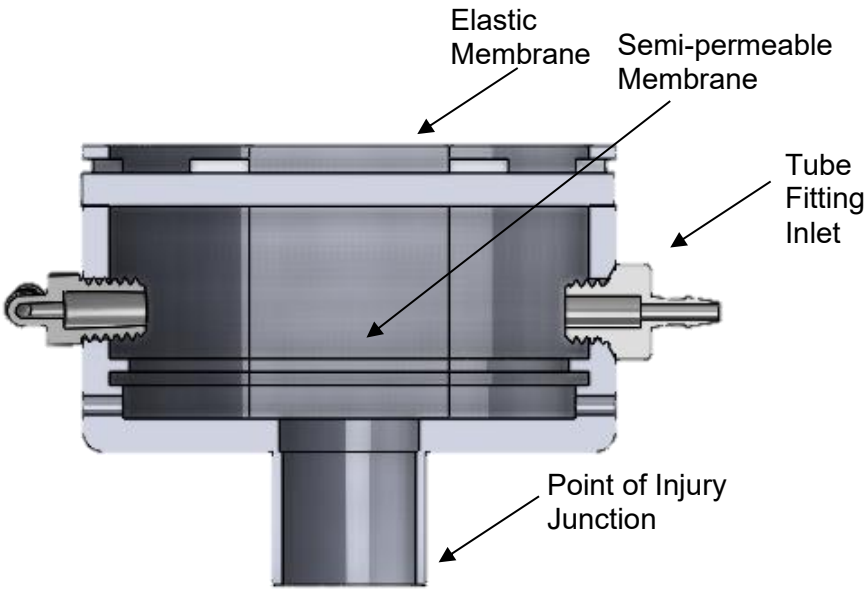

Figure 5.2 Swine pTBI-OTD CAD representation

Due to pigs being much larger animals than rodents, an IV bag could not be used as a solution reservoir; therefore, a closed loop system was devised which allowed the device and components to be affixed to the pig. The higher volume of the device required a different inlet and outlet system that would allow fully formed tangential flow to eliminate air bubbles and prevent crystallization of the highly concentrated protein solution. A small pump system was designed to fill and circulate the solution through the tubing to achieve this goal. The closed system also prevented the outflow of edematous fluid that was drawn from the subject and so a small tube fitting with a 3-way luer-lock valve system was implemented downstream of the device. When the valve is turned, fluid is released to an outlet tubing container and the volume of the system is reduced to ensure that the elastic membrane does not break during the study.

5.1.1 Manufacturing Cost and Production

A brief mention on the cost of the devices is discussed here to show the benefits of SLA manufacturing over traditional manufacturing methods. The devices were manufactured using the previously mentioned Formlabs Biomed Clear resin which has a cost of 350 dollars per kilogram with 1 kg of resin making about 200 device shells carrying a per device cost of $1.75. The Sterlitech 10kda molecular weight cutoff UF010 CF 042 membranes cost $159.79 for 5 membranes which can be further cut to fit 15 devices at a cost of $10.65 per device. The barbed tube fittings that allow inlet/outlet tangential flow cost $1.57 and $0.66 respectively for a cost of $2.23 per device. The elastic material Formlabs elastic resin 50a that allows device expansion costs 200 dollars per kilogram with 1 kg of resin making about 300 device shells for a per device cost of $0.66. The final total cost of a single pTBI-OTD is therefore estimated to be $15.29 with most of the cost associated with the membrane.

5.2 Quantitative and Qualitative Testing of pTBI-OTD

The stretching of the elastic membrane is an integral part of the pTBI-OTD. The soft material stretches to accommodate the uptake of edematous fluid in a closed-loop system. The theoretical amount that the device can uptake before breaking is about 7.5mL but devices were shock tested to check integrity up to 5mL uptake. The shock test also checked for leaks at the semi-permeable membrane and tube fittings as well as the integrity of the elastic membrane. This was accomplished via a syringe with luer-lock connection that connected to the inlet with another tube with a tubing clip attached to the outlet. The syringe filled the lumen reservoir with water until it was cleared of air bubbles, but the elastic membrane was not under strain. The outlet tube was then clipped,

and the syringe was pushed to test the pressure seal of the semi-permeable and elastic membrane. A successful device would show no leaks in either membrane and return to conformity after the test. Devices that failed and leaked the elastic membrane would be resealed with UV resin while devices that had leaks in the semi-permeable membrane would be discarded as there was no way to reseal the membrane without disassembling the device.

The hydraulic permeability of the device determined the ease through which water would pass through the membrane under pressure. The manufacturer hydraulic permeability is used as a reference. Similarly, to the shock test, a syringe was used to fill the pTBI-OTD with water and the outlet tubing was connected to an Elveflow MPS pressure sensor. The syringe was then loaded on to a syringe pump and pressure was increased in the device until it reached 5 psi at which it was immediately set to pump at a prescribed rate of 0.135 mL/min to maintain pressure for 1 minute. The water buildup in the chamber below the membrane was then weighed and the device was categorized based on the hydraulic permeability.

The theoretical hydraulic permeability of the flat sheet membrane is given by the manufacturer as 116/58 Gallons per feet per day per psi which when converted to standard units show in Figure 5.3 incorporate the area component of the membrane. Using this term, we can calculate the theoretical hydraulic permeability of the membrane at a specific pressure and time frame. For these membranes with an area of 569 mm^2 at around 5 psi over 1 minute the theoretical volume of water pushed through the membrane

is 0.6486 milliliters which volume is our theoretical limit of the hydraulic permeability for the membrane based on manufacturer specifications.

$$\frac{J_v}{P} = 9.5\ x\ 10^{-4}\frac{mm^3}{(mm^2 * s)Psi}$$

Figure 5.3 Hydraulic permeability of the flat sheet membrane.

Another challenging aspect when preparing the devices for shipment to our collaborators was the membrane degradation over time. Theoretically, the flat sheet membranes have an indefinite shelf life as long as they are in dry conditions. The membranes only activate when wetted and if they subsequently dry out then the pores close and render the device useless. The pTBI-OTD would then be stored with a volume of water in chamber 1 to prevent the membrane from drying out. Therefore, after shock testing and hydraulic permeability qualification, the membranes would be stored in a vacuum sealed bag with most of the air removed via a food storage vacuum sealer (Bonsenkitchen, Flowery Branch, GA). The inlet and outlet were shut with tubing clips and bound together to prevent the negative pressure from the vacuum sealing process with interfering with the device. A small piece of cotton was also inserted at the elastic membrane to help prevent negative pressure from putting too much strain and to evaluate the elastic membrane integrity.

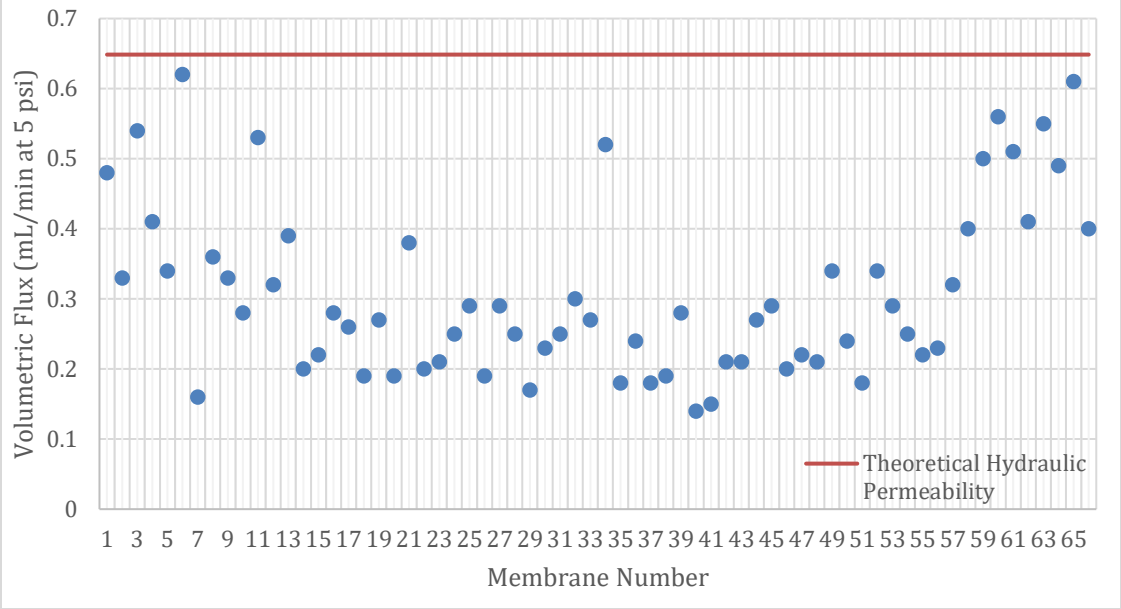

Figure 5.4 Hydraulic permeability of membranes prior to storage.

Figure 5.5 Vacuum Sealed pTBI-OTD Ready for Shipment.

The hydraulic permeability of the devices that were not vacuum sealed showed lower hydraulic permeability after a week as shown in Figure 5.4. The vacuum sealed devices in Figure 5.5 show excellent stability and membrane integrity with an average

drop of 0.122 mL over 87 days. However, these devices faced issues that exceeded the original timescale. Figure 5.4 shows a range of 8 devices that were not vacuum sealed with some membranes showing a drop of over 50% flux. These devices were most likely contaminated from bacteria that were trapped within the device that could not be sterilized by the UV cure process. These devices could still be sealed and used “wet” by introducing an antibacterial agent or a salt solution that may prevent the fluid that keeps the membrane from drying from developing bacterial growth that would block the pores from functioning. The addition of alternate staging fluids is a gamble as any antibacterial agents may influence the animal, but it is a promising future research direction for long term storage. As a precaution, a set of untested and unqualified membranes were set aside as “dry”. These membranes would be backup in case the vacuum membranes degraded to a point where they were unusable. These would be shock tested and qualified on site before the surgery to ensure no contamination or degradation in the membrane.

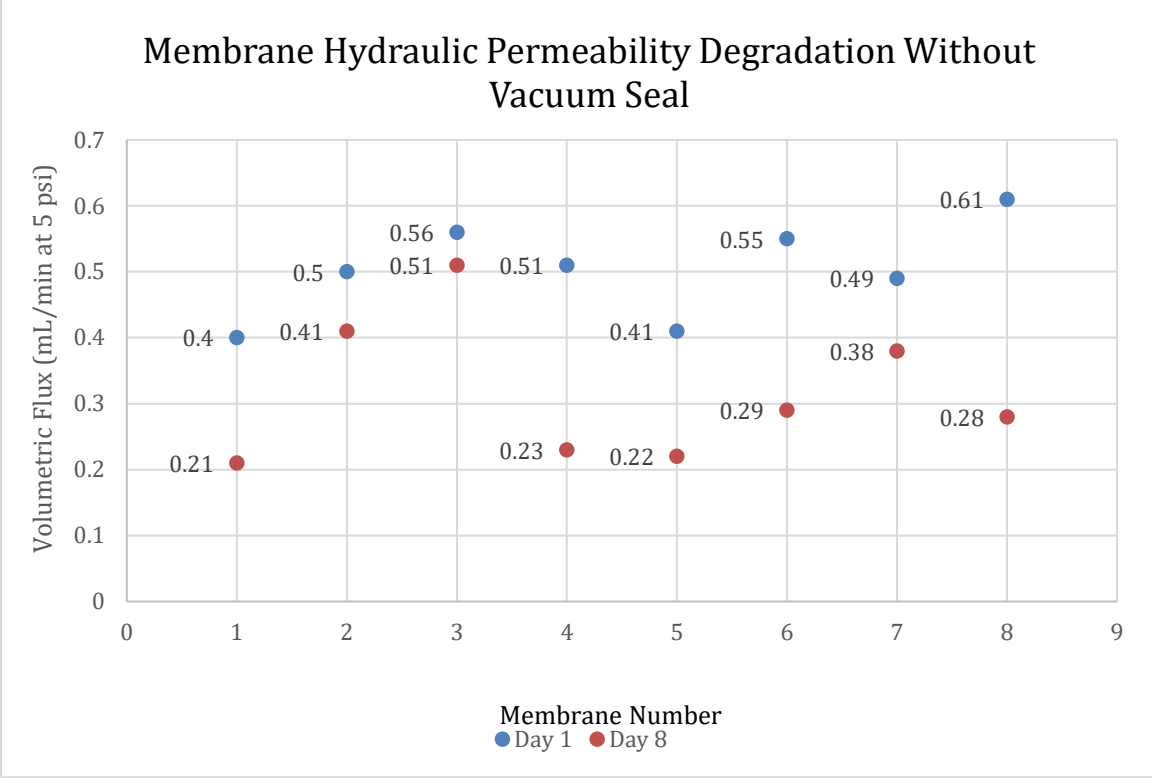

Figure 5.6 Membrane degradation without vacuum seal to protect membrane

Hydraulic permeability tests were also conducted to determine the long-term efficacy of the membranes and if there was any degradation of the membrane hydraulic permeability over a time frame of 4 months in sealed conditions as shown in Figure 5.4. Despite the vacuum seal, the device hydraulic permeability degraded over 50% and signs of bacterial growth were actively observed in some of the devices. The vacuum seal was not sufficient to prevent membrane degradation for long term storage. Therefore, the best storage option for the device would be to store the devices “dry” and shock test immediately before use.

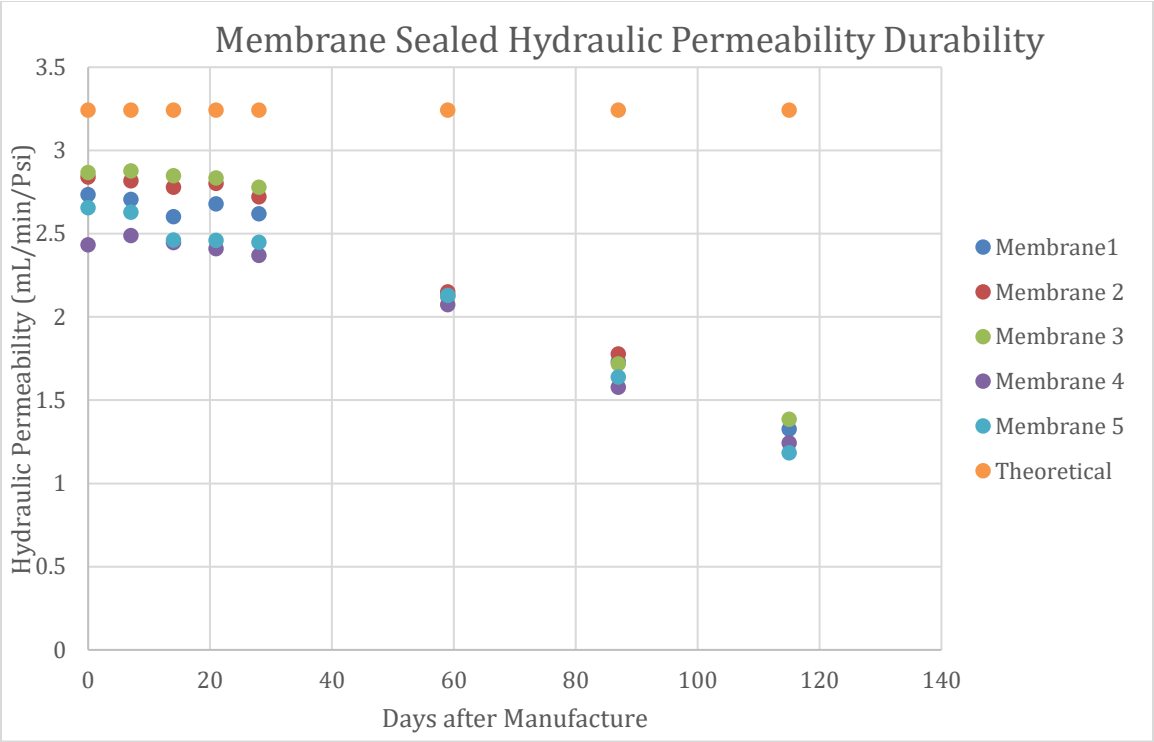

Figure 5.7 Degradation of Hydraulic Permeability of pTBI-OTD Membrane.

5.3 Swine Helmet and Vest

After consulting with several porcine experts in the research field, it was determined that a helmet would need to be developed to protect the OTD on the animal skull since a cone would not fit firmly around the neck and ensure that the animal would not destroy it immediately. Several workarounds were discussed with our collaborators, the most efficient of which is a helmet which can protect the OTD by surrounding it in a soft foam which would insulate it from any impact the animal may impart. This helmet occupied a large portion of the cranium around the OTD and added stability and protection while the device was in action. The helmet was designed after a cosplay helmet and was constructed out of 10mm thick EVA foam. This foam is moldable under

heat, easily modified with precision cuts, padded for impact and comfortable with prolonged skin contact making it an ideal protective material. Each helmet was specialized for each individual patient to fit them best over the study. Initially this helmet was designed to fit over the chin of the subject and secured via clip straps. However, initial test fittings of this showed that pigs do not have chins like humans and the helmet would slide off the snout easily. The size of the helmet would be drastically reduced to just surround the OTD and would be anchored at the base of the neck to a support vest that had custom pockets to house ancillary monitoring equipment. Evaluation of the helmet seemed to not add more protection and remains to be evaluated with animals before the experiment.

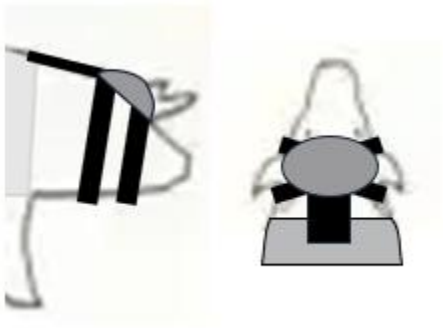

Figure 5.8 Helmet prototype design and connection to vest

The vest was fitted over the subject front and rear legs to provide a stable base for monitoring equipment and a circulation pump.

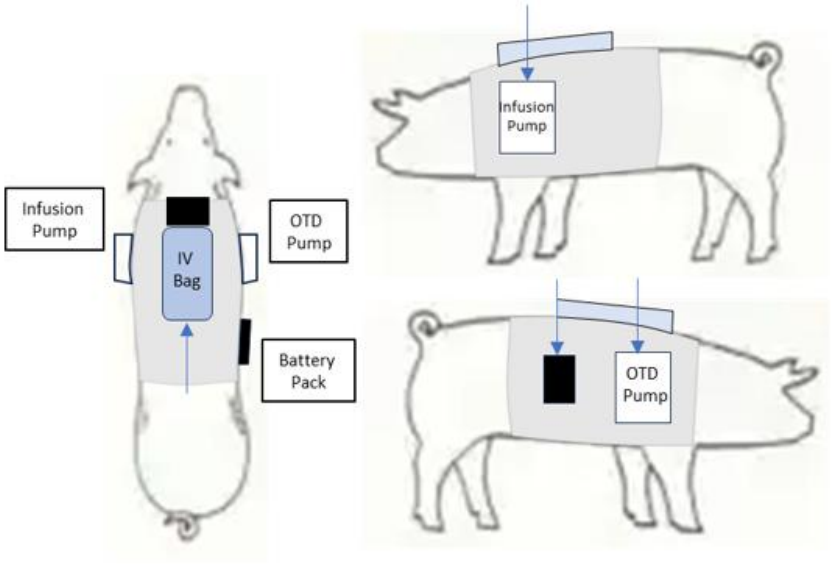

Figure 5.9 Vest with OTD BoxPump, Battery pack, and infusion system for the 3-day study courtesy of Dr. Joseph Dwyer

5.3.1 Circulation BoxPump

The high concentration of protein required to create the osmotic pressure gradient necessary for flux to occur is very viscous. In a controlled environment, this viscosity is not an issue but with an animal experiment there is a concern that the protein solution may coagulate and cause blockages in the tubing. Furthermore, internal concentration polarization due to forward osmosis will dilute the protein concentration and will lower the osmotic pressure gradient. A small simple circulation pump system was designed to intermittently circulate the protein solution to prevent crystallization in the system.

The experiment parameters required the pump to function on a living animal for an expected 3-day study, the pump required an independent battery system that would not interfere with the subject minute movements and bodily functions. The battery limitation prevented the pump from constant mixing and required a timer that would power the system on and off at specific intervals to save on battery. The previous data on mixing

showed that the pump required less than 1 minute of mixing at full speed to mix the protein solution and prevent any blockages or buildup in the tubing. The pump itself would have to be small enough to fit on the test subject and use low power consumption.

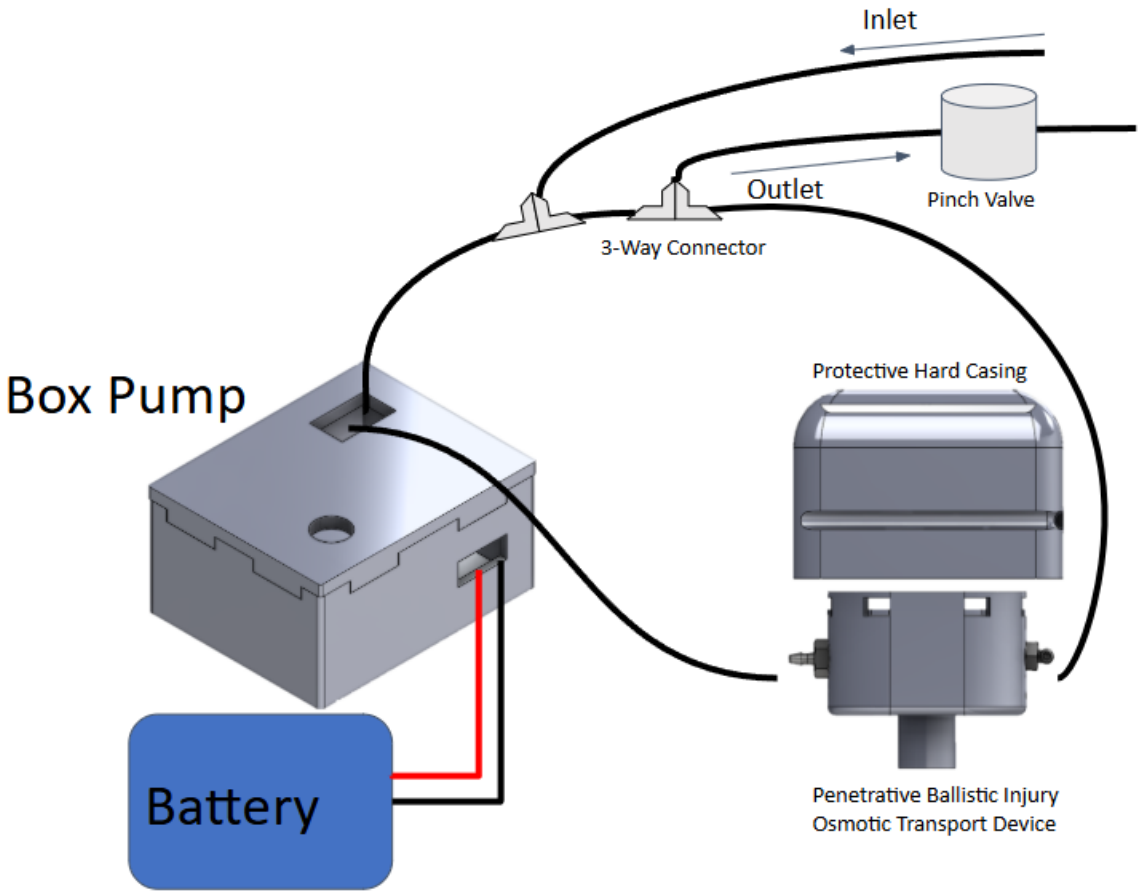

Figure 5.10 BoxPump schematic during porcine experimenation

With these parameters in mind, an Arduino UNO R3 board (Arduino Inc, Lombardia, Italy) was used as the prototype framework to control and modulate a small 6V pump. The Arduino is low power and has the digital and analog input and outputs required to control the system. The peristaltic pumps (3910, Adafruit Industries, Brooklyn, New York) are small solenoid motors that operate a clover three-wheel system

on a soft nylon tubing. A simple always on smartphone power banks battery system was used which would output 5V 20,000 mAh and would power the pump, Arduino, and the pinch valve. The Arduino requires only 50mAh of power to function as a timer and switch for the pump. The high capacity of the battery allows the pump to function without battery replacement for the entirety of the study.

The elastic would be put under strain under the intake of fluid from the edematous fluid into the device from the test subject. In some cases, the relatively high pressure that occurs when filling the device with high density protein solution would cause micro fissure cracks in the UV resin holding the elastic in place and leak. The failure rate when filling the devices in this manner was 18.5% and would compromise the membrane with all resealing methods ineffective. To circumvent this the pump speed was lowered via pulse width modulation and a small pinch valve (Neptune Research, West Caldwell, NJ) was attached to an outlet tubing in a normally closed configuration. In intervals of 1 hour the pinch valve would open and close rapidly every second for 5 seconds to release pressure buildup.

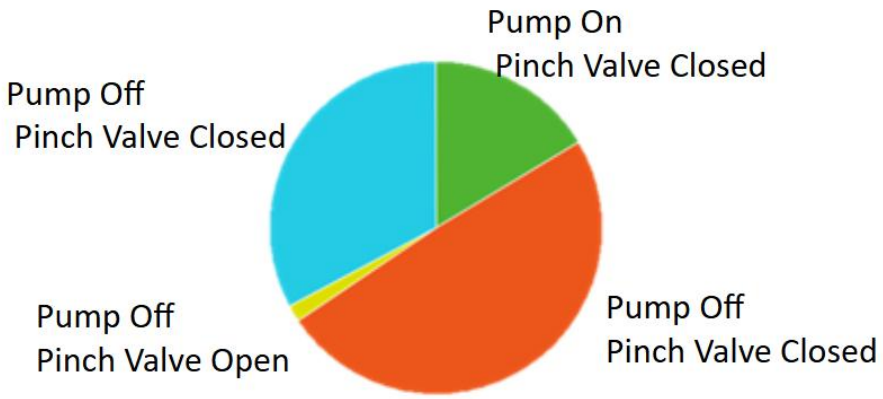

Figure 5.11 Box pump activity pie chart per hour.

5.4 Device Efficacy and Quantitative Analysis

The volumetric flowrate of the system should have no effect on the efficacy of an osmotic transport device. To test this theory, a study was conducted to test the pTBI-OTD at three different flowrates using a peristaltic pump. These speeds are modulated using an Arduino motherboard with pulse width modulation capabilities at 100% pump power and 55% pump power denoted as “high speed” and “low speed” respectively. A no flow condition was also tested with the pump run at high speed at the conclusion of the study to mix the fluid in the system and determine the final density.

The flowrate of these speeds was examined by pumping the BSA through the system and measuring the density of the solution and the weight of the flow per minute. With the density being actively measured, the flowrate could then be calculated for each speed. High concentration 350 g/L BSA solution was used to draw artificial cerebrospinal fluid (aCSF) from a reservoir situated on a balance and the change in density in the draw solution was monitored with a densimeter (LDens2300, Anton Paar, Austria).

Prior to the start of the experiment, the membranes were fouled for two hours and the hydraulic permeability of the feed solution was measured. Then the aCSF feed solution density, volume of the system, and the system flowrate with BSA was measured before the draw solution density was loaded. Hydrogel was then loaded on the feed solution side within the membrane housing and allowed to cool to room temperature to facilitate the connection between the reservoir and the membrane. The device was then placed onto the reservoir and run at high speed for an hour then refilled with solution and run at low speed for an hour. The speed of the pump was controlled via pulse width modulation circuitry built directly into the Arduino system for this study. High speed was

at full voltage, 255/255, while low speed was modulated to be 140/255 which is about 55% of high pump speed. This was conducted 3 times each per membrane resulting in 6 datasets. Pressure in the system was released at pressure intervals throughout the study to preserve the integrity of the device. At the end of the experiment, the initial volume of the device system was measured with BSA and then compared to the final volume of the system, and the final weight of the reservoir was compared to the initial weight.

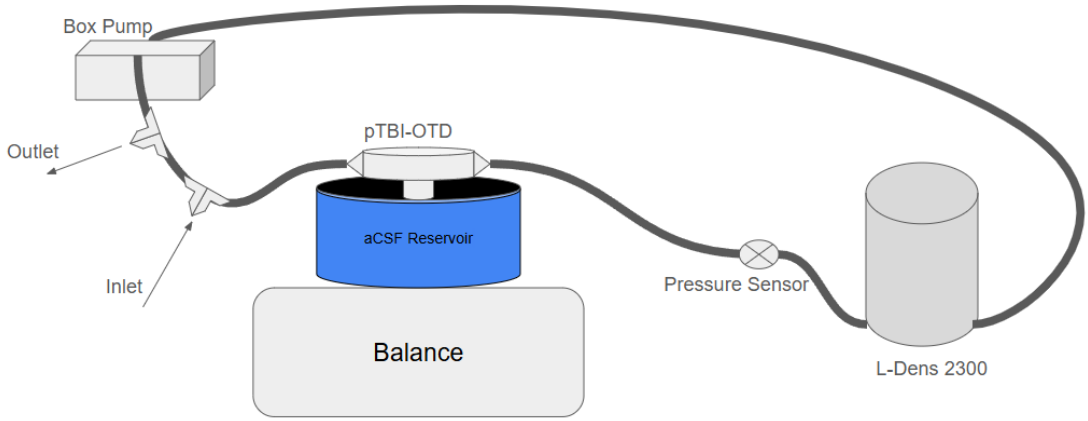

Figure 5.12 Schematic of device efficacy experiment

MATLAB was used to regress the data and create a model that would return the inflow rate of fluid from the aCSF reservoir into a semi-permeable device system driven by the osmotic pressure gradient. After cleaning and smoothing the raw data, the script fits a physics-based model to the data by solving a governing differential equation and minimizing the mean absolute percentage error (MAPE) between the measured and simulated ρ. The model assumes ideal mixing, negligible membrane fouling, and no reverse solute flux. By estimating the osmotic inflow rate F, this approach quantitatively captures the mass transfer behavior across the membrane under controlled experimental

conditions, allowing us to evaluate device performance and fluid uptake over time. This inflow rate (F) is dictated by the dynamic volume, $V(t)$, increase observed in the system as shown below. Since the volume of the system was taken at the beginning and end of the experiment, 5.4.1 can be linearized to represent the overall change in volume with respect to time as a function of inflow rate.

$$\frac{dV}{dt} = F \rightarrow V(t) = V_0 + Ft \tag{5.4.1}$$

The change in the system density over time is modelled in Equation 5.4.2 and describes the change in density over time in the draw system, (ρ), as a function of the constant density from the aCSF reservoir (ρ_{in}), volume, and inflow rate.

$$\frac{d\rho}{dt} = \frac{F}{V(t)}(\rho_{in} - \rho) \tag{5.4.2}$$

The model that accurately predicts the inflow rate of the system in $\frac{L}{min}$.

Parameter	Value	Units	Description
V0	0.0233	L	Initial volume in the draw chamber
ΔT	3600	s	Total experiment time
ρ _in	1.00527	g/ccm	Density of the incoming aCSF solution for Membrane 1
ρ _in2	1.00460	g/ccm	Density of the incoming aCSF solution for Membrane 2

Table 5.2 Parameters for 1% agarose hydrogel tangential flow study.

Dataset	Vf (L)	F (L/min) e-7	rho_0 (g/ccm)	MAPE (%)	Time (hour)
DHigh1	0.0253	2.08	1.0917	0.002978	1
DLow1	0.0251	2.11	1.0946	0.006404	2
DHigh2	0.0253	1.4	1.0933	0.007948	3
DLow2	0.0253	0.814	1.0927	0.000685	4
DHigh3	0.0253	1.11	1.0930	0.003999	5
DLow3	0.0258	0.722	1.0927	0.000859	6
DHigh21	0.0253	1.87	1.095	0.00193	1
DLow21	0.0253	1.65	1.0958	0.004351	2
DHigh22	0.0251	1.47	1.0953	0.007208	3

DLow22	0.0253	1.71	1.0955	0.003781	4
DHigh23	0.0253	1.42	1.0955	0.004047	5
DLow23	0.0258	0.783	1.0958	0.000372	6

Table 5.3 Flux data for the 1% agarose tangential flow study

Parameter	Value	Units	Description
V0	0.02454	L	Initial volume in the draw chamber
ΔT	2700	s	Total experiment time
ρ _in	1.00443	g/ccm	Density of the incoming aCSF solution for Membrane 1
ρ _in2	1.00473	g/ccm	Density of the incoming aCSF solution for Membrane 2

Table 5.4 Parameters for 2% agarose hydrogel tangential flow study

Dataset	Vf (L)	F (L/min) e-7	rho_0 (g/ccm)	MAPE (%)	Time (hour)
DHigh1	0.0253	0.528	1.0971	0.004705	1
DLow1	0.0251	0.523	1.0967	0.000835	2
DHigh2	0.0253	0.594	1.0958	0.001823	3
DLow2	0.0253	0.544	1.0956	0.000984	4
DHigh3	0.0253	0.521	1.0951	0.003647	5
DLow3	0.0258	0.571	1.0942	0.002141	6
DHigh21	0.0255	0.626	1.0964	0.003567	1
DLow21	0.25	0.601	1.0960	0.000648	2
DHigh22	0.0253	0.615	1.0951	0.002165	3
DLow22	0.0258	0.676	1.0949	0.003564	4
DHigh23	0.0254	0.565	1.0945	0.007986	5
DLow23	0.0255	0.699	1.0937	0.003421	6

Table 5.5 Flux data for the 2% agarose tangential flow study

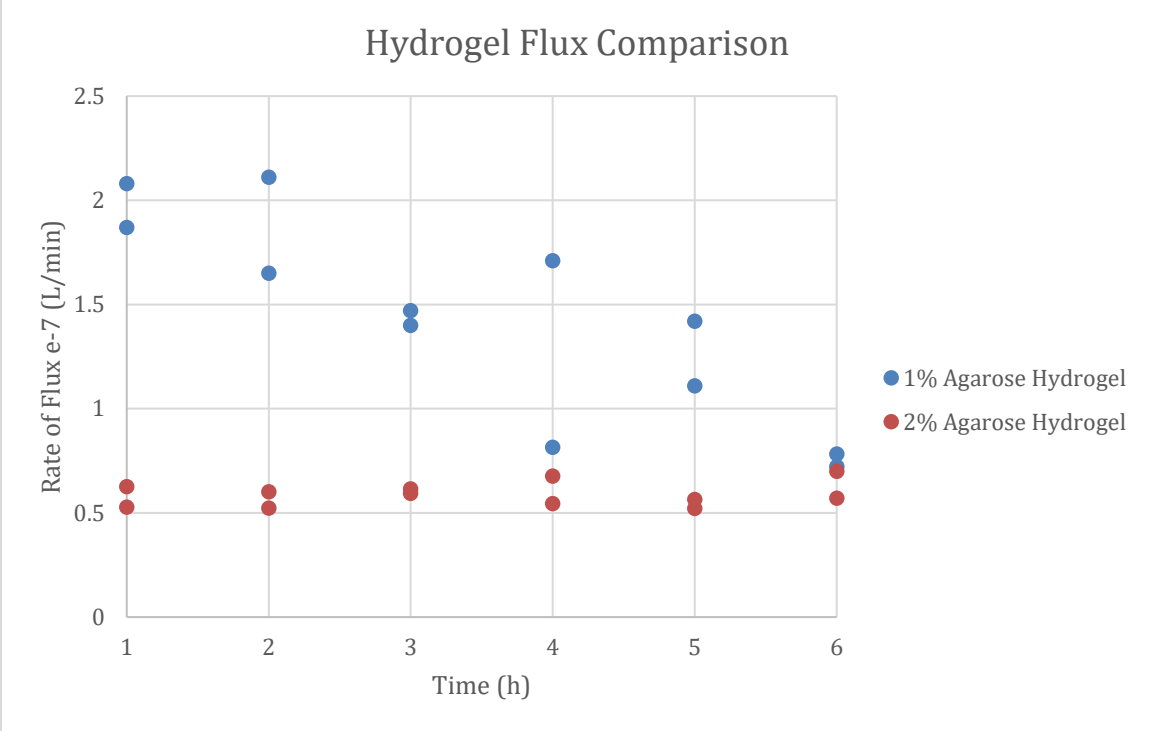

Figure 5.13 Flux comparison of 1% and 2% agarose hydrogel at different tangential flow rates

The inherent design of the OTD with a flat sheet membrane ensures that any force within the chamber will introduce bowing forces to the membrane. The high shear rate introduced to the chamber at either speed introduced high forces on the membrane which caused it to bow towards the agar gel. The agar gel at 1% is an excellent conductive material to facilitate the connection between the aCSF reservoir and the membrane. However, in the proposed animal studies the membrane will need a functionally stronger material that will handle minor displacements and movements over three days. Figure 5.13 shows that a higher concentration hydrogel provides similar flux while maintaining the structural integrity necessary for a multi-day experiment.

Analysis of the effect of shear rate on the effective volumetric flowrate through the membrane of the 1% hydrogel showed no dependency on the shear rate but did

exhibit the same hydrogel degradation as shown in figure 5.14. While this study shows no dependence on the shear rate on the effect of the volumetric flux the degradation of the agarose hydrogel layer made it difficult to ascertain the effectiveness of this study so a second study was conducted for a 2% agarose hydrogel.

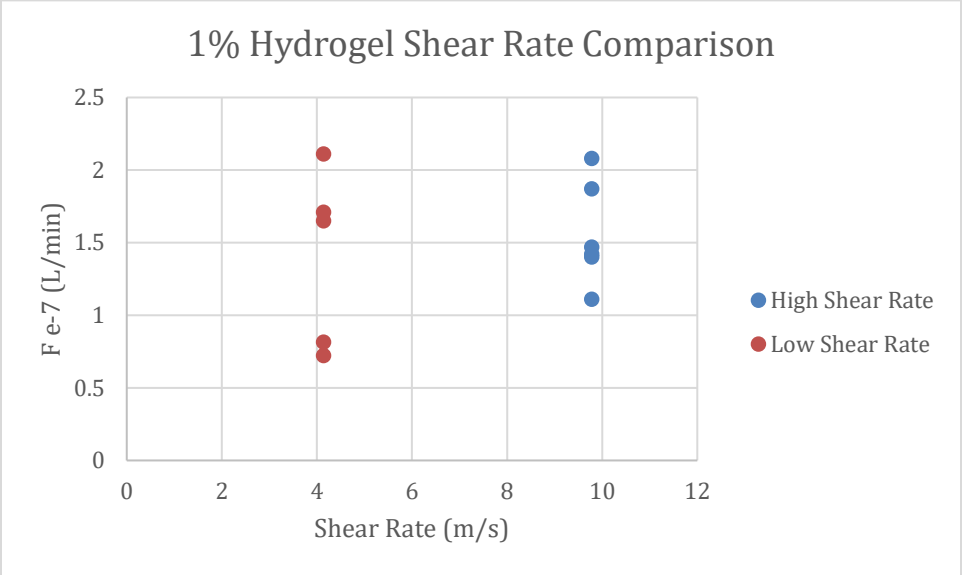

Figure 5.14 Results of shear comparison for the 1% agarose hydrogel study.

The 2% hydrogel study showed no degradation and exhibited a constant flux for both membranes in the study as shown in figure 5.15. This data was uniform and showed only slight variations demonstrating that the shear rate had a negligible effect on the volumetric flux for the pTBI-OTD application. Next, we examined the effectiveness of a no tangential flow condition where the device was active, but the pump was not circulating fluid through the system. At the end of the study the OTD was removed from the reservoir, and the pump ran at a high flow rate until the device was well mixed, and the density stabilized. These experiments were conducted with 3 different membranes for each hydrogel condition as shown in figures 5.16 and 5.17.

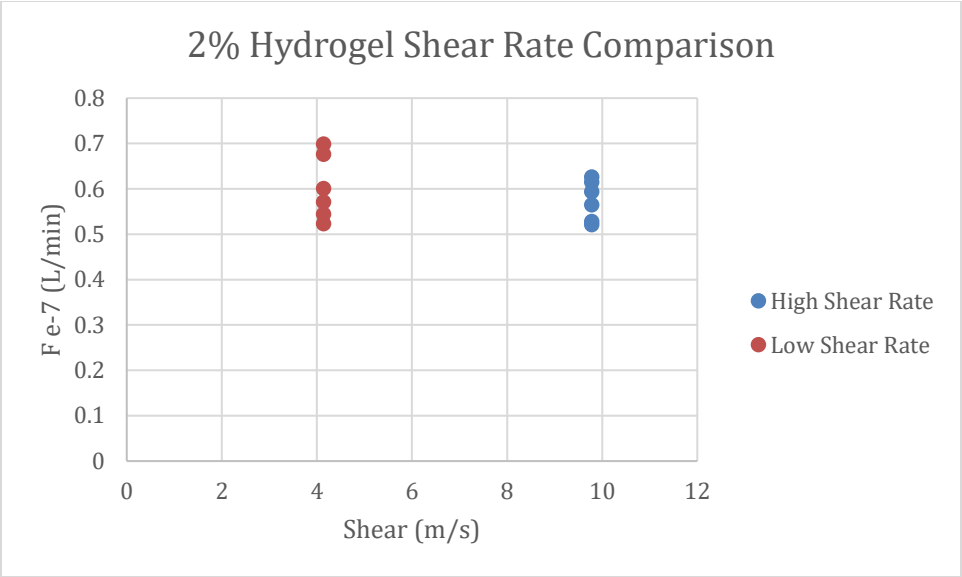

Figure 5.15 Results of shear comparison for the 2% agarose hydrogel study.

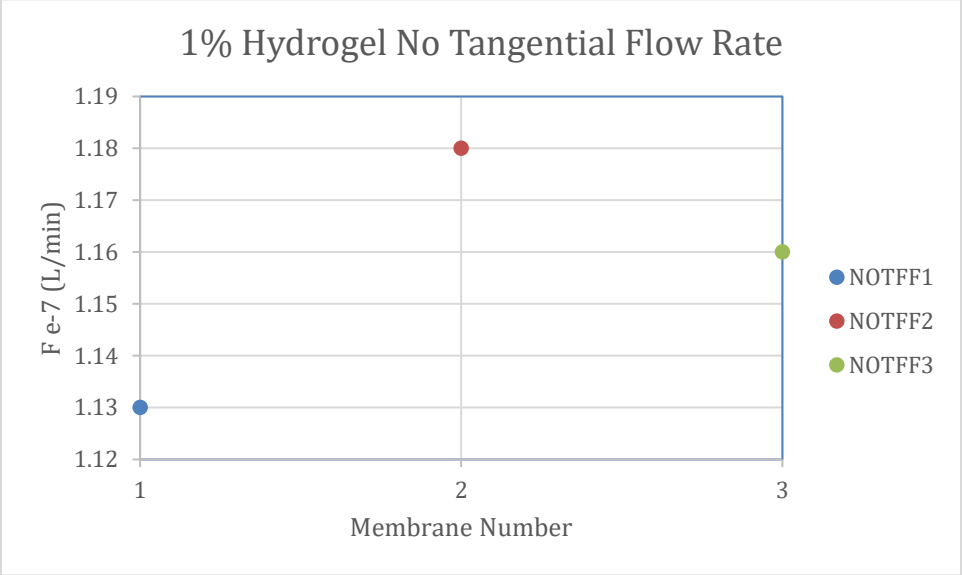

Figure 5.16 No tangential flow rate for the 1% agarose hydrogel.

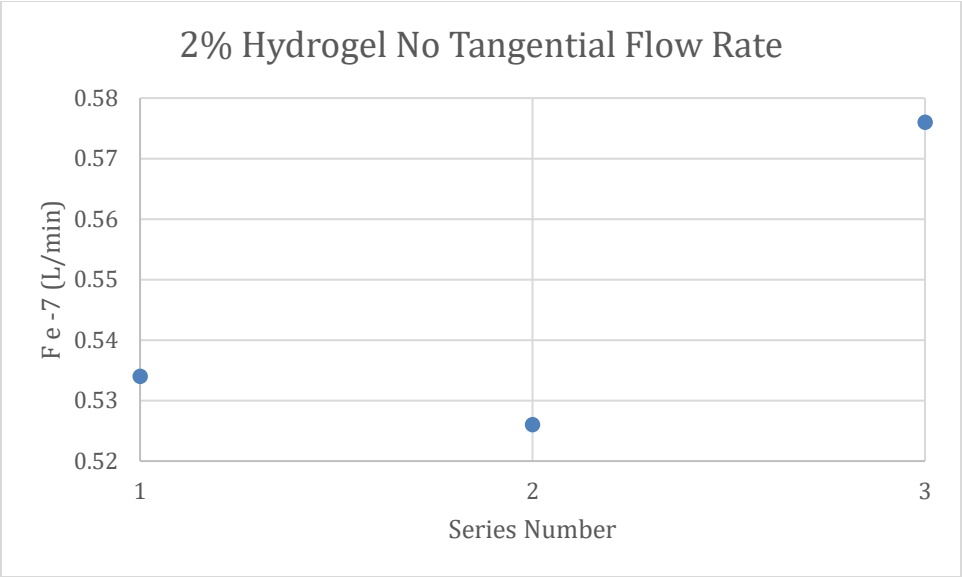

Figure 5.17 No tangential flow rate for the 2% agarose hydrogel.

5.5 Conclusion

The tangential flow studies, while minor in the greater context of this work, have implications on the mathematical model developed in this work. The relevance of the shear rate in regard to the volumetric flow rate is an important factor for that piece of work.

While untested, the pTBI-OTD is a promising platform to test the effectiveness of reducing intracranial pressure on a porcine model. The device is effective at removing fluid from a reservoir in a laboratory setting. Even a slight drop in ICP can greatly reduce intracellular pressure and improve neurological outcomes. The benefits of the device will be tested to address the lack of intervention strategies at the point-of-injury following pTBI but the device may be influential throughout the continuum of care when

decompressive craniectomies are performed since cerebral edema is a persistent challenge following TBI.

Positive findings may have widespread implications in multi-domain operations and have the potential to greatly extend the window of salvage in pTBI patients in situation of prolonged field care and until definitive medical treatment and surgical capabilities can be reached. At the time of writing, the porcine experiments are in progress and the OTD cohorts are scheduled to run in late 2025. I look forward to finding out what impact the OTD will have on neuropathologies in a swine model of pTBI.

Chapter 6. Conclusions

6.1 Findings in This Work

Herein, the osmotic transport device was developed and modified to reduce intraspinal pressure and improve neurological outcomes in non-severed spinal cord injury. The device was based on a previous design our lab had developed and manufactured using SLA technology. The device-maintained contact with the dura of the spinal cord of a rodent for 3-day study and removed fluid to reduce intraspinal pressure.

A device for enhancing decompressive craniectomy was developed for rodents with a hollow fiber module was modified and retrofitted to a custom craniotomy fitting as a fieldable solution to high intracranial pressure from penetrative traumatic brain injury. Additionally, a flat sheet membrane device was developed to reduce the ICP of rodents in a penetrative ballistic injury study. This device was modified for a porcine study for penetrative ballistic injury which is currently underway.

6.2 Future Directions

The osmotic transport device continues to show promise for treating secondary edema injury at the point of injury. The porcine study currently underway will shed light on the extent of damage that can be mitigated in penetrating injury. The neuropathology and histology from this study will form a basis for advancing to human trials. This device can be further developed into a fieldable version.

Schematics of Flat Sheet Membrane OTD Versions and Full Assemblies

A1. Schematic of Base v1.2

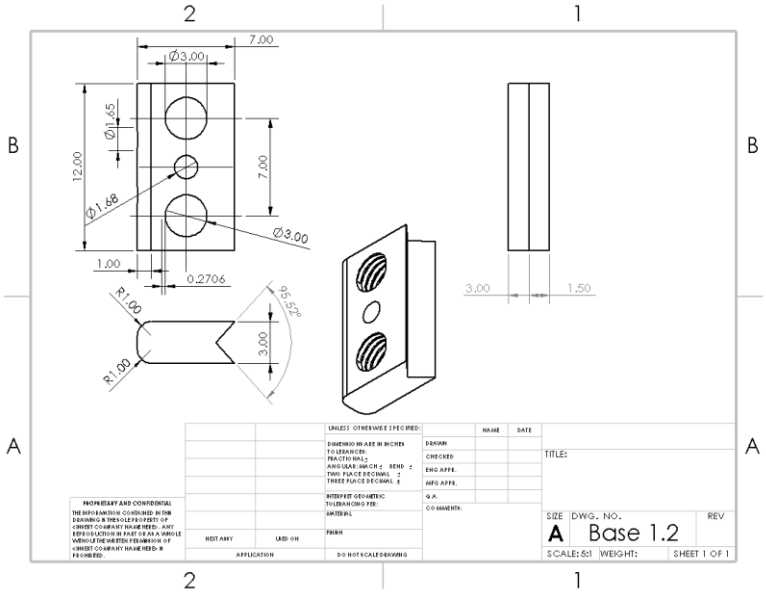

Figure 0.1 Schematic of Base v1.2

A2. Schematic of Bracket v1.2

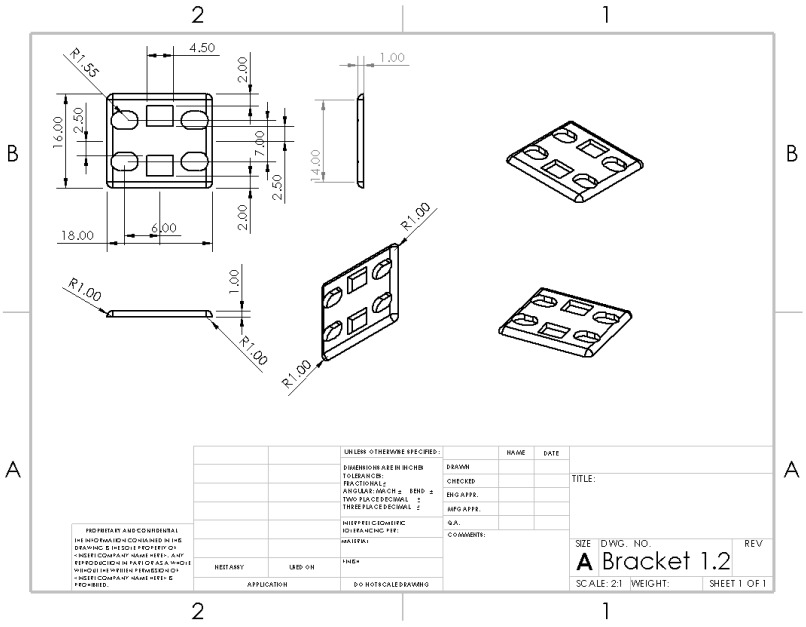

Figure 0.2 Schematic of Bracket v1.2

A3. Schematic of OTD v1.2

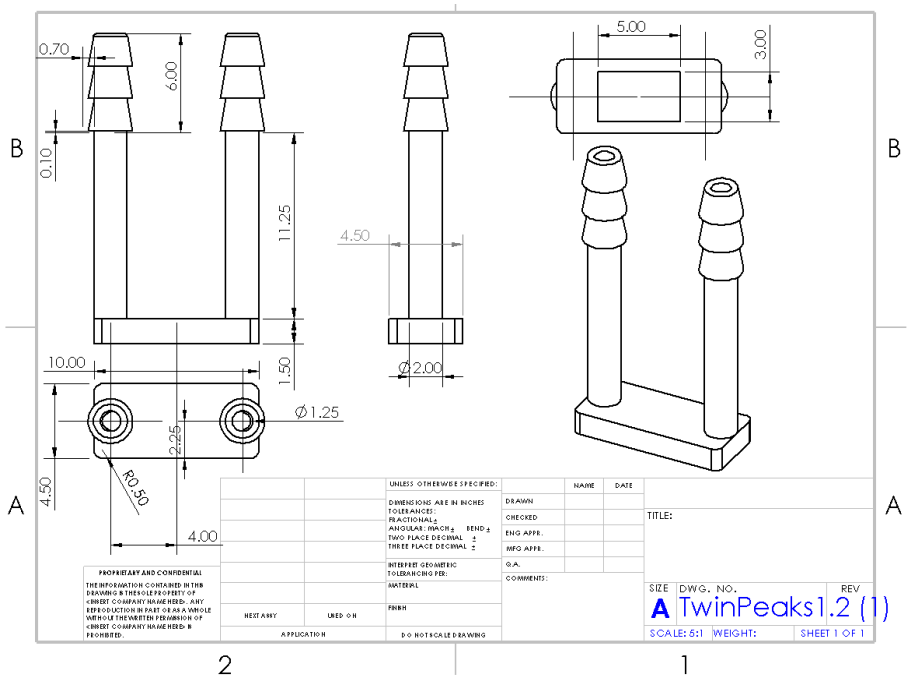

Figure 0.3 Schematic of OTD v1.2

A4. Schematic of v1.2 Assembly

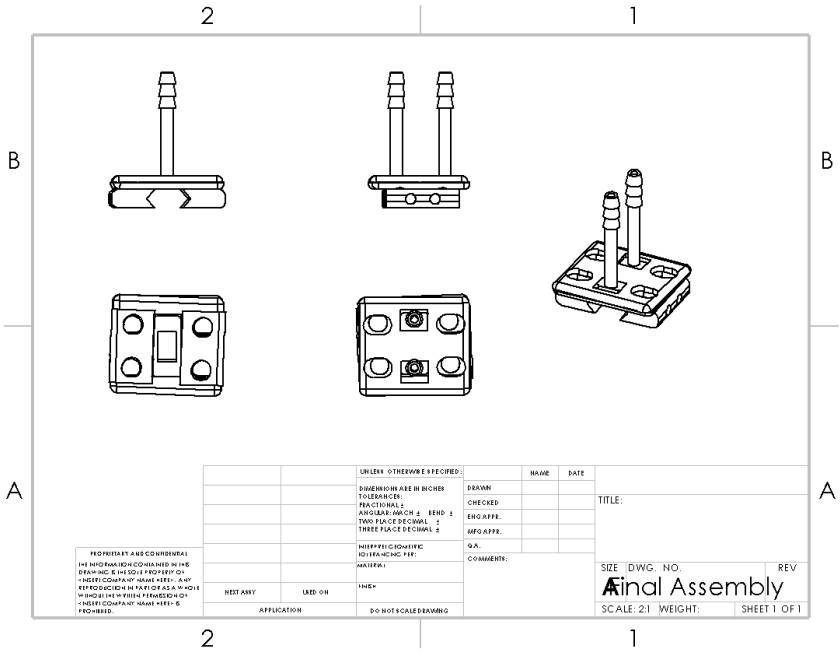

Figure 0.4 Schematic of v1.2 Assembly

A5. Schematic of Bracket 1.3

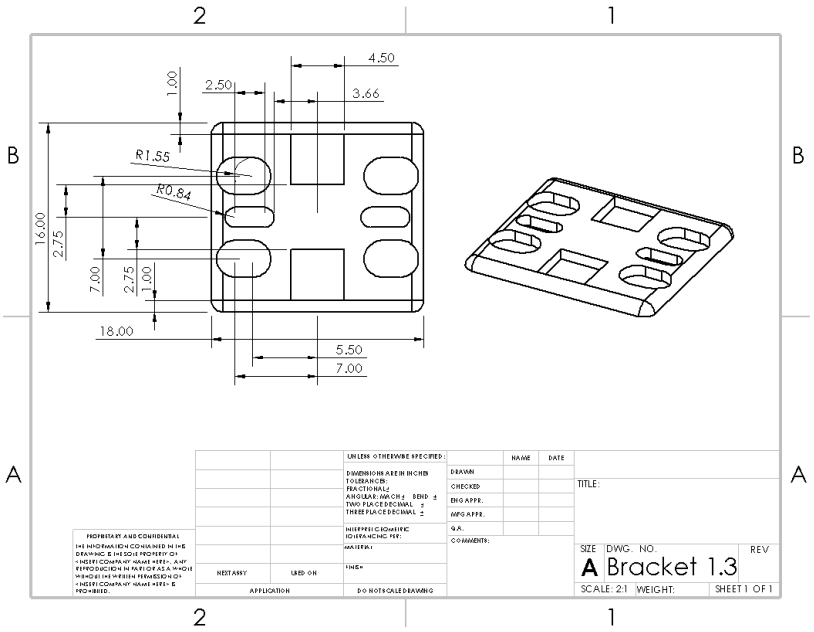

Figure 0.5 Schematic of Bracket v1.3

A6. Schematic of Base 1.3

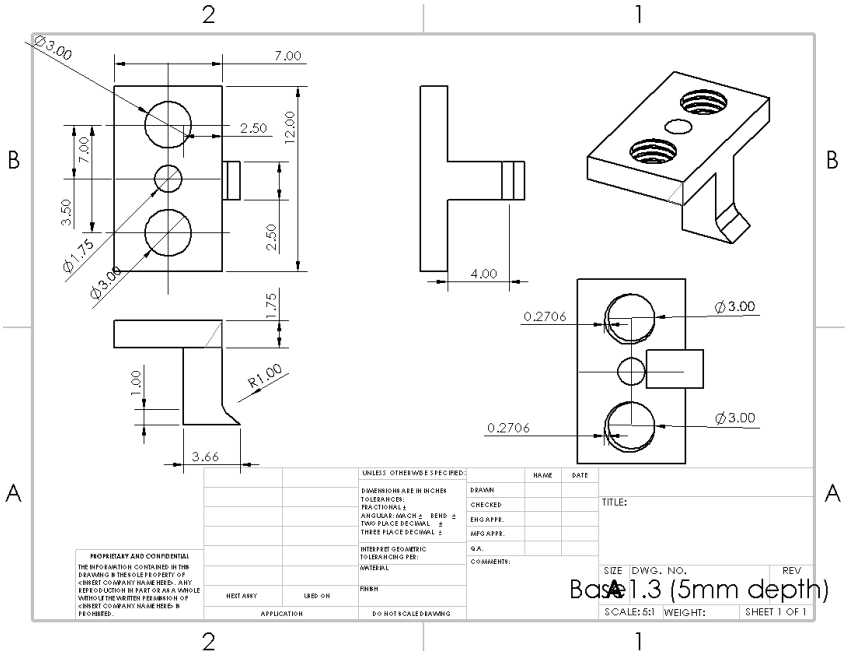

Figure 0.6 Schematic of Base v1.3

A7. Schematic of OTD 1.3 Assembly

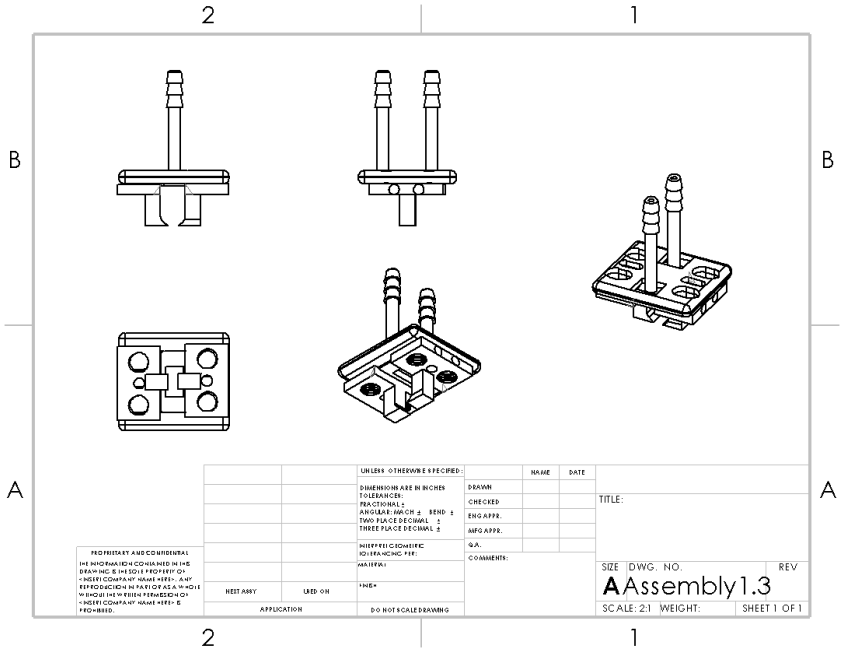

Figure 0.7 Schematic of Assembly v1.3

A8. Schematic Base 1.4

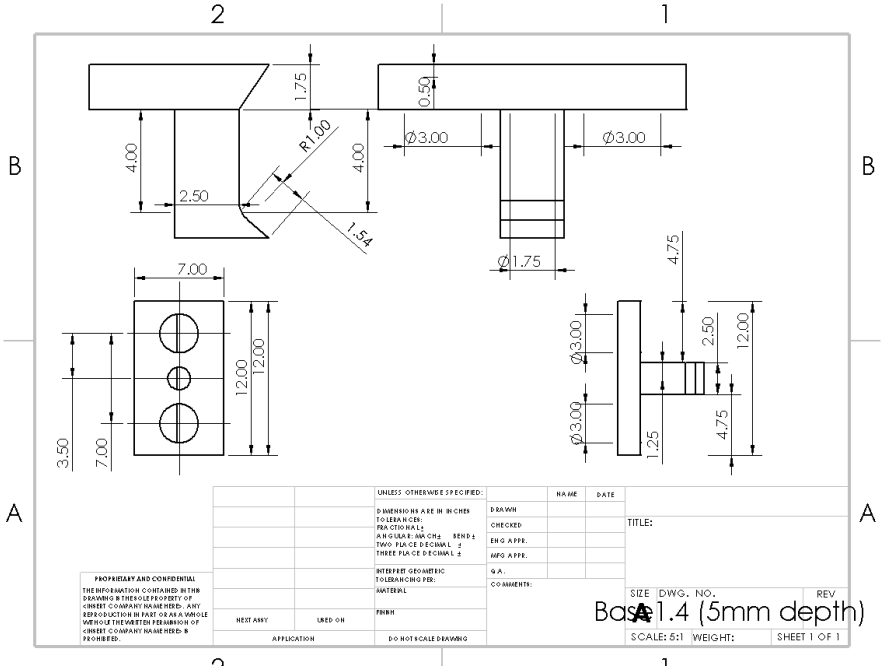

Figure 0.8 Schematic of Base v1.4

A9. Schematic Bracket 1.4

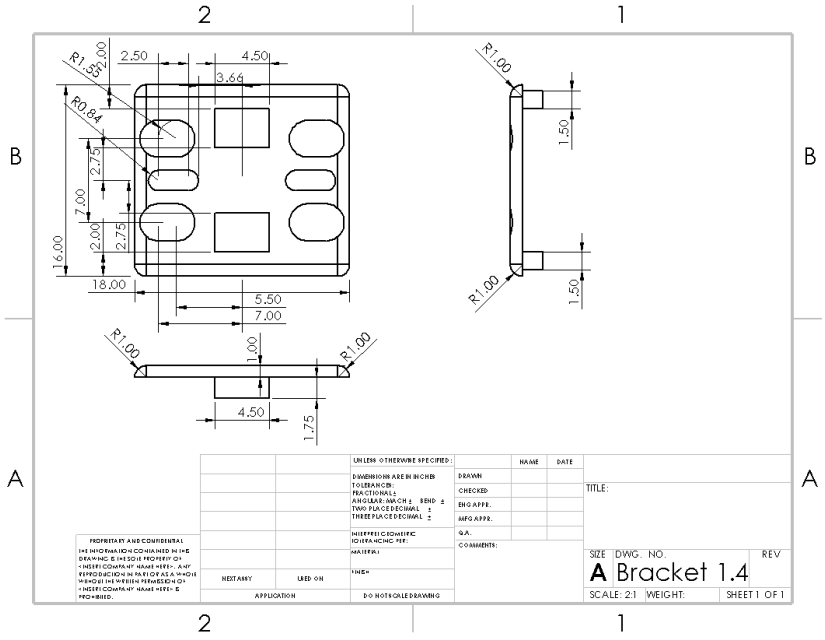

Figure 0.9 Schematic of Bracket v1.4

A10. Schematic of OTD v1.4 Assembly

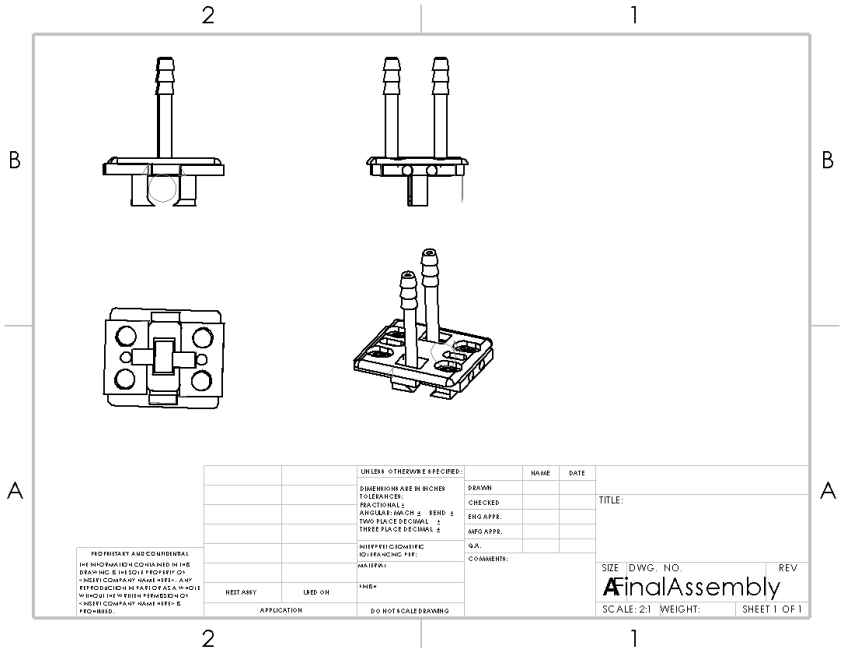

Figure 0.10 Schematic of Assembly v1.4

A11. Schematic of Base 1.6

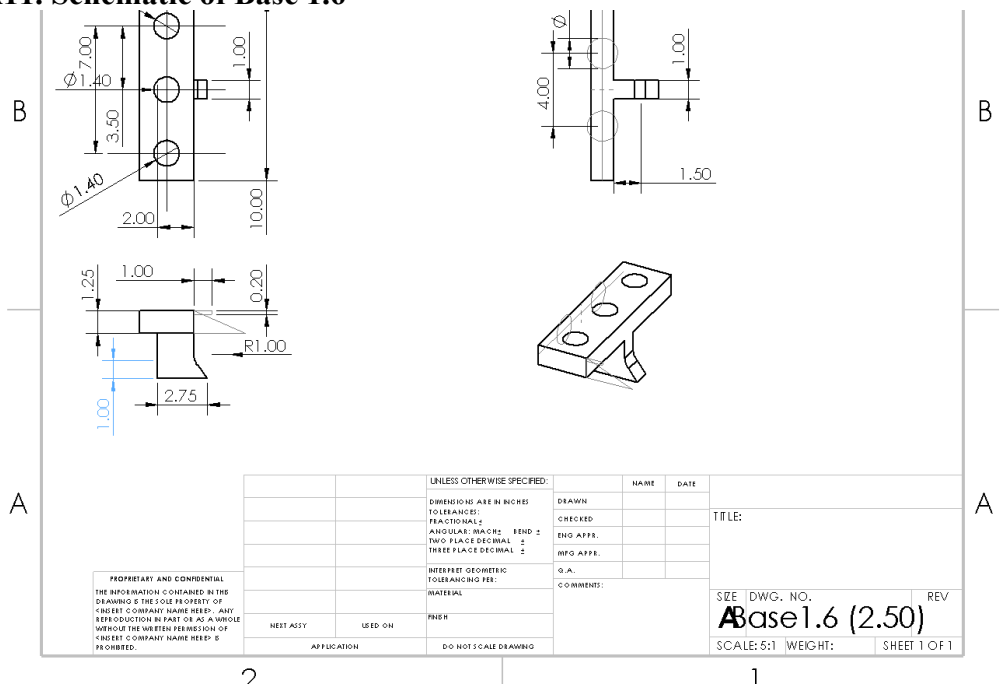

Figure 0.11 Schematic of Base v1.6

A12. Schematic of Bracket 1.6

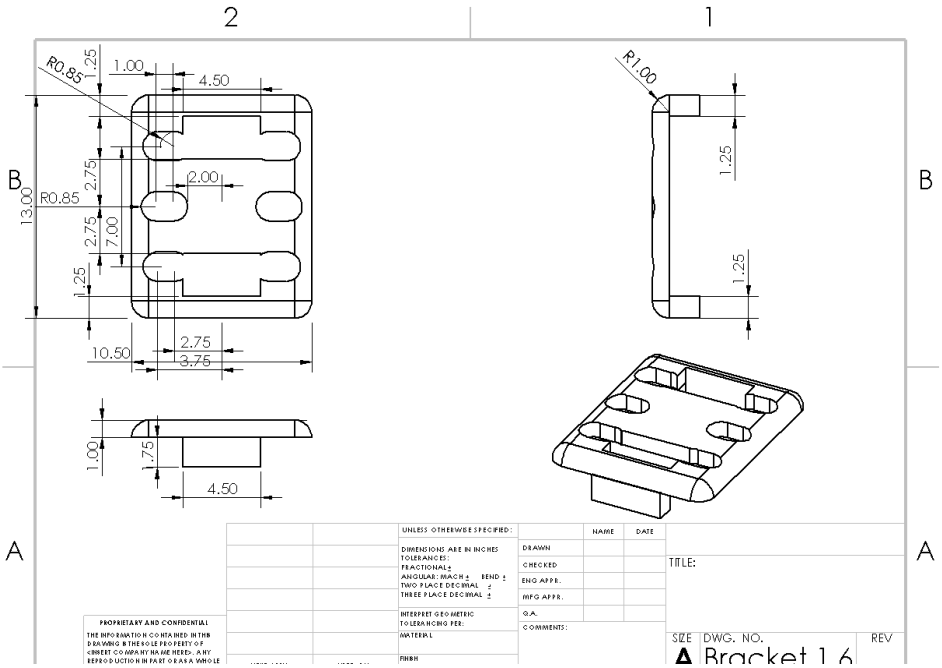

Figure 0.12 Schematic of Bracket v1.6

A13. Schematic of OTD v1.6 Assembly

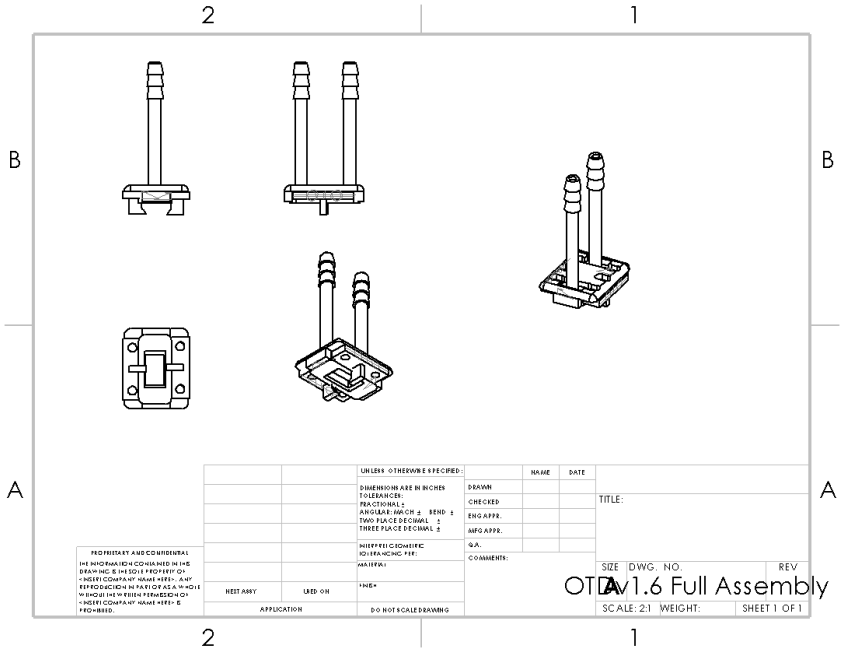

Figure 0.13 Schematic of Assembly v1.6

A14. Schematic of OTD v1.8 Base

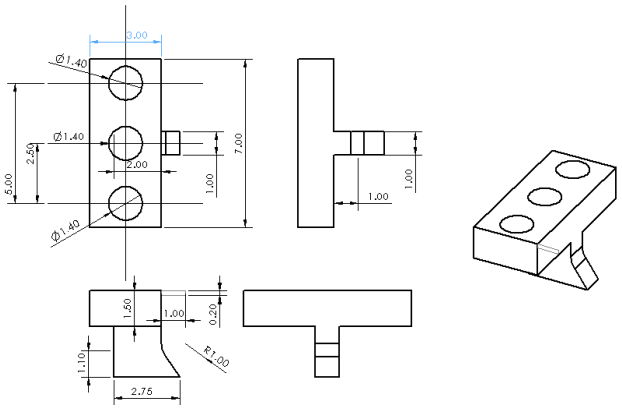

Figure 0.14 Schematic of Base v1.8

A15. Schematic of OTD v1.8 Bracket

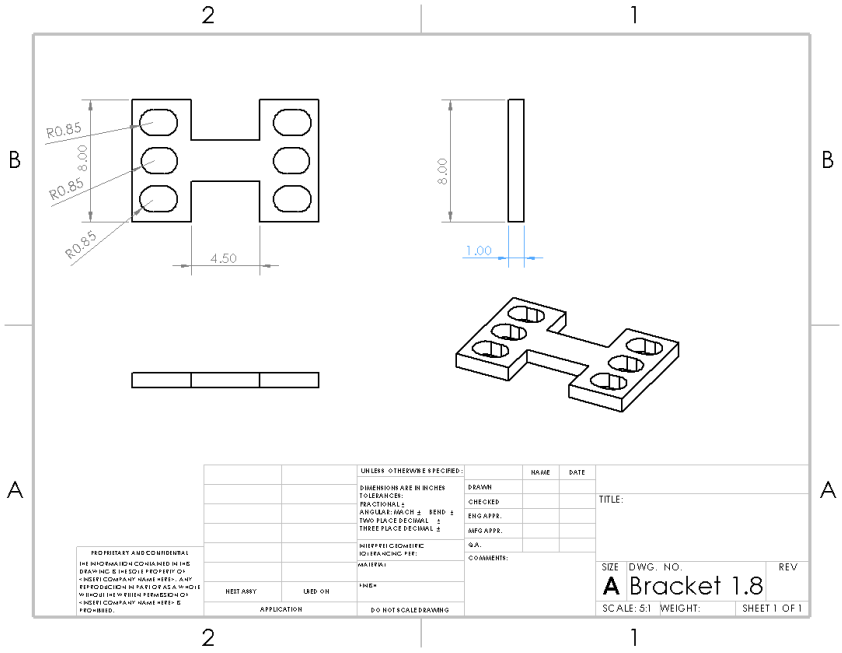

Figure 0.15 Schematic of Bracket v1.8

A16. Schematic of OTD v1.8 Assembly

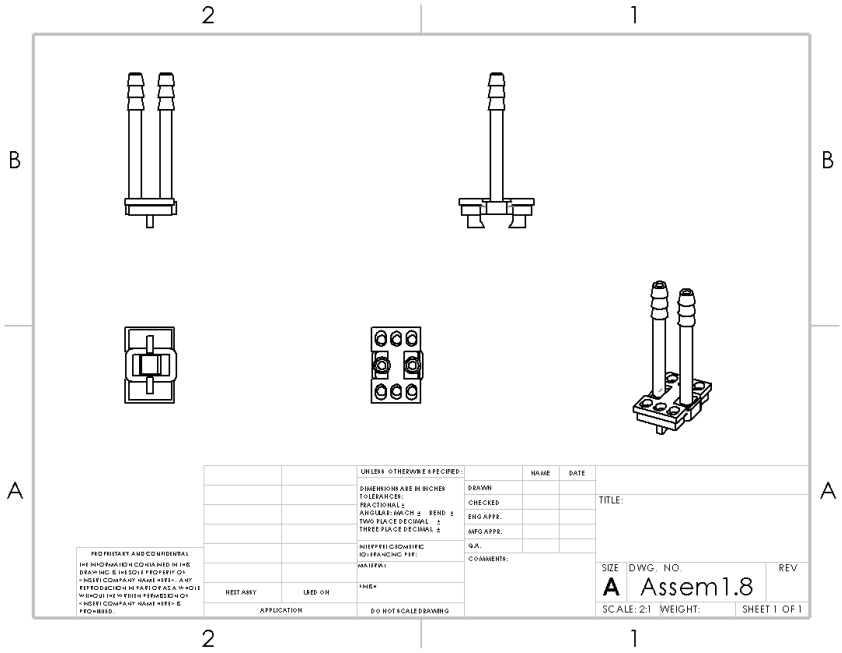

Figure 0.16 Schematic of Assembly v1.8

A17 Schematic of Rat Spinal Cord Harness

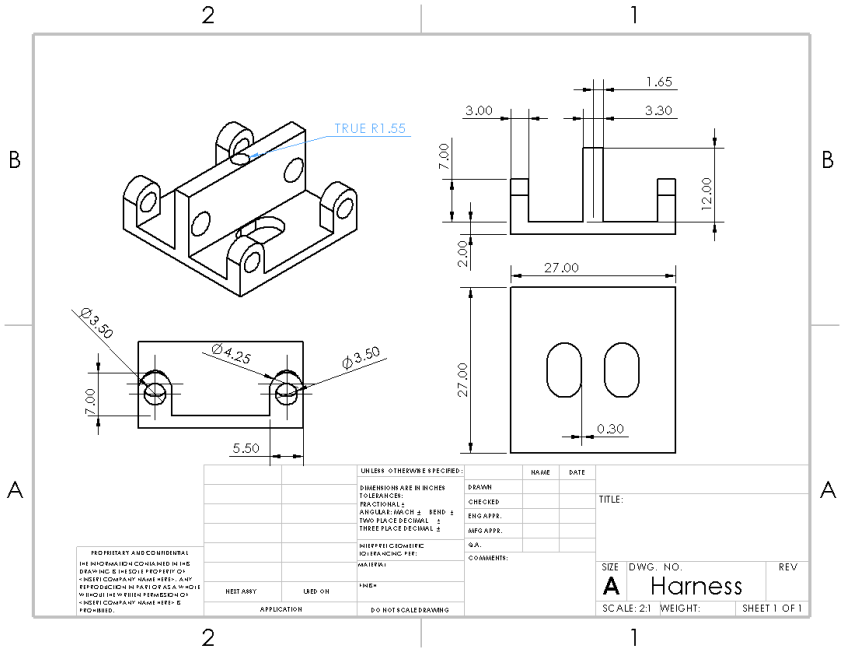

Figure 0.17 Schematic of Rat Harness

Appendix b. Hollow Fiber OTD Schematics

B1. Schematic of Hollow Fiber Skull Attachment

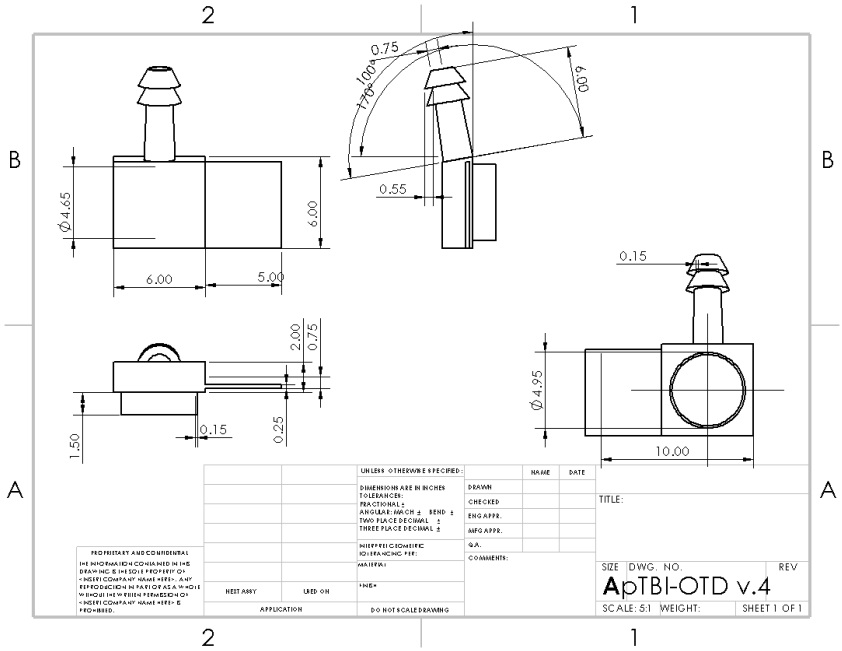

Figure b.1 Schematic of Hollow Fiber Prototype Skull Attachment

B2. Schematic of Hollow Fiber Housing Bottom

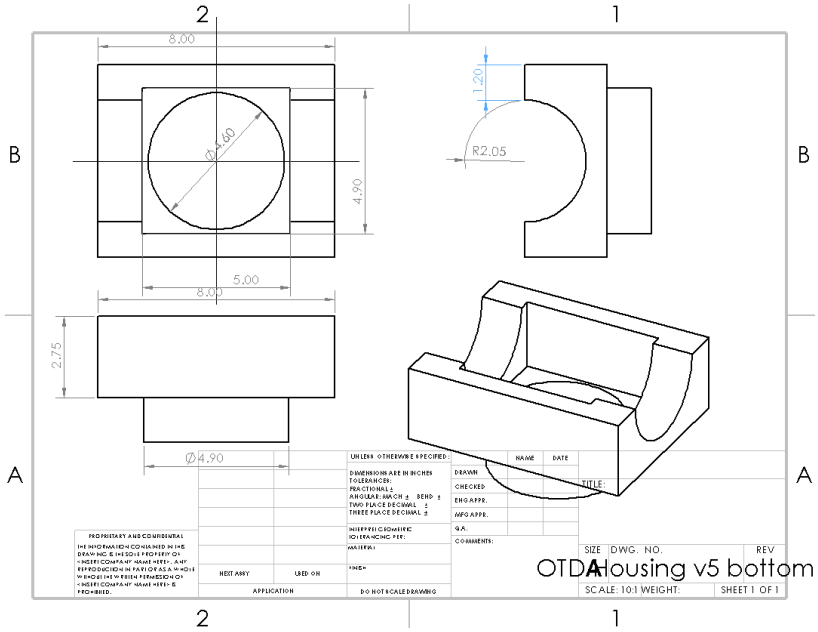

Figure b.2 Schematic of Hollow fiber housing Bottom v.5

B3. Schematic of Hollow Fiber Housing Top

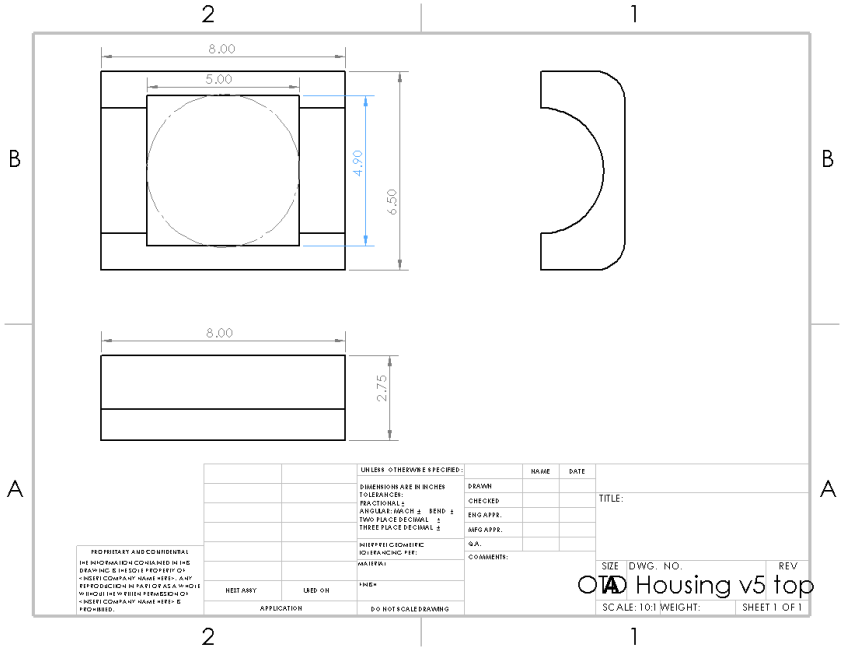

Figure b.3 Schematic of Hollow Fiber Housing Top v.5

B4. Schematic of Hollow Fiber Housing Barbed Tubing Connection

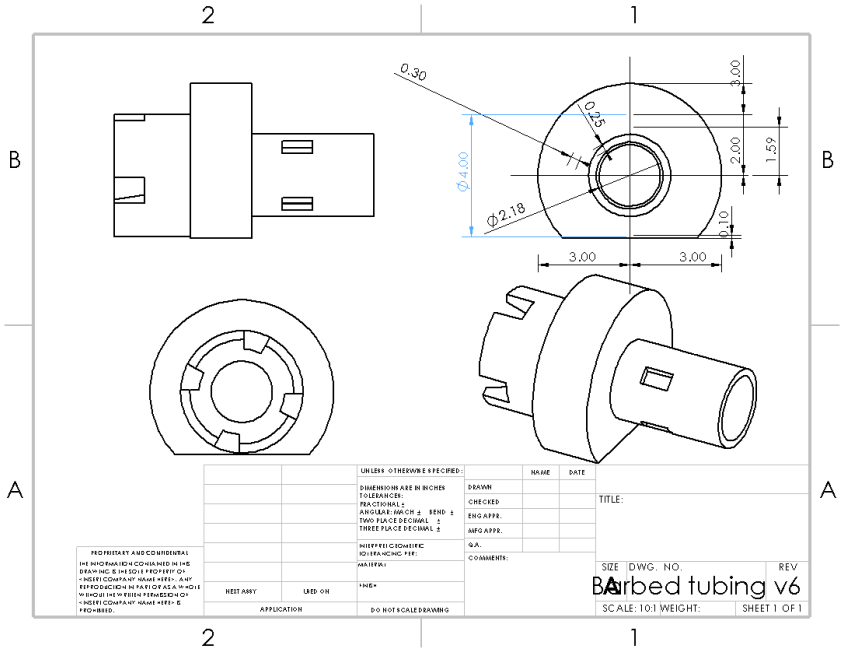

Figure b.4 Schematic of Hollow Fiber Housing Barbed Tubing Connector v.6

B5. Schematic of Barbed Cap

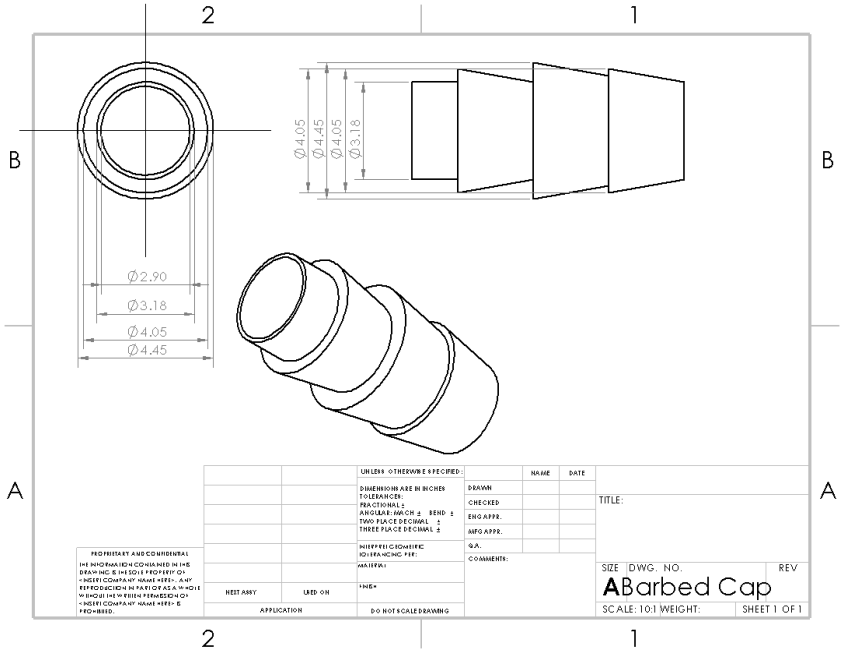

Figure b.5 Schematic of Hollow Fiber Housing Barbed Cap

B6. Schematic of 180 Degree Barbed Cap

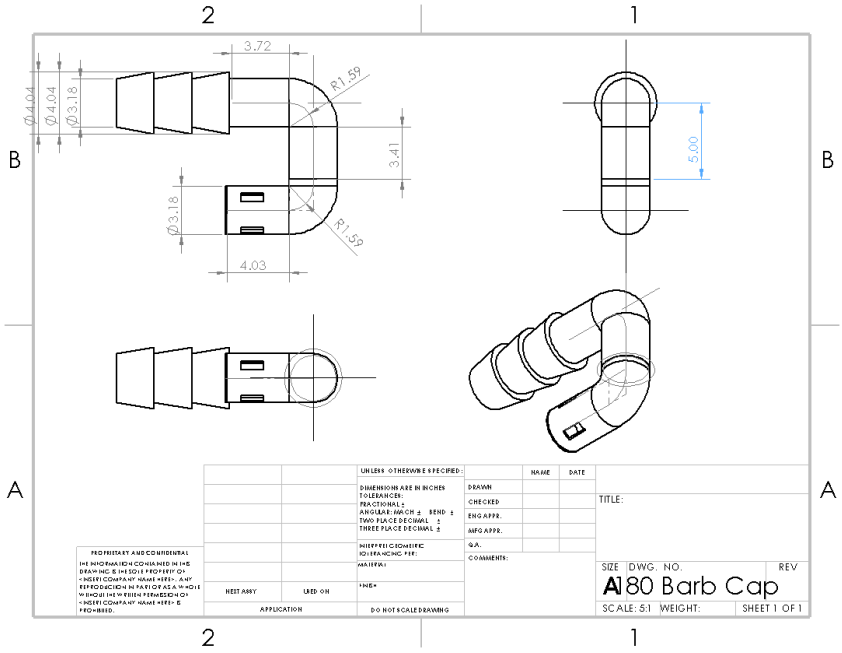

Figure b.6 Schematic of 180 Degree Barbed Cap

B7. Schematic of Hollow Fiber Assembly

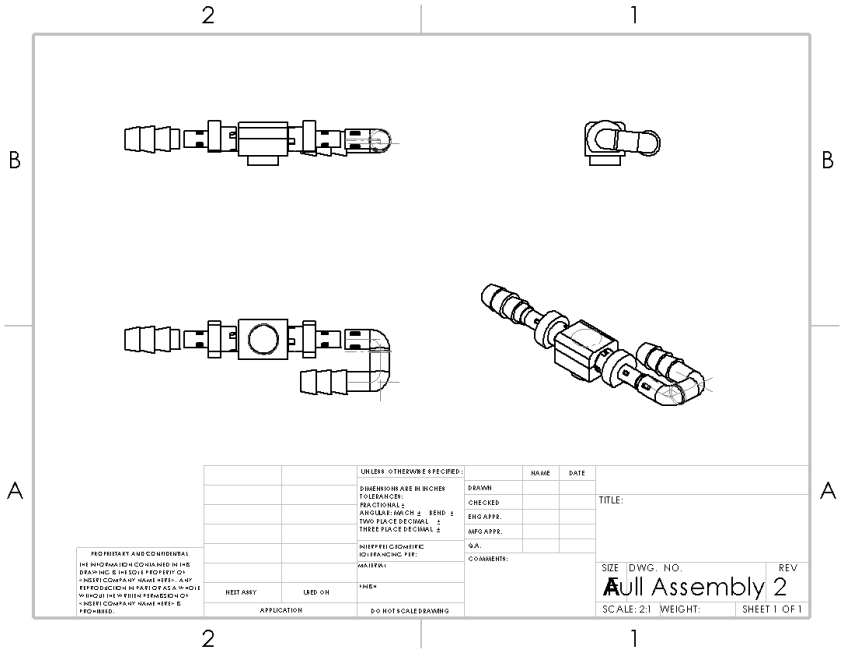

Figure b.7 Schematic of Hollow Fiber Assembly

Appendix c. Rodent Flat Sheet Membrane OTD Schematics

C1. Schematic of Flat Sheet Membrane Rodent Model Base

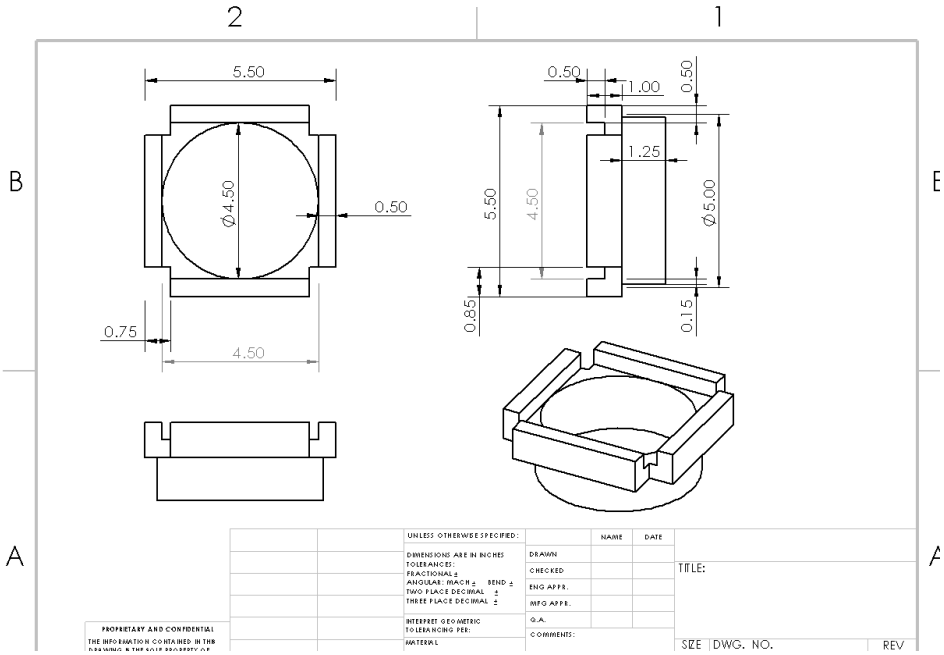

Figure c.1 Schematic of Flat Sheet Membrane Rodent Model Base

C2. Schematic of Flat Sheet Membrane Rodent Model Top

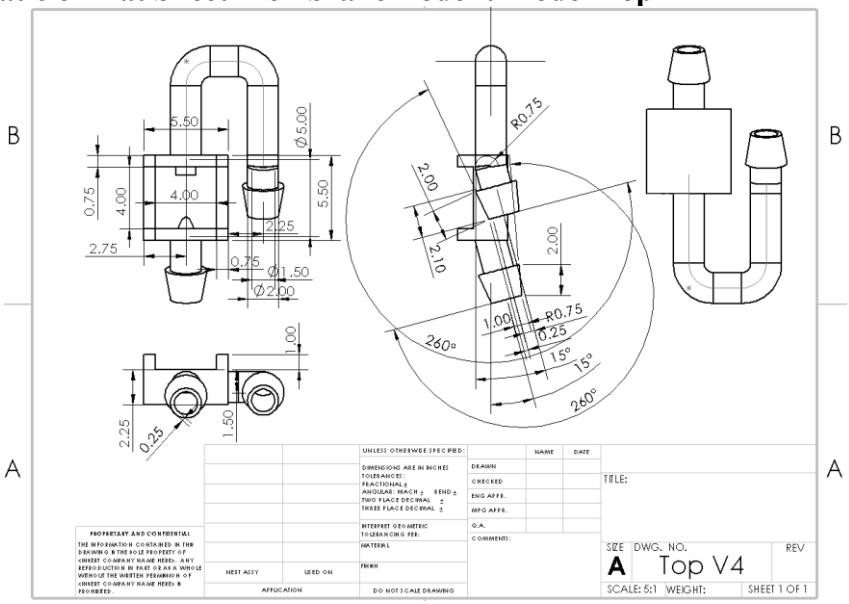

Figure c.2 Schematic of Flat Sheet Membrane Rodent Model Top

C3. Schematic of Flat Sheet Membrane Rodent Model Assembly

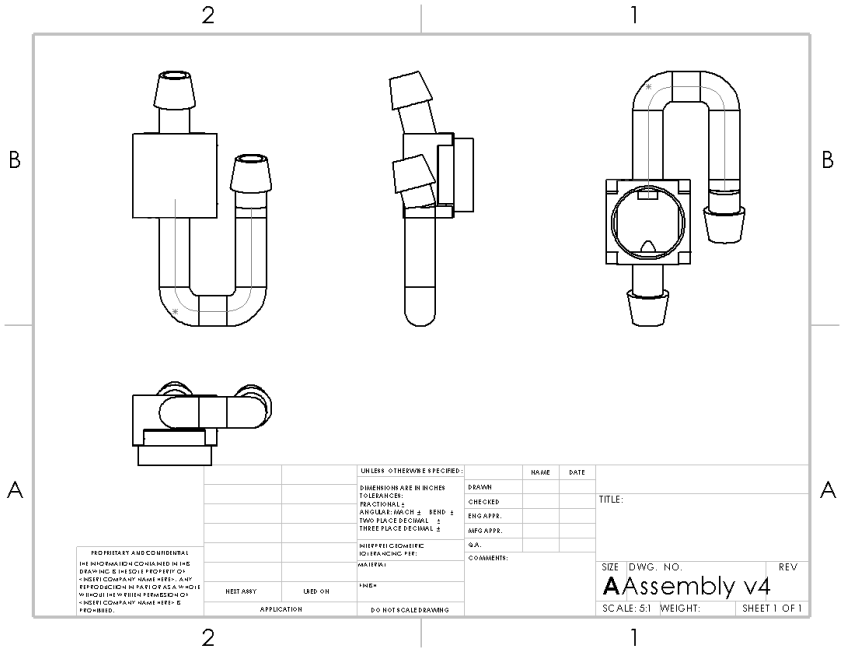

Figure c.3 Schematic of Flat Sheet Membrane Rodent Model Assembly

D1. Schematic of Impermeable Elastic Membrane for Porcine Model OTD

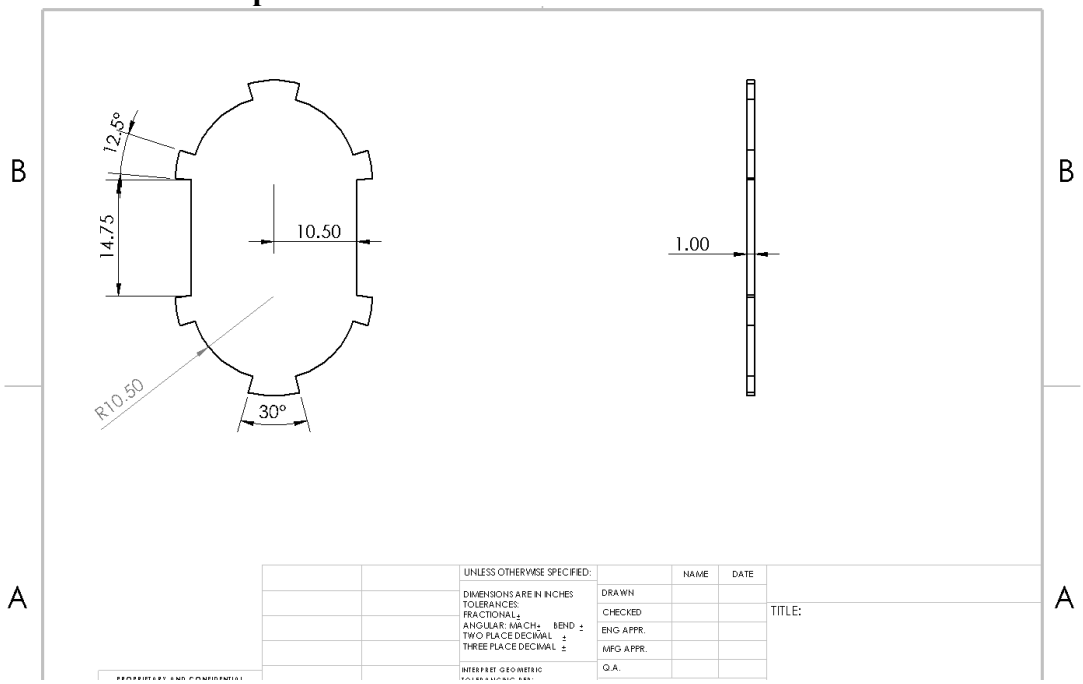

Figure d.1 Schematic of Impermeable Elastic Membrane for Porcine Model OTD

D2. Schematic of Membrane Housing for Porcine Model OTD

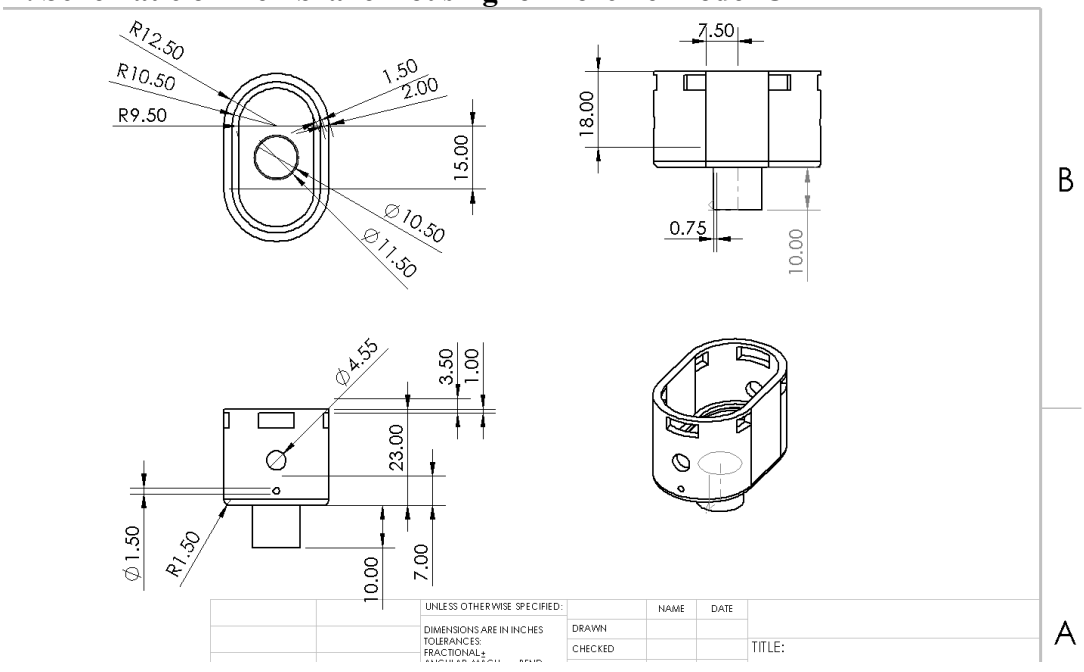

Figure d.2 Schematic of Membrane Housing for Porcine Model OTD

D3. Schematic of Porcine Model OTD Assembly

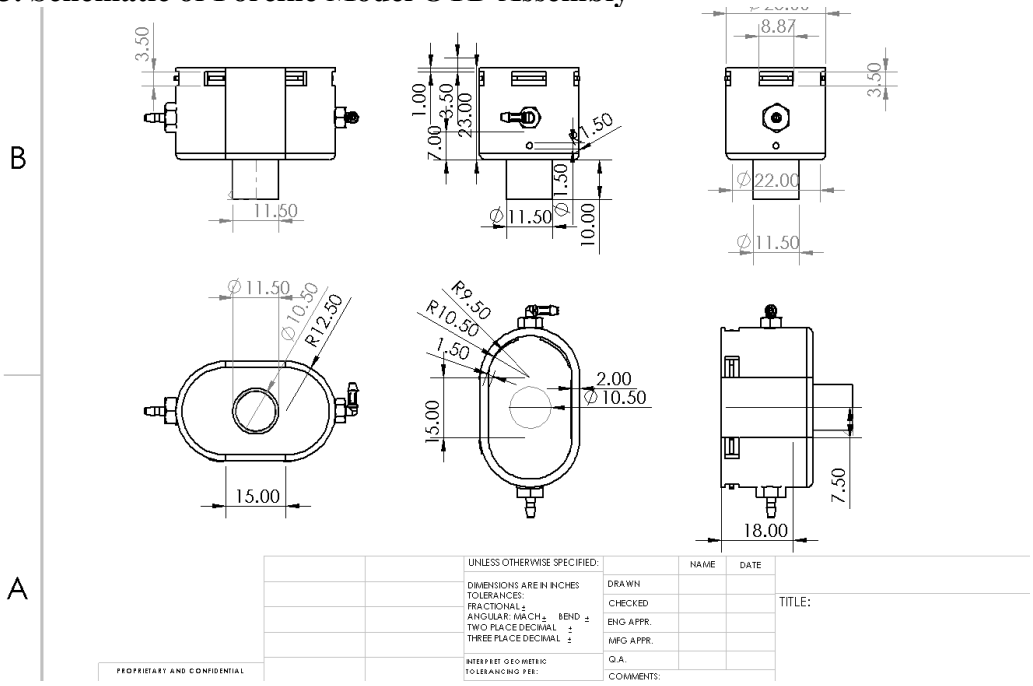

Figure d.3 Schematic of Porcine Model OTD Assembly

Appendix e. Matlab Code for the Analysis of Tangential Flux

E1. Code for Membrane Series 1

```
clc;
clear;

% List of datasets and their corresponding Vf values
datasets = {'DHigh1', 'DHigh2', 'DHigh3', 'DLow1', 'DLow2', 'DLow3'};
Vf_values = struct(...
    'DHigh1', 0.0253, ...
    'DHigh2', 0.0253, ...
    'DHigh3', 0.0253, ...
    'DLow1', 0.0251, ...
    'DLow2', 0.0253, ...
    'DLow3', 0.0258);

deltaT = 3600;  % Fixed deltaT for all datasets

for i = 1:length(datasets)
    process_density_data(datasets{i}, Vf_values.(datasets{i}), deltaT);
end

function process_density_data(filename, Vf, deltaT)
    fprintf('\nProcessing %s.mat...\n', filename);

    % Load data
    data = load([filename, '.mat']);
    raw_data = data.(filename);

    % Clean up rows
    raw_data(end, :) = [];
    raw_data(1:207, :) = [];
    if size(raw_data,1) >= 3663
        raw_data(3663,:) = [];
    end

    % Extract and clean density column
    rho_raw = fillmissing(raw_data.VarName5, 'linear');
    rho_raw(rho_raw < 0.90) = NaN;
    rho_raw = fillmissing(rho_raw, 'linear');
    smoothed = smooth(rho_raw, 0.5);

    % Remove outliers
    residuals = abs(rho_raw - smoothed);
    threshold = std(residuals);
    valid_idx = residuals <= threshold;
    rho_data = rho_raw(valid_idx);
    t_data = (1:length(rho_raw))';
    t_data = t_data(valid_idx);

    % Constants
    rho_in = 1.00527;
```

```
    V0 = 0.0233;

    % Estimate initial flow rate
    F0 = (Vf - V0) / deltaT * 60;  % Convert to L/min
    rho0 = rho_data(1);


    % Optimization
    objFun = @(F) compute_error(F, rho0, t_data, rho_data, rho_in, V0);
    F_est = fminsearch(objFun, F0);
    fprintf('Estimated Flow Rate F: %.8f L/min\n', F_est);

    % Simulate using best-fit F
    [~, rho_fit] = ode45(@(t, rho) odefun(t, rho, F_est, rho_in, V0), t_data,
rho0);

    % Plot results
    figure;
    plot(t_data, rho_data, 'ro', 'DisplayName', 'Measured \rho');
    hold on;
    plot(t_data, rho_fit, 'b-', 'LineWidth', 2, 'DisplayName', 'Model Fit');
    xlabel('Time (seconds)');
    ylabel('\rho (Density in Draw Solution)');
    title(sprintf('Model Fit for %s\nFlow Rate F = %.6g L/min', filename,
F_est));

    % Annotate with equation and error
    fit_error = mean(abs((rho_fit - rho_data) ./ rho_data)) * 100;
    xlims = xlim();
    ylims = ylim();
    eqn_text = sprintf(['d\\rho/dt = F/V(t)·(\\rho_{in} - \\rho)\n' ...
                        'F = %.2e L/min\nMAPE = %.6f%%'], F_est, fit_error);
    x_pos = xlims(1) + 0.05 * range(xlims);
    y_pos = ylims(2) - 0.9 * range(ylims);
    text(x_pos, y_pos, eqn_text, 'FontSize', 10, 'BackgroundColor', 'w',
'EdgeColor', 'k');

    legend('Measured \rho', 'Model Fit');
    grid on;
    hold off;
    disp(rho0)
end

function drho = odefun(t, rho, F, rho_in, V0)
    Vt = V0 + F * t;
    drho = (F / Vt) * (rho_in - rho);
end

function err = compute_error(F, rho0, t_data, rho_data, rho_in, V0)
    [~, rho_model] = ode45(@(t, rho) odefun(t, rho, F, rho_in, V0), t_data,
rho0);
    if length(rho_model) ~= length(rho_data)
```

```
        rho_model = interp1(1:length(rho_model), rho_model, ...
            linspace(1, length(rho_model), length(rho_data)), 'linear',
'extrap');
    end
    err = mean(abs((rho_model - rho_data) ./ rho_data)) * 100;
end
```

E2. Code for Membrane Series 2 Low Speed

```
clc;
clear;

% List of datasets and their corresponding Vf values
datasets = {'DHigh21', 'DHigh22', 'DHigh23', 'DLow21', 'DLow22', 'DLow23'};
Vf_values = struct(...
    'DHigh21', 0.0253, ...
    'DHigh22', 0.0253, ...
    'DHigh23', 0.0253, ...
    'DLow21', 0.0251, ...
    'DLow22', 0.0253, ...
    'DLow23', 0.0258);

deltaT = 3600;  % Fixed deltaT for all datasets

for i = 1:length(datasets)
    process_density_data(datasets{i}, Vf_values.(datasets{i}), deltaT);
end

function process_density_data(filename, Vf, deltaT)
    fprintf('\nProcessing %s.mat...\n', filename);

    % Load data
    data = load([filename, '.mat']);
    raw_data = data.(filename);

    % Clean up rows
    raw_data(end, :) = [];
    raw_data(1:207, :) = [];
    if size(raw_data,1) >= 3663
        raw_data(3663,:) = [];
    end

    % Extract and clean density column
    rho_raw = fillmissing(raw_data.VarName5, 'linear');
    rho_raw(rho_raw < 0.90) = NaN;
    rho_raw = fillmissing(rho_raw, 'linear');
    smoothed = smooth(rho_raw, 0.1);

    % Remove outliers
    residuals = abs(rho_raw - smoothed);
    threshold = std(residuals);
```

```
    valid_idx = residuals <= threshold;
    rho_data = rho_raw(valid_idx);
    t_data = (1:length(rho_raw))';
    t_data = t_data(valid_idx);

    % Constants
    rho_in = 1.00460;
    V0 = 0.02307;

    % Estimate initial flow rate
    F0 = (Vf - V0) / deltaT * 60;  % Convert to L/min
    rho0 = rho_data(1);


    % Optimization
    objFun = @(F) compute_error(F, rho0, t_data, rho_data, rho_in, V0);
    F_est = fminsearch(objFun, F0);
    fprintf('Estimated Flow Rate F: %.8f L/min\n', F_est);

    % Simulate using best-fit F
    [~, rho_fit] = ode45(@(t, rho) odefun(t, rho, F_est, rho_in, V0), t_data,
rho0);

    % Plot results
    figure;
    plot(t_data, rho_data, 'ro', 'DisplayName', 'Measured \rho');
    hold on;
    plot(t_data, rho_fit, 'b-', 'LineWidth', 2, 'DisplayName', 'Model Fit');
    xlabel('Time (seconds)');
    ylabel('\rho (Density in Draw Solution)');
    title(sprintf('Model Fit for %s\nFlow Rate F = %.6g L/min', filename,
F_est));

    % Annotate with equation and error
    fit_error = mean(abs((rho_fit - rho_data) ./ rho_data)) * 100;
    xlims = xlim();
    ylims = ylim();
    eqn_text = sprintf(['d\\rho/dt = F/V(t)·(\\rho_{in} - \\rho)\n' ...
                    'F = %.2e L/min\nMAPE = %.6f%%'], F_est, fit_error);
    x_pos = xlims(1) + 0.05 * range(xlims);
    y_pos = ylims(2) - 0.9 * range(ylims);
    text(x_pos, y_pos, eqn_text, 'FontSize', 10, 'BackgroundColor', 'w',
'EdgeColor', 'k');

    legend('Measured \rho', 'Model Fit');
    grid on;
    hold off;
    disp(rho0)
end

function drho = odefun(t, rho, F, rho_in, V0)
    Vt = V0 + F * t;
```

```
    drho = (F / Vt) * (rho_in - rho);
end

function err = compute_error(F, rho0, t_data, rho_data, rho_in, V0)
    [~, rho_model] = ode45(@(t, rho) odefun(t, rho, F, rho_in, V0), t_data,
rho0);
    if length(rho_model) ~= length(rho_data)
        rho_model = interp1(1:length(rho_model), rho_model, ...
            linspace(1, length(rho_model), length(rho_data)), 'linear',
'extrap');
    end
    err = mean(abs((rho_model - rho_data) ./ rho_data)) * 100;
end
```

BoxPump Code and Schematic Design

F1. Code for Arduino Boxpump

```
#define PUMP_PIN 10       // PWM capable pin
#define VALVE_PIN 12
#define LED_PIN 6
#define RED_LED_PIN 5
#define BUTTON_PIN 7

bool systemRunning = false;
unsigned long startTime = 0;
unsigned long lastOffTime = 0;
unsigned long valveCycleStart = 0;
bool valveHasCycled = false;

const unsigned long runTime = 600000;         // 10 min ON (full power)
const unsigned long restTime = 3000000;      // 50 min OFF (PWM)
const unsigned long valveActivationTime = 1800000; // 30 min
const unsigned long valveCycleDuration = 1000; // 10s
const int pwmOffSpeed = 0;                 // PWM value during "off" state
(0-255)

void setup() {
  pinMode(PUMP_PIN, OUTPUT);
  pinMode(VALVE_PIN, OUTPUT);
  pinMode(LED_PIN, OUTPUT);
  pinMode(RED_LED_PIN, OUTPUT);

  digitalWrite(PUMP_PIN, LOW);
  digitalWrite(VALVE_PIN, LOW);
  digitalWrite(RED_LED_PIN, LOW);
```

```
  digitalWrite(LED_PIN, HIGH);

  pinMode(BUTTON_PIN, INPUT_PULLUP);

  lastOffTime = millis();
  systemRunning = false;
}

void loop() {
  // Handle button press
  if (digitalRead(BUTTON_PIN) == LOW) {
    delay(50);
    if (digitalRead(BUTTON_PIN) == LOW) {
      toggleSystem();
    }
    while (digitalRead(BUTTON_PIN) == LOW);
  }

  // Pump state machine
  if (systemRunning) {
    if (millis() - startTime >= runTime) {
      shutDownSystem();
    } else {
      analogWrite(PUMP_PIN, 200); // Full speed when running
    }
  } else {
    // Auto-restart condition
    if (millis() - lastOffTime >= restTime) {
      startSystem();
    } else {
      analogWrite(PUMP_PIN, pwmOffSpeed); // Reduced speed during "off"
    }

    // Valve control
    if (!valveHasCycled && (millis() - lastOffTime >=
valveActivationTime)) {
      valveCycleStart = millis();
      valveHasCycled = true;
    }

    if (valveHasCycled) {
      if (millis() - valveCycleStart < valveCycleDuration) {
```

```
        // 10Hz cycling
        static unsigned long lastToggle = 0;
        if (millis() - lastToggle >= 100) {
          digitalWrite(VALVE_PIN, !digitalRead(VALVE_PIN));
          lastToggle = millis();
        }
      } else {
        digitalWrite(VALVE_PIN, LOW);
      }
    }
  }

  // LED control
  digitalWrite(LED_PIN, systemRunning ? LOW : (millis() % 1000 < 500 ?
HIGH : LOW));
}

void toggleSystem() {
  if (systemRunning) shutDownSystem();
  else startSystem();
}

void startSystem() {
  systemRunning = true;
  valveHasCycled = false;
  startTime = millis();
  analogWrite(PUMP_PIN, 255); // Full speed
  digitalWrite(VALVE_PIN, LOW);
}

void shutDownSystem() {
  systemRunning = false;
  valveHasCycled = false;
  lastOffTime = millis();
  analogWrite(PUMP_PIN, pwmOffSpeed); // Reduced speed
  digitalWrite(VALVE_PIN, LOW);
}
```

F2. Electric Schematic for the BoxPump Device

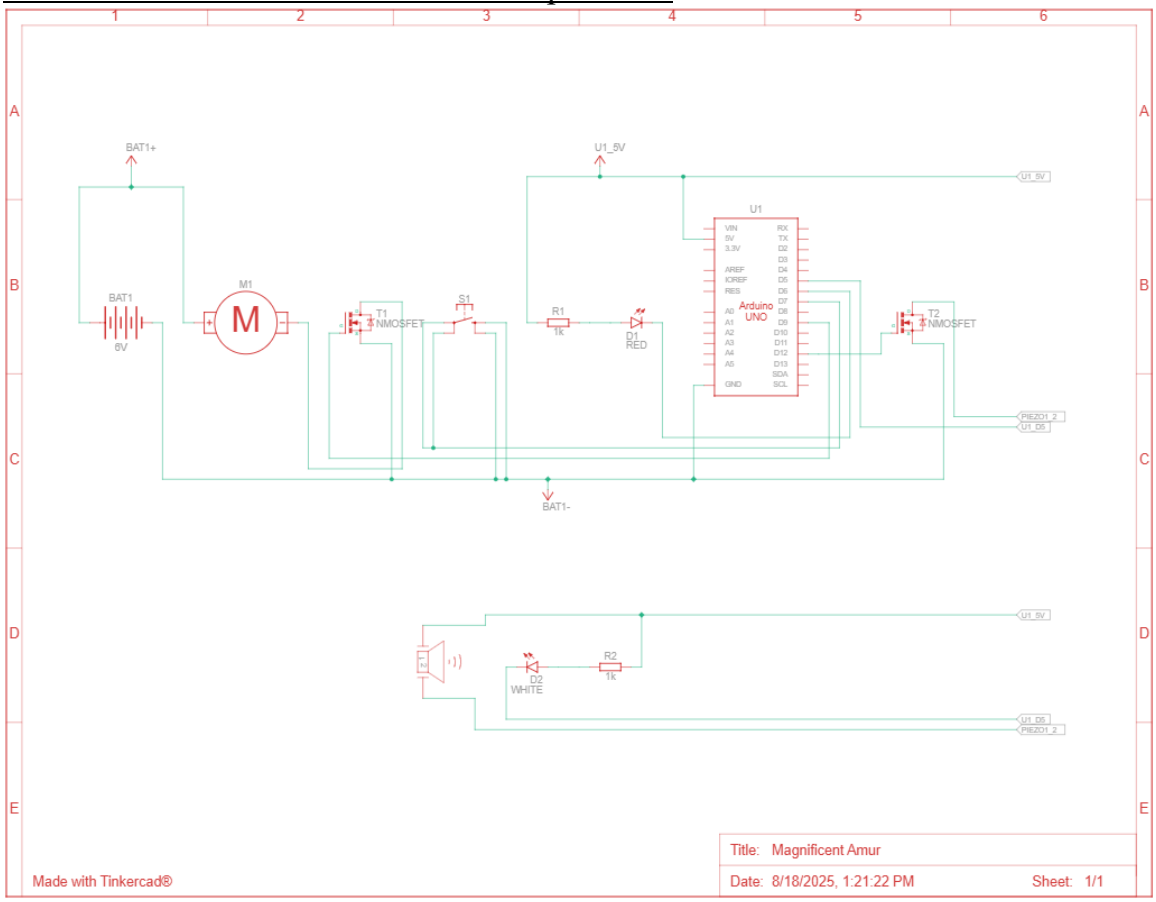

References

1. Philbert, M.A., M.L. Billingsley, and K.R. Reuhl, *Mechanisms of Injury in the Central Nervous System.* Toxicologic Pathology, 2000. **28**(1): p. 43-53.
2. Gennarelli, T.A., *The Pathobiology of Traumatic Brain Injury.* The Neuroscientist, 1997. **3**(1): p. 73-81.
3. Borgens, R.B. and P. Liu-Snyder, *Understanding secondary injury.* The Quarterly review of biology, 2012. **87**(2): p. 89-127.
4. Hale, C., et al., *Implantable osmotic transport device can reduce edema after severe contusion spinal cord injury.* Frontiers in bioengineering and biotechnology, 2020. **8**: p. 806.
5. Hawryluk, G., et al., *Mean Arterial Blood Pressure Correlates with Neurological Recovery after Human Spinal Cord Injury: Analysis of High Frequency Physiologic Data.* Journal of Neurotrauma, 2015. **32**(24): p. 1958-1967.
6. Thal, S.C., et al., *Brain edema formation and neurological impairment after subarachnoid hemorrhage in rats: Laboratory investigation.* Journal of Neurosurgery JNS, 2009. **111**(5): p. 988-994.
7. Rungta, R.L., et al., *The Cellular Mechanisms of Neuronal Swelling Underlying Cytotoxic Edema.* Cell, 2015. **161**(3): p. 610-621.
8. D'Agostino, R., et al., *Management of Penetrating Traumatic Brain Injury: Operative versus Non-Operative Intervention.* J Surg Res, 2021. **257**: p. 101-106.
9. Deng, H., et al., *Adult Firearm-Related Traumatic Brain Injury in United States Trauma Centers.* Journal of Neurotrauma, 2019. **36**(2): p. 322-337.
10. Kochanek, K.D., et al., *Deaths: Final Data for 2017.* Natl Vital Stat Rep, 2019. **68**(9): p. 1-77.
11. Kazim, S.F., et al., *Management of penetrating brain injury.* Journal of Emergencies, Trauma, and Shock, 2011. **4**(3): p. 395-402.
12. du Trevou, M.D. and J.R. van Dellen, *Penetrating Stab Wounds to the Brain: The Timing of Angiography in Patients Presenting with the Weapon Already Removed.* Neurosurgery, 1992. **31**(5): p. 905-912.
13. Hagan, M.J., et al., *Spinal cord injury in adult and pediatric populations.* Interdisciplinary Neurosurgery-Advanced Techniques and Case Management, 2022. **29**.
14. Ackery, A., C. Tator, and A. Krassioukov, *A global perspective on spinal cord injury epidemiology.* Journal of Neurotrauma, 2004. **21**(10): p. 1355-1370.
15. Society, W.H.O.I.S.C., *International perspectives on spinal cord injury*. 2013.
16. Torre-Healy, A., N.F. Marko, and R.J. Weil, *Hyperosmolar therapy for intracranial hypertension.* Neurocritical care, 2012. **17**(1): p. 117-130.

17. Keyrouz, S.G., R. Dhar, and M.N. Diringer, *Variation in osmotic response to sustained mannitol administration.* Neurocritical Care, 2008. **9**(2): p. 204-209.

18. Papadopoulos, M., et al., *Molecular mechanisms of brain tumor edema.* Neuroscience, 2004. **129**(4): p. 1009-1018.

19. Saadoun, S., et al., *The dura causes spinal cord compression after spinal cord injury.* British Journal of Neurosurgery, 2016. **30**(5): p. 582-584.

20. Bell, R.S., et al., *Early decompressive craniectomy for severe penetrating and closed head injury during wartime.* Neurosurg Focus, 2010. **28**(5): p. E1.

21. Cooper, D., *DECRA Trial Investigator; Australian and New Zealand Intensive Care Society Clinical Trials Group: Decompressive craniectomy in diffuse traumatic brain injury.* N Enigl J Med, 2011. **364**: p. 1493-1502.

22. Hachem, L.D., C.S. Ahuja, and M.G. Fehlings, *Assessment and management of acute spinal cord injury: From point of injury to rehabilitation.* J Spinal Cord Med, 2017. **40**(6): p. 665-675.

23. Yang, C.-H., et al., *Elevated intraspinal pressure in traumatic spinal cord injury is a promising therapeutic target.* Neural Regeneration Research, 2022. **17**(8): p. 1703.

24. Soubeyrand, M., et al., *Rat model of spinal cord injury preserving dura mater integrity and allowing measurements of cerebrospinal fluid pressure and spinal cord blood flow.* European Spine Journal, 2013. **22**(8): p. 1810-1819.

25. Hurlbert, R.J., *Methylprednisolone for acute spinal cord injury: an inappropriate standard of care.* Journal of Neurosurgery: spine, 2000. **93**(1): p. 1-7.

26. Wilson, J.R. and M.G. Fehlings, *Riluzole for acute traumatic spinal cord injury: a promising neuroprotective treatment strategy.* World neurosurgery, 2014. **81**(5-6): p. 825-829.

27. Papadopoulos, M.C. and S. Saadoun, *The INSPIRE studies for spinal cord injury.* Journal of Neurosurgery-Spine, 2021. **35**: p. 684-685.

28. McBride, D.W., et al., *Reduction of cerebral edema after traumatic brain injury using an osmotic transport device.* Journal of neurotrauma, 2014. **31**(23): p. 1948-1954.

29. McBride, D.W., et al., *Reduction of cerebral edema via an osmotic transport device improves functional outcome after traumatic brain injury in mice*, in *Brain Edema XVI*. 2016, Springer. p. 285-289.

30. Pickstone, J.V., *Science and Public-Health - Hodgkinson,R.* Annals of Science, 1976. **33**(4): p. 407-407.

31. Lewis, G.N., *The osmotic pressure of concentrated solutions, and the laws of the perfect solution.* Journal of the American Chemical Society, 1908. **30**(5): p. 668-683.

32. Yousef, M.A., R. Datta, and V.G.J. Rodgers, *Confirmation of free solvent model assumptions in predicting the osmotic pressure of concentrated globular proteins.* Journal of Colloid and Interface Science, 2001. **243**(2): p. 321-325.

33. Kedem, O. and A. Katchalsky, *Thermodynamic Analysis of the Permeability of Biological Membranes to Non-Electrolytes.* Biochimica Et Biophysica Acta, 1958. **27**(2): p. 229-246.

34. Vilker, V.L., C.K. Colton, and K.A. Smith, *The Osmotic-Pressure of Concentrated Protein Solutions - Effect of Concentration and Ph in Saline Solutions of Bovine Serum-Albumin.* Journal of Colloid and Interface Science, 1981. **79**(2): p. 548-566.

35. Farrar, M.J. and C.B. Schaffer, *A Procedure for Implanting a Spinal Chamber for Longitudinal In Vivo Imaging of the Mouse Spinal Cord*. Vol. 94. 2014: 1940-087X. e52196.

36. Alvis-Miranda, H., S.M. Castellar-Leones, and L.R. Moscote-Salazar, *Decompressive Craniectomy and Traumatic Brain Injury: A Review.* Bull Emerg Trauma, 2013. **1**(2): p. 60-8.

37. Daugherty, J., et al., *Traumatic Brain Injury-Related Deaths by Race/Ethnicity, Sex, Intent, and Mechanism of Injury - United States, 2000-2017.* Mmwr-Morbidity and Mortality Weekly Report, 2019. **68**(46): p. 1050-1056.

38. Keyrouz, S.G., R. Dhar, and M.N. Diringer, *Variation in osmotic response to sustained mannitol administration.* Neurocrit Care, 2008. **9**(2): p. 204-9.

39. Castillo, L.B., G.A. Bugedo, and J.L. Paranhos, *Mannitol or hypertonic saline for intracranial hypertension? A point of view.* Crit Care Resusc, 2009. **11**(2): p. 151-4.

40. Bingaman, W.E. and J.I. Frank, *Malignant cerebral edema and intracranial hypertension.* Neurol Clin, 1995. **13**(3): p. 479-509.

41. Hariri, R.J., *Cerebral edema.* Neurosurg Clin N Am, 1994. **5**(4): p. 687-706.

42. Schwarz, S., et al., *Effects of hypertonic (10%) saline in patients with raised intracranial pressure after stroke.* Stroke, 2002. **33**(1): p. 136-40.

43. Nakagawa, K., et al., *Treatment of refractory intracranial hypertension with 23.4% saline in children with severe traumatic brain injury.* J Clin Anesth, 2012. **24**(4): p. 318-23.

44. Cooper, D.J., et al., *Decompressive craniectomy in diffuse traumatic brain injury.* N Engl J Med, 2011. **364**(16): p. 1493-502.

45. Orman, J.A., et al., *Epidemiology of moderate-to-severe penetrating versus closed traumatic brain injury in the Iraq and Afghanistan wars.* Journal of Trauma and Acute Care Surgery, 2012. **73**(6): p. S496-S502.

46. Jha, R.M., P.M. Kochanek, and J.M. Simard, *Pathophysiology and treatment of cerebral edema in traumatic brain injury.* Neuropharmacology, 2019. **145**(Pt B): p. 230-246.

47. Cavaliere, R., et al., *Gunshot wounds of the brain in civilians.* Acta Neurochir (Wien), 1988. **94**(3-4): p. 133-6.

48. Bailey, Z.S., et al., *The Effects of Balloon Occlusion of the Aorta on Cerebral Blood Flow, Intracranial Pressure, and Brain Tissue Oxygen Tension in a Rodent Model of Penetrating Ballistic-Like Brain Injury.* Front Neurol, 2019. **10**: p. 1309.

49. Shear, D.A., et al., *Severity Profile of Penetrating Ballistic-Like Brain Injury on Neurofunctional Outcome, Blood–Brain Barrier Permeability, and Brain Edema Formation.* Journal of Neurotrauma, 2011. **28**(10): p. 2185-2195.

50. Gajavelli, S., et al., *Glucose and oxygen metabolism after penetrating ballistic-like brain injury.* J Cereb Blood Flow Metab, 2015. **35**(5): p. 773-80.

51. Williams, A.J., et al., *Characterization of a new rat model of penetrating ballistic brain injury.* J Neurotrauma, 2005. **22**(2): p. 313-31.

52. Williams, A.J., et al., *Penetrating ballistic-like brain injury in the rat: differential time courses of hemorrhage, cell death, inflammation, and remote degeneration.* J Neurotrauma, 2006. **23**(12): p. 1828-46.

53. Corporation, B.H. *Revaclear 300/400/500 Dialyzer*. Baxter Kidney Care 2014 [cited 2023 08/24]; Available from: https://renalcareus.baxter.com/sites/g/files/ebysai3581/files/2023-05/US-RC38-230001%20V2%20-%20Revaclear%20300%20400%20and%20500%20Datasheet.pdf.

54. Schulze, J.O., et al., *Structural and functional characterization of human Iba proteins.* The FEBS Journal, 2008. **275**(18): p. 4627-4640.

55. Farrell Jr, R.E., *RNA Methodologies: laboratory guide for isolation and characterization*. 2009: Academic Press.

56. KO, U., *Effect of receptor protein kinase inhibition on the morphogenesis of experimental diabetic retinopathy.* Journal of Ophthalmology (Ukraine)/Oftal′mologičeskij Žurnal, 2025(1).

57. Sauleau, P., et al., *The pig model in brain imaging and neurosurgery.* Animal, 2009. **3**(8): p. 1138-51.